AD NUMBER

AD485829

NEW LIMITATION CHANGE

TO

Approved for public release, distribution unlimited

FROM

Distribution authorized to U.S. Gov't. agencies and their contractors; Administrative/Operational Use; APR 1966. Other requests shall be referred to Ballistic Systems and Space Systems Div., AFSC, Los Angeles Air Force Station, CA.

AUTHORITY

SAMSO ltr, 25 Nov 1968

AD 485829

Detection Probabilities for Log-Normally Distributed Signals

APRIL 1966

Prepared by G. R. HEIDBREDER and R. L. MITCHELL
Electronics Research Laboratory
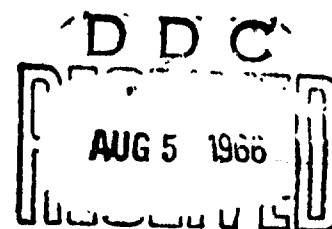Laboratories Division
Laboratory Operations

AEROSPACE CORPORATION

D D C

AUG 5 1966

E

Best Available Copy

Air Force Report No. . Aerospace Report No.
TR-669(9990)-6

DETECTION PROBABILITIES FOR LOG-NORMALLY
DISTRIBUTED SIGNALS

Prepared by

G. R. Heidbreder and R. L. Mitchell
Electronics Research Laboratory

Laboratories Division
Laboratory Operations
AEROSPACE CORPORATION

April 1966

Prepared for

BALLISTIC SYSTEMS AND SPACE SYSTEMS DIVISIONS
AIR FORCE SYSTEMS COMMAND
LOS ANGELES AIR FORCE STATION
Los Angeles, California

FOREWORD

This report is published by Aerospace Corporation, El Segundo, California, under Contract No. AF 04(695)-669.

This report, which documents research conducted between 1 January and 15 February 1966, was submitted on 12 May 1966 to Captain Ronald J. Starbuck, SSTRT, for review and approval.

The authors wish to acknowledge Mr. Arlyn Boekelheide for helpful discussions, and Dr. B. J. DuWaldt for pointing out the significance of the problem and contributing many helpful suggestions. The authors also wish to express appreciation to Maj. R. W. Kennedy (AFAL) for supplying the data presented in Fig. 1.
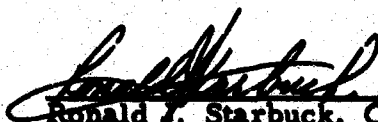
Information in this report is embargoed under the U. S. Export Control Act of 1949, administered by the Department of Commerce. This report may be released by departments or agencies of the U. S. Government to departments or agencies of foreign governments with which the United States has defense treaty commitments. Private individuals or firms must comply with Department of Commerce export control regulations.

Approved

D. D. King, Director
Electronics Research Laboratory
Laboratories Division
Laboratory Operations

Publication of this report does not constitute Air Force approval of the report's findings or conclusions. It is published only for the exchange and stimulation of ideas.

Ronald J. Starbuck, Captain
Space Systems Division
Air Force Systems Command

-ii-

ABSTRACT

The amplitude and power of a large family of radio signals
are observed to have log-normal probability density func-
tions. Among these are signals propagated through random
inhomogeneous media, a notable example being low frequency
atmospheric radio noise. Of greater importance are certain
radar targets that have been observed to have essentially
log-normal density functions. Both ships and space vehicles
may fall into this category. Curves of probability of detection
versus signal-to-noise ratio for the case of log-normal signals
in Gaussian noise have been computed and are presented in
this paper. The curves apply for square-law detection with
varying degrees of post-detection linear integration. Both
slowly and rapidly fluctuating signals are considered. It is
shown that for log-normal signal distributions having large
variances the probability of detection differs significantly
from that obtained using curves based on an assumed Rayleigh
signal distribution.

CONTENTS

TABLE

FIGURES

I. INTRODUCTION

The detection of fluctuating signals in the presence of Gaussian noise has been studied widely [1]-[4] since the extensive pioneering treatment of detection theory for constant amplitude pulsed signals in noise by Marcum [5]. All of these studies are extensions of Marcum's work. In almost all cases, the fluctuating signal amplitude has been assumed to be Rayleigh distributed. This choice is due to the well-known fact that the sum of a large number of independent random vectors having uniform phase distributions is a Rayleigh vector, i.e., one having a uniform phase distribution and a Rayleigh amplitude distribution, provided only that the number of contributing vectors is very large and that no single vector contributes significantly to the total power [6]. Swerling [1] has presented curves of the probability of detection as a function of the signal-to-noise ratio for both Rayleigh-distributed signals and for signals whose power is distributed Chi-square with four degrees of freedom. Since N, the number of pulses integrated, is presented as a parameter, and since a square-law detector is assumed, results for signals whose power is distributed Chi-square with 2N degrees of freedom may be inferred. It is only necessary to observe that the sum of a Rayleigh noise vector and a Rayleigh signal vector is, itself, a Rayleigh vector and that the post-detection sum of N independent signal plus noise variates is then the sum of the squares of 2N independent Gaussian variates and, hence, is Chi-square with 2N degrees of freedom. As Swerling has noted [2], one can construct a wide variety of probability density functions from the Chi-square family. In choosing a member of the Chi-square family to fit a particular distribution, one is free

to choose two parameters, e.g., the mean and the number of degrees of freedom. Different degrees of skewness are obtained as the number of degrees of freedom is varied.

The assumption of signals composed of a large number of small independent random contributions appears to be reasonable in many cases, e.g., the signals scattered by many radar targets consist of contributions from numerous and diverse reflecting elements. It has become common practice to treat most fluctuating radar returns as having Rayleigh-distributed amplitudes. The experimental evidence for the existence of Rayleigh-distributed radar returns is not altogether conclusive, however. Early investigators [7] found that, while target cross section distributions followed the Rayleigh law reasonably well for low cross sections, they often exhibited a pronounced high cross section tail, i.e., higher probability density at the high cross sections than indicated by the Rayleigh law. This difference is consistent with the idea that a few large surfaces predominate in the target. The case of aircraft appears to be a notable exception where experimental data are conclusively Rayleigh. There has been some disagreement on this point [8], but the major body of opinion supports the Rayleigh interpretation [9], [10]. More recently, Harrison [11] in analyzing the statistics of the radar returns from ships has found that the return signal strength distribution closely follows a log-normal law. Space vehicle and satellite cross sections have also typically exhibited non-Rayleigh statistics. They are usually characterized by a very large dynamic range and variance [12]. Kennedy [13] has obtained statistical data on the radar cross section of a satellite, examining the distribution over aspect angle and frequency. The resulting

-2-

cross section probability density functions are shown in Fig. 1. One of the density functions was obtained by measuring over aspect angle alone with all aspect angles assumed to be equiprobable. The same aspect measurement procedure was followed in obtaining the other density function, with frequency averaging being obtained by stepping the frequency of alternate radar pulses. The density functions appear to be log-normal and, significantly, exhibit mean values about 10 dB above the median values. The high ratio of mean-to-median values is due to the pronounced high cross section tail of the distribution. It is not possible to obtain such a mean-to-median ratio with any member of the Chi-square family suggested by Swerling.

Weinstock [14] has studied the modeling of certain classes of satellite bodies and has attempted to fit empirical data to Chi-square models. The difficulty in fitting members of the Chi-square family is evident when one considers the variance and mean-to-median ratio. Starting with Swerling's generalized distribution [2]

$$f(x, \bar{x}) = \frac{1}{\Gamma(k)} \left(\frac{kx}{\bar{x}} \right)^{k-1} \exp\left(-\frac{kx}{\bar{x}} \right) \frac{k}{\bar{x}}$$

we have for the variance

$$D^2(x) = \frac{\bar{x}^2}{k}$$

where k is one-half the number of degrees of freedom of the Chi-square distribution. The median, x_m, is given by the solution of

$$\int_0^{x_m} \frac{1}{\Gamma(k)} \left(\frac{kx}{\bar{x}}\right)^{k-1} \exp\left(-\frac{kx}{\bar{x}}\right) \frac{kdx}{\bar{x}} = \frac{1}{2}$$

or

$$\frac{1}{\Gamma(k)} \int_0^{kx_m/\bar{x}} u^{k-1} \exp(-u) \, du = \frac{1}{2}$$

The latter expression is recognized as a form of the incomplete gamma function. Solving for $\bar{x}/x_m$ with $k = 1$, the result is $\bar{x}/x_m = 1.44$. For $k = 2$, it is 1.18, and it approaches unity with increasing k. Since large variances and mean-to-median ratios may characterize radar targets of interest, the Chi-square family with integral k may be unsuitable. Weinstock [13] has allowed $k < 1$ in order to fit the variance and mean to empirical data but has found disagreement of higher order moments and a lack of fit on the tails of the distributions. He found that for a class of bodies of the conducting cylinder type a reasonable fit could be obtained by varying k between 0.3 and 0.7.

Current system analysis and design practice uses the Swerling Chi-squared models almost exclusively, with the mean characterizing the distributions treated. Both Weinstock [14] and Swerling have observed that if a single parameter is to be used to characterize a distribution the median is preferred over the mean. The median is less influenced by high cross section tails of distributions and leads to a more conservative choice of design parameters. To conclusively check the validity of this assertion, it is necessary to compute the probability

-4-

of detection as a function of median signal-to-noise ratio for distributions having large ratios of mean-to-median values. The log-normal distribution, in addition to being one that is found to occur in practice, is one that represents an extreme in high cross section tails. It is therefore suitable for checking the accuracy of design procedures that use existing cross section models but characterize distributions by their medians.

This paper presents the results of a numerical computation of the probability of detection for a large family of fluctuating signal distributions that are log-normal.

II. LOG-NORMAL SCATTERING MECHANISMS

The nature of the scattering mechanisms that lead to log-normal density functions for radar targets is not understood, and no attempt at a complete analysis is made in this paper. Nevertheless, a brief conjecture on this point seems in order.

If a random signal amplitude has a log-normal distribution, it can be represented by

$$x = A e^{-\psi}$$

where ψ is normally distributed. A log-normal distribution occurs in radio propagation through inhomogeneous media, the logarithmic variable ψ being interpreted as the sum of independent attenuation factors associated with statistically independent regions or "blobs" in the medium [15]. In the case of the radar cross section measurements referred to above, however,

it seems clear that the signal fluctuations are due to statistical effects associated with the targets. One possible explanation for log-normal target statistics has been suggested by DuWaldt [16] who noted that the effect of surface roughness on the specular return from a flat plate is to reduce the cross section relative to that of a smooth plate by a factor $e^{-\psi}$, where ψ is proportional to the mean-square surface depth fluctuation. If the radar return at any aspect angle is that from a single surface selected from an ensemble having a normally distributed degree of roughness, log normal amplitude statistics result. Since the return from a ship at any given aspect angle is largely due to a single predominant dihedral corner, the log-normal character of ship returns might thus be explained.

III. THE PROBABILITY OF DETECTION FOR LOG-NORMALLY DISTRIBUTED SIGNALS

The computational procedures are based on the receiver models used by Marcum and Swerling, i.e., a linear receiver preceding a square-law detector and followed by post-detection integration which gives equal weight to all the pulses added. As in Swerling [1], two extremes of pulse-to-pulse correlation are treated. These are:

Case 1: All pulses occurring during an integration period are perfectly correlated. Pulses in successive integration periods are independent. In the case of a scanning radar, this implies independent fluctuations from scan to scan but with no fluctuation during a scan.

Case 2:   The fluctuations are independent from pulse to pulse.

The probability density, $f_N(y)$, of N integrated signal plus noise variates at the detector output is integrated to obtain the probability of detection,

$$P_D(\bar{x}) = \int_{Y_b}^{\infty} f_N(y, \bar{x}) \, dy \qquad (1)$$

The density function of signal plus noise and the probability of detection are functions of some measure of power in the signal distribution. The average signal-to-noise power ratio, $\bar{x}$, is used. The normalization is the same as that used by Marcum, and, hence, the detection threshold level, Y_b, is as given therein, namely, the solution of

$$1 - \left(\frac{1}{2}\right)^{N/n} = \int_{Y_b}^{\infty} f_N(y, 0) \, dy \qquad (2)$$

where n is the number of pulses in the time required for the false alarm probability to reach 0.5. Values of Y_b as a function of N and n are tabulated in Table I.

In Case 1, the density function, $f_N(y, \bar{x})$, is obtained by averaging Marcum's density function for a constant signal plus noise over the distribution of the signal-to-noise power ratio. Thus,

$$f_N(y, \bar{x}) = \int_0^{\infty} f_N(y/x) \, f(x, \bar{x}) \, dx \qquad (3)$$

where $f_N(y/x)$ is the conditional probability density of the integrated detector output signal plus noise variate y, given a signal-to-noise power ratio x and where $f(x,\bar{x})$ is the density function for the signal-to-noise power ratio. For a log-normally distributed signal,

$$f(x,\bar{x}) = \frac{1}{\sqrt{2\pi}\ \sigma x}\ \exp\left[-\frac{(\ln x - \overline{\ln x})^2}{2\sigma^2}\right]$$

where σ^2 is the variance of ln x.

For the presentation of the results, it is more convenient to characterize $f(x,\bar{x})$ by the parameters $\bar{x}$ and ρ, the ratio of mean to median values. In terms of σ and $\overline{\ln x}$,

$$\bar{x} = \exp\left(\frac{\sigma^2}{2} + \overline{\ln x}\right)$$

$$\rho = \exp\left(\frac{\sigma^2}{2}\right)$$

In case 2, $f_N(y,\bar{x})$ is the result of an N-fold self-convolution of $f_1(y,\bar{x})$ as given by Eq. (3).

Details of the numerical computation are given in the appendix.

IV. RESULTS AND CONCLUSIONS

Curves of the probability of detection as a function of average signal-to-noise ratio are presented in Figs. 2 - 28 for Cases 1 and 2, with the number of pulses integrated, N, as a parameter. Fixed values of ρ and the false alarm number n were used in plotting the curves, namely,

-8-

$\rho = 1, 2, 4, 8, 16$ and $n = 10^6, 10^8, 10^{10}$. Figures 2 - 4 are identical to those in Marcum since for $\rho = 1$ the variance is zero and, hence, the target is not fluctuating. Cases 1 and 2 are thus identical for $\rho = 1$. In Figs. 29 - 43, the curves have been replotted with ρ as a parameter. These figures are useful for interpolation in ρ.

To improve the accuracy of interpolation in ρ, it may be advantageous to first plot the curves with ρ as a parameter as a function of the median signal-to-noise ratio (or to normalize R to unity median signal-to-noise ratio). A set of such curves for $n = 10^8$ is presented in Figs. 44 - 50. The curves for Case 1 intersect near 50-percent probability of detection and, hence, facilitate interpolation. A very different behavior is observed in Case 2 when the curves are plotted versus the median signal-to-noise ratio. The point at which the curves intersect shifts to higher values of probability as the number of pulses integrated is increased.

The form of presentation is that of Marcum and Swerling. While it is recognized that this format is not always convenient, it seems preferable in view of the wide circulation of the curves compiled by the aforementioned authors and the resulting ease of comparison. A secondary reason is the compression of the curves afforded by plotting probability of detection versus normalized radar range which is inversely proportional to the quarter-power of the signal-to-noise ratio. This compression is desirable because of the flattening of the curves with increasing variance of the signal distribution. A nonlinear dB scale for the signal-to-noise ratio is added for convenience.

As ρ is increased from unity at constant average signal-to-noise ratio, the probability of detection is reduced at high signal-to-noise ratios and increased at low signal-to-noise ratios. The sensitivity to a change in ρ is seen to be greatest for small ρ. As ρ is increased to very large values, the probability density function approaches a delta function at the origin. To show this, it is first noted that the mode of the log-normal distribution is at

$$x_{mode} = e^{\overline{\ln x} - \sigma^2} = \frac{\bar{x}}{\rho^3}$$

The peak value of the density function is

$$f(x_{mode}, \bar{x}) = \frac{\rho^2}{2\sqrt{\pi \ln \rho}\, \bar{x}}$$

Hence,

$$\lim_{\rho \to \infty} x_{mode} = 0$$

$$\lim_{\rho \to \infty} f(x_{mode}, \bar{x}) \to \infty$$

It can be shown that unit weight is associated with the delta function on examination of the probability that the signal-to-noise ratio exceeds some positive value ϵ

$$P(x>\epsilon) = \int_{\epsilon}^{\infty} f(x, \overline{x})\, dx$$

$$= \frac{1}{\sqrt{\pi}} \int_{E}^{\infty} e^{-z^2}\, dz$$

where $z = (\ln x - \overline{\ln x})/\sqrt{2}\,\sigma$, and

$$E = \frac{\ln \epsilon - \ln \overline{x} + \ln \rho}{\sqrt{2\, \ln \rho}}$$

Then, if ϵ is fixed at any finite positive value,

$$\lim_{\rho \to \infty} P(x>\epsilon) = 0$$

As a consequence, the probability of detection for any finite average signal-to-noise ratio approaches zero as ρ is increased without limit.

The relative insensitivity of the probability of detection to a change in ρ at $\rho = 16$ is due to the fact that the mode of the distribution is already 36 dB below the average value. Hence, the probability weighting in the vicinity of the mode is not significant for all but the very highest signal-to-noise ratios. At larger values of ρ, the probability of detection is governed by the relatively flat and slowly decreasing tail of the density function. The behavior of $f(x, 1)$ with increasing ρ in the range of values used for the calculations is illustrated in Figs. 61 and 62. These curves are indicative of the behavior for all $\overline{x}$ since

$$f(x, k\overline{x}) = \frac{1}{k}\, f\left(\frac{x}{k}, \overline{x}\right)$$

-11-

The effect of variation in $\bar{x}$ at constant ρ is illustrated in Fig. 63.

It is of interest to compare the results with those obtained by Swerling using Rayleigh-distributed signal amplitude. Figures 51 - 56 show the comparison for $n = 10^8$ and $\rho = 2$, 16 (Case 1) and $\rho = 2$, 4, 8, 16 (Case 2). For $\rho = 2$, there is relatively good agreement between the curves over a wide range of signal-to-noise ratios. (It should be recalled that for the Rayleigh distribution ρ equals 1.44.) The agreement is particularly good for Case 2 when a large number of pulses is integrated. This is to be expected since the sum of a large number of independent variates approaches a normal distribution regardless of the distribution of the individual variates. The curves differ widely for $\rho = 16$, however, thereby illustrating the inapplicability of Swerling's curves when the mean-to-median signal power ratio is very large. The probability of detection for Case 2 based on the normal approximation to the density function of the detector output is also shown in Figs. 53 - 56. The details of the computation are given in the appendix.

Figures 57 - 60 show the above data plotted versus the median signal-to-noise ratio. For the curves from Swerling, the signal-to-noise ratio is the average signal-to-noise power ratio. Thus, R_o is to be interpreted as that range for which the log-normal target has unity median signal-to-noise ratio and the Rayleigh target has unity average signal-to-noise ratio. These curves permit judgment of the efficacy of entering Swerling's curves with median signal-to-noise ratio in the hope of obtaining a conservative estimate of performance. It is seen that a conservative estimate is obtained for $\rho = 2$ in both Cases 1 and 2. For larger values of ρ, the curves for the

log-normal distribution fall below those for the Rayleigh distribution over a portion of their range. Nevertheless, conservative estimates are obtained almost everywhere for $\rho = 16$ in Case 2. In Case 1 for $\rho = 16$, the blip-scan ratio predicted by the Rayleigh curves never exceeds the actual one by as much as 10 percent.

When the statistical description of a radar target is obtained by averaging over all of the aspect angles and assuming them to be equally probable, some discretion must be applied in using the resulting model. It is entirely possible that a high cross section tail in the density function results from specular returns at relatively few aspect angles. If, then, the target attitude is relatively stable during a radar intercept, the equally probable aspect assumption can lead to very erroneous results. Conservatively, it may be best to neglect the high cross section tail of the density function when a lower bound on detection probability is desired. Thus, the procedure of using the Rayleigh curves with a median signal-to-noise ratio would be a good one. On the other hand, if one is interested in an upper bound on detection probability, the tail of the density function must be considered. The Rayleigh curves are then completely unsuitable.

Table I. Detection Threshold (Bias) Level, Y_b

	Detection Threshold (Bias) Level, Y_b (Accurate to 0.002)		
	$n = 10^6$	$n = 10^8$	$n = 10^{10}$
N = 1	14.182	18.787	23.392
2	16.342	21.194	25.995
4	20.168	25.438	30.574
8	26.910	32.857	38.544
10	30.037	36.277	42.202
20	44.485	51.944	58.864
40	70.718	80.024	88.454
80	119.303	131.371	142.051
100	142.681	155.898	167.510
200	255.526	273.399	288.756
400	472.717	497.484	518.321
800	895.459	930.451	959.289
1000	1104.188	1143.432	1175.559
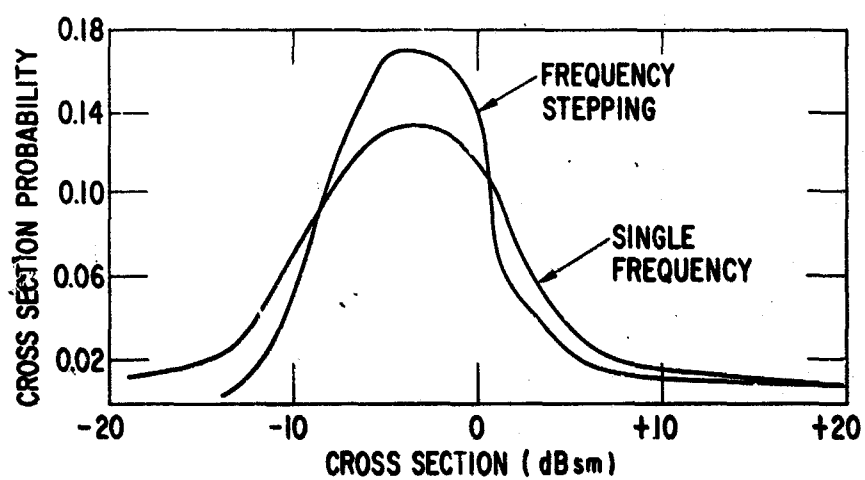
Fig. 1.   Probability Density Function, Radar
Cross Section of Satellite
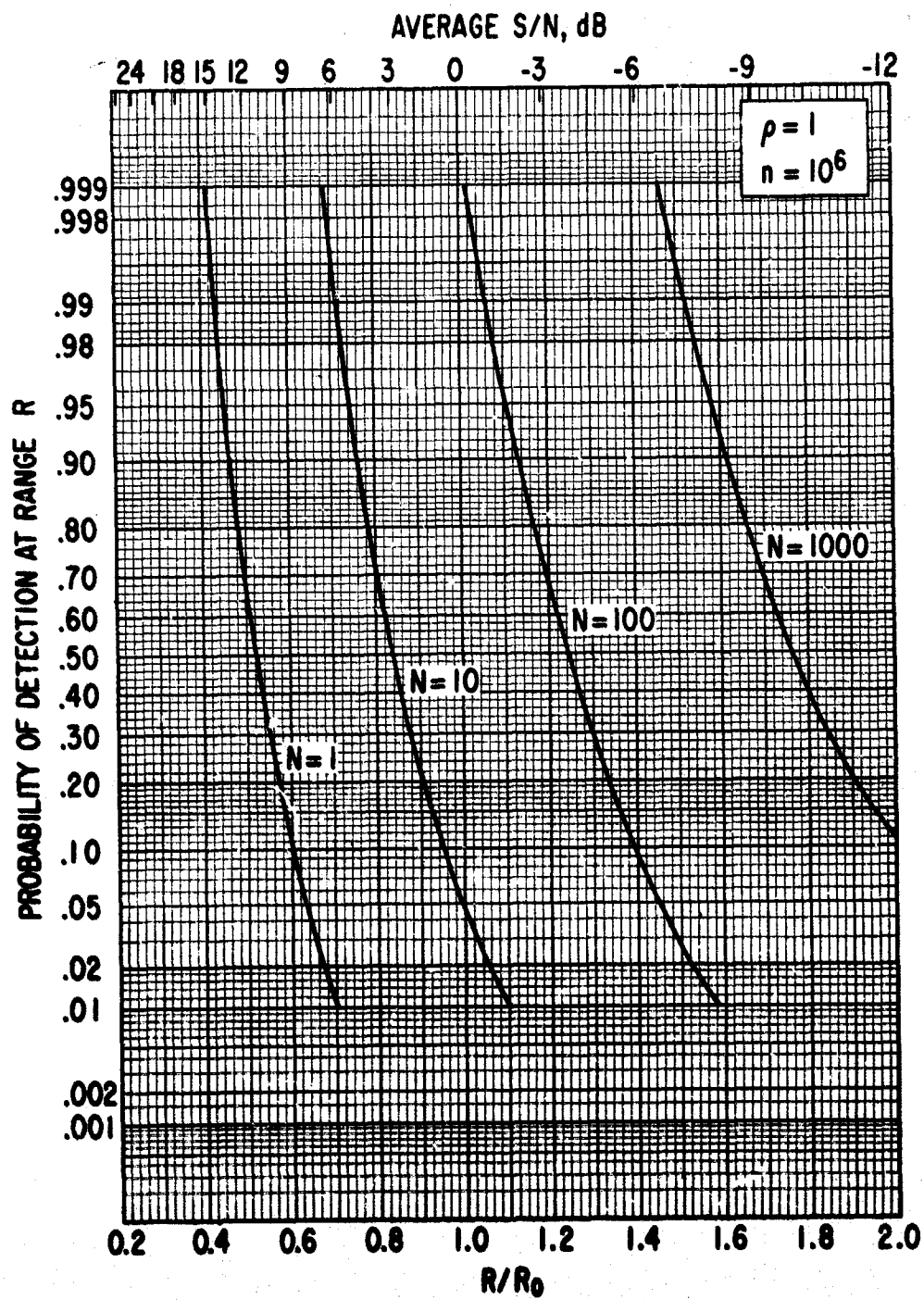
Fig. 2. Nonfluctuating Target (Marcum), $\rho = 1$ and $n = 10^6$
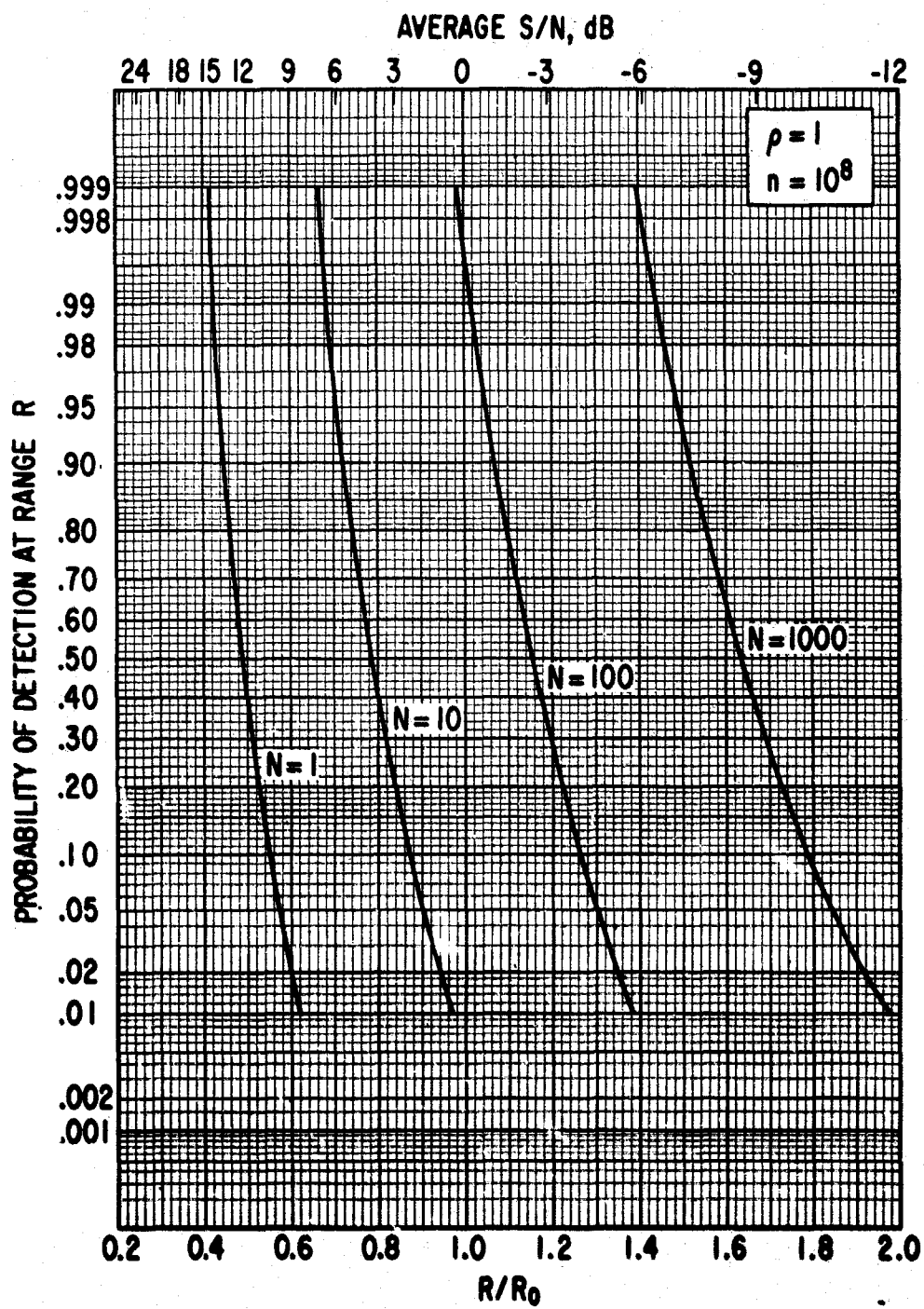
Fig. 3. Nonfluctuating Target (Marcum), $\rho = 1$ and $n = 10^6$
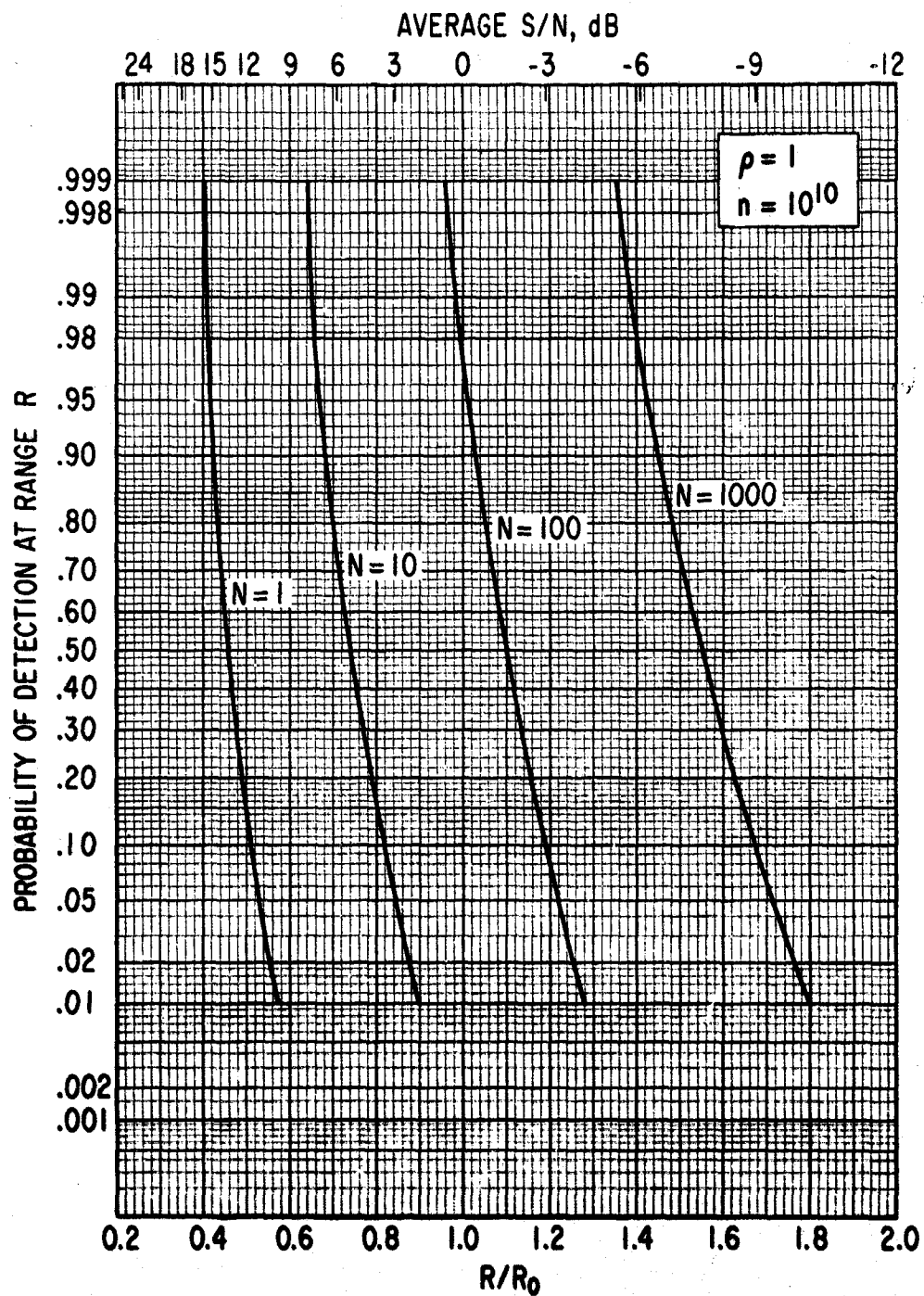
Fig. 4. Nonfluctuating Target (Marcum), $\rho = 1$ and $n = 10^{10}$
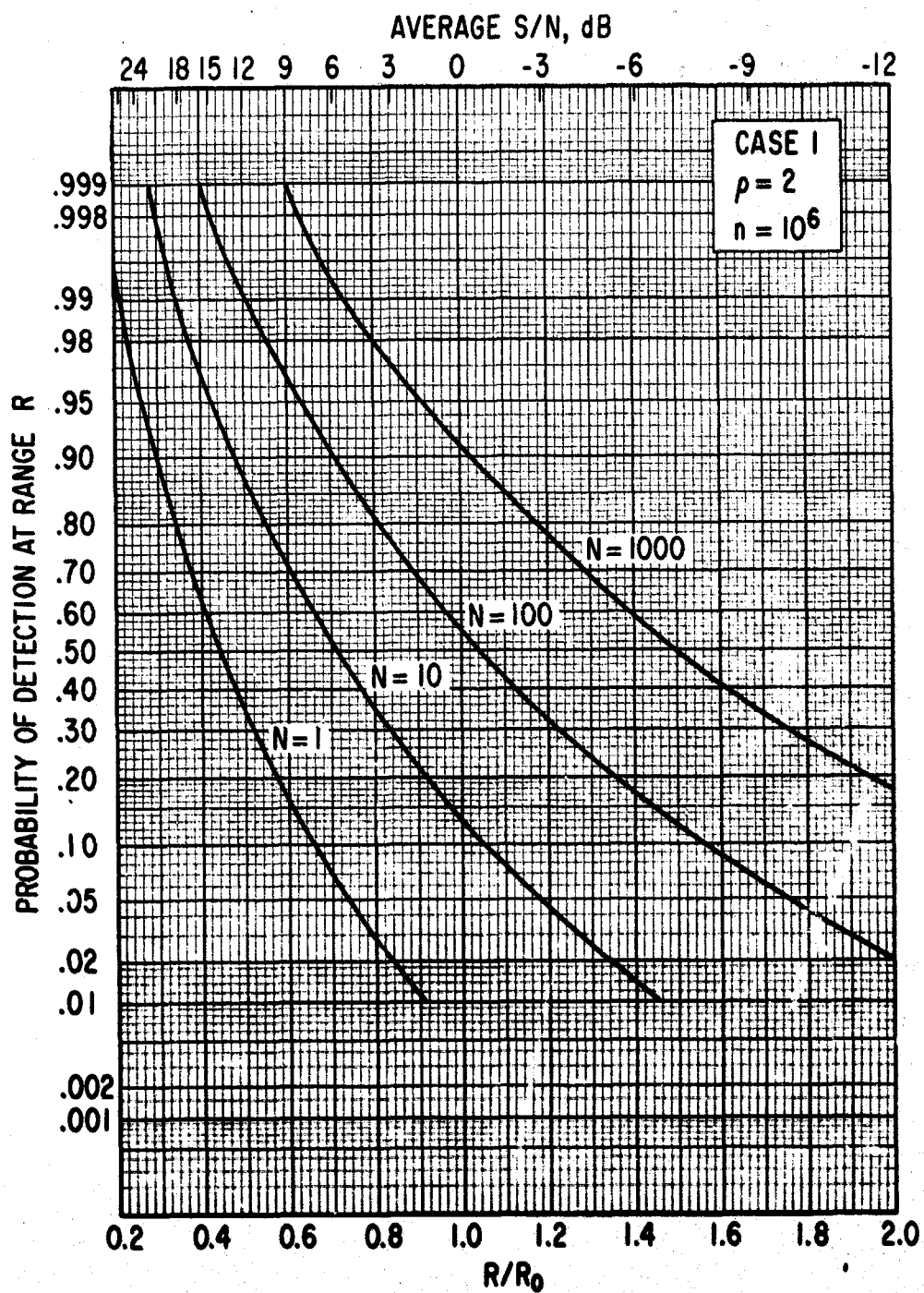
Fig. 5. Case 1, $\rho = 2$, $n = 10^6$, with N as a Parameter
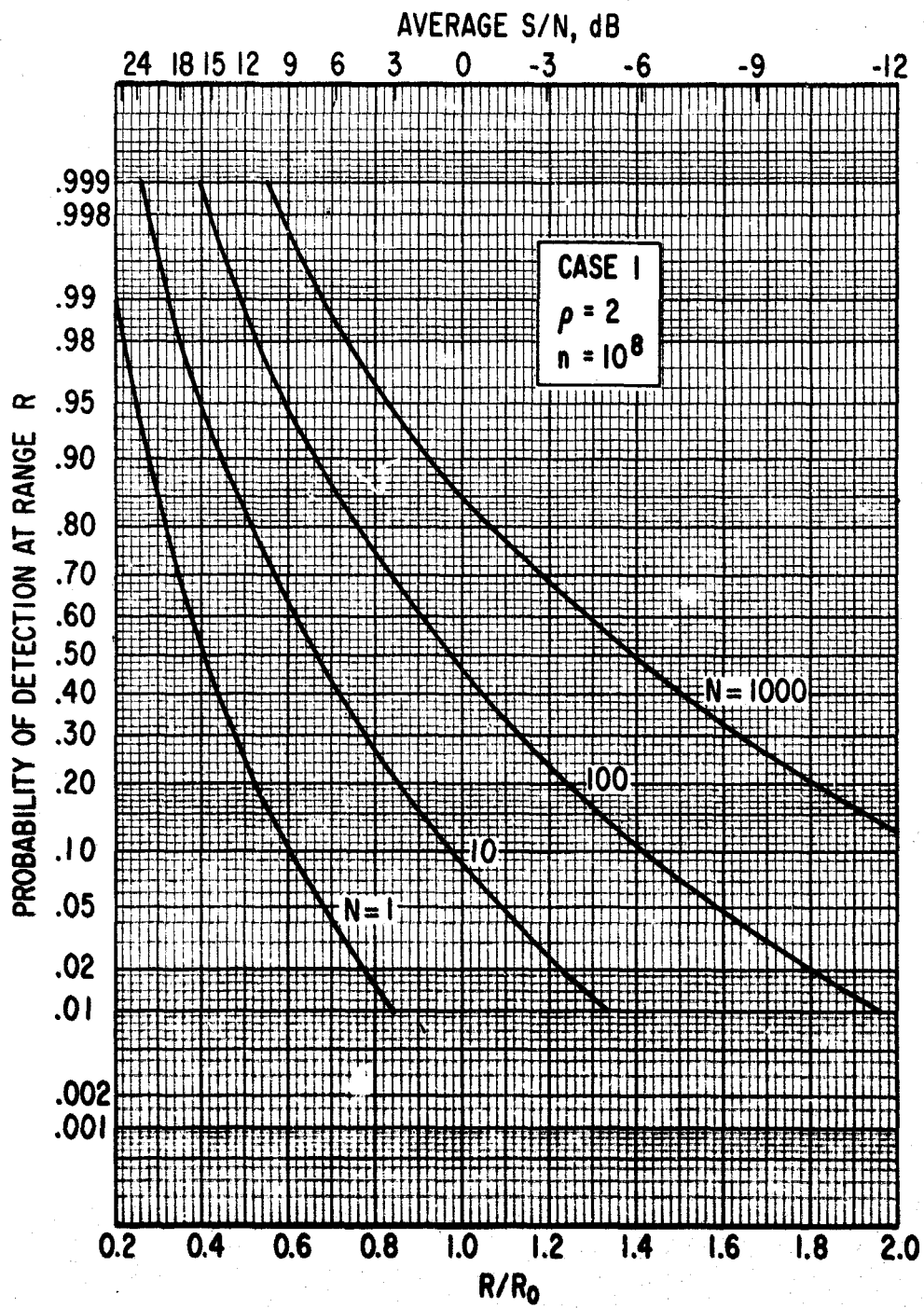
Fig. 6. Case 1, $\rho = 2$, $n = 10^8$, with N as a Parameter
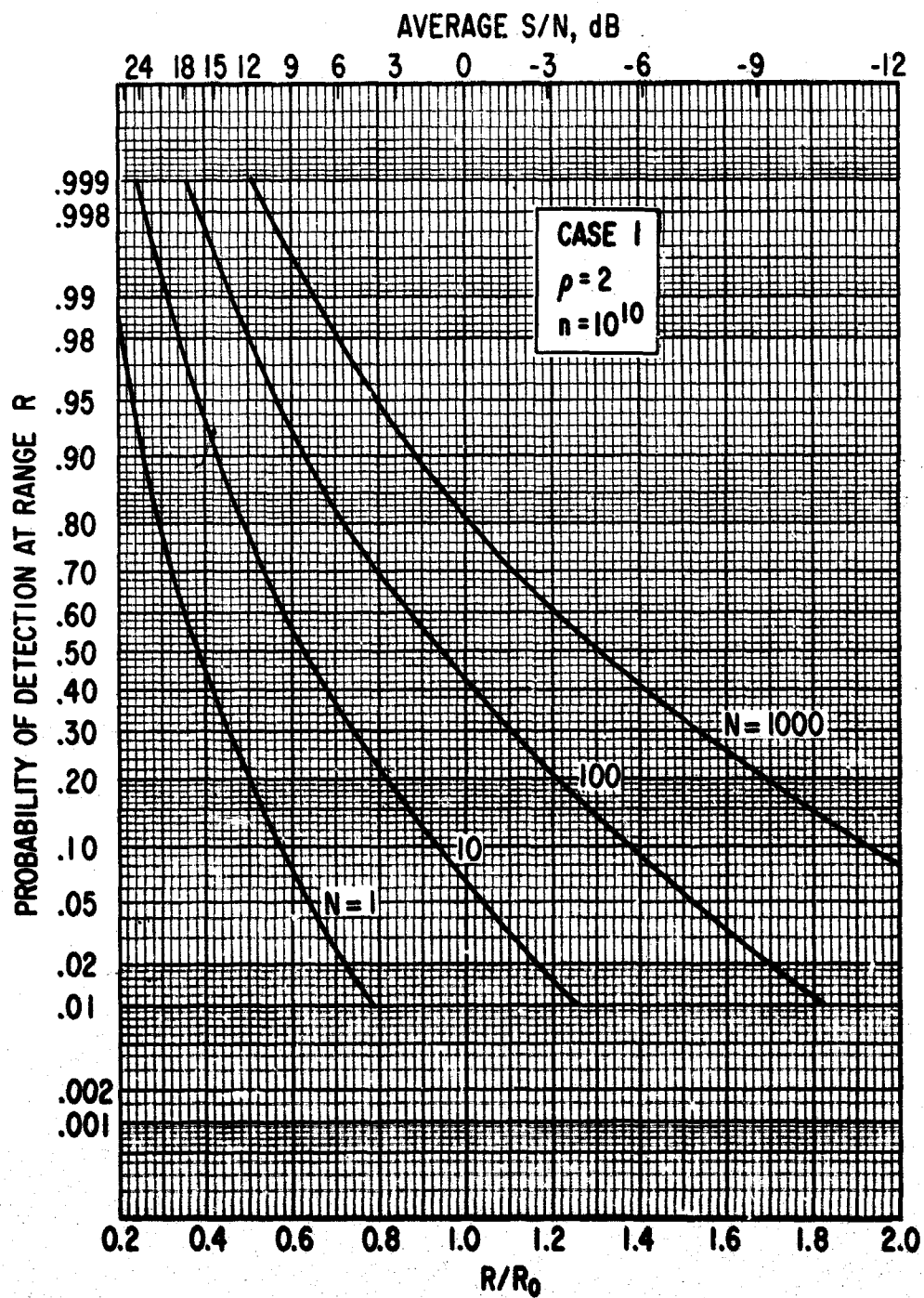
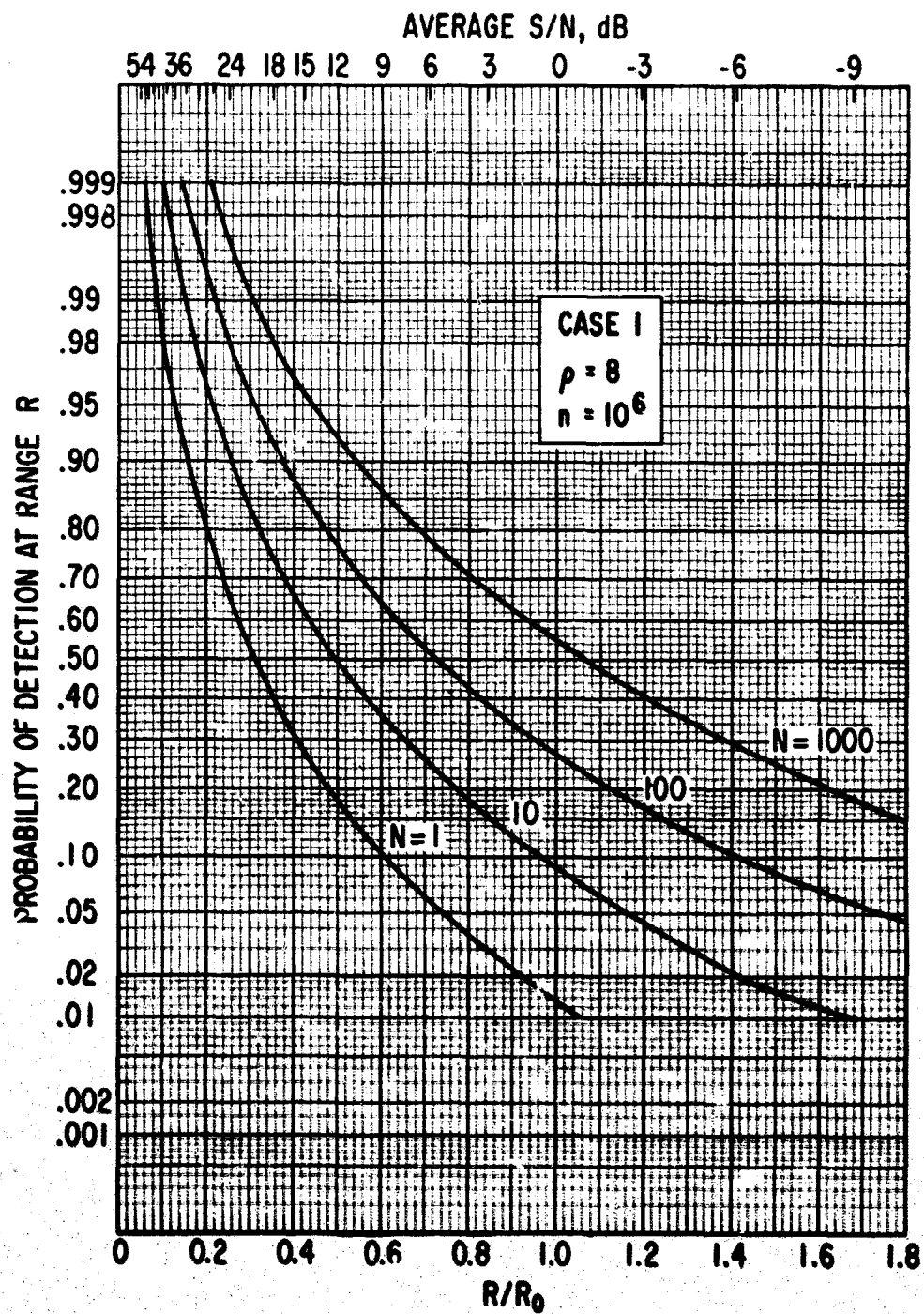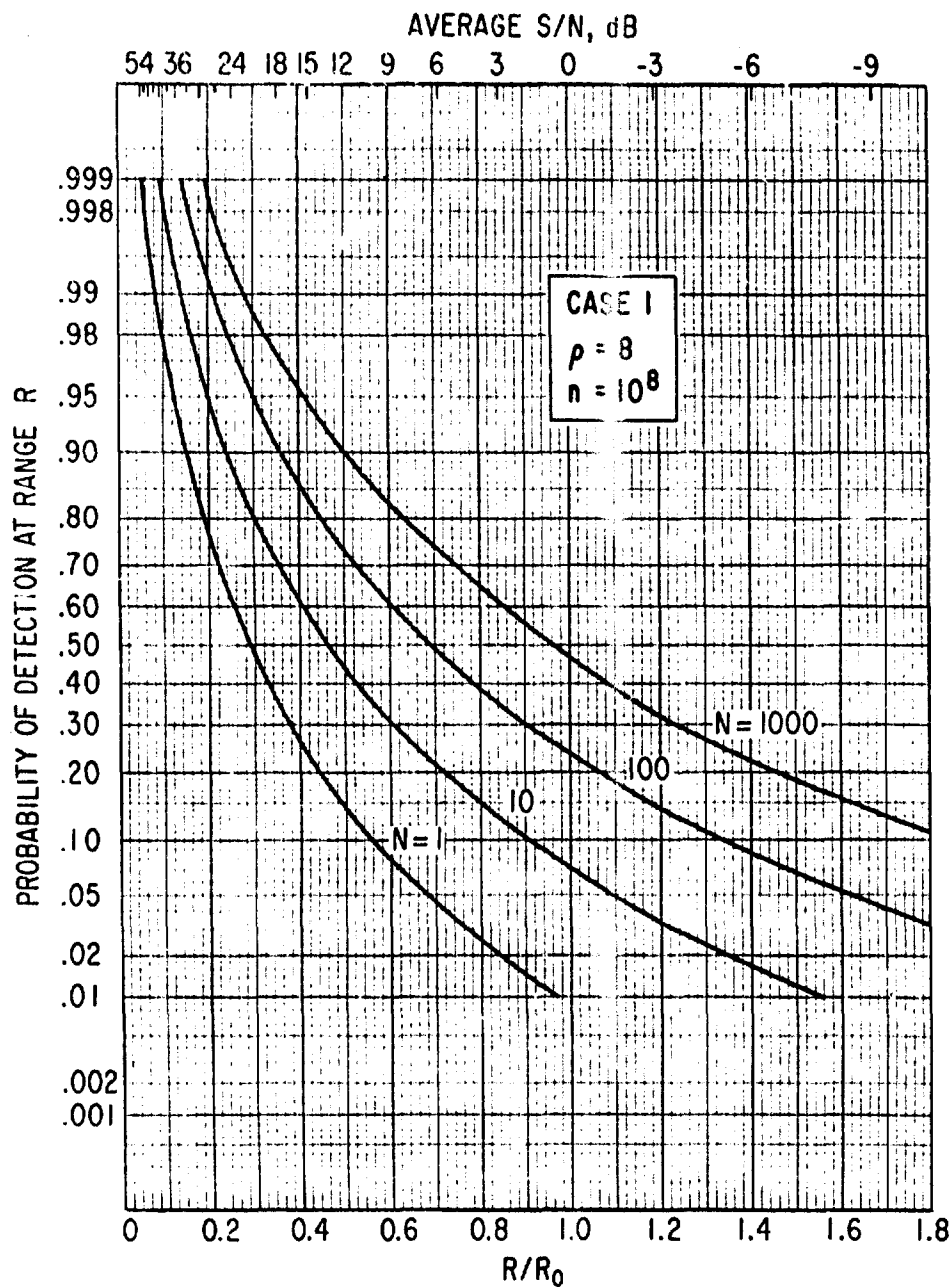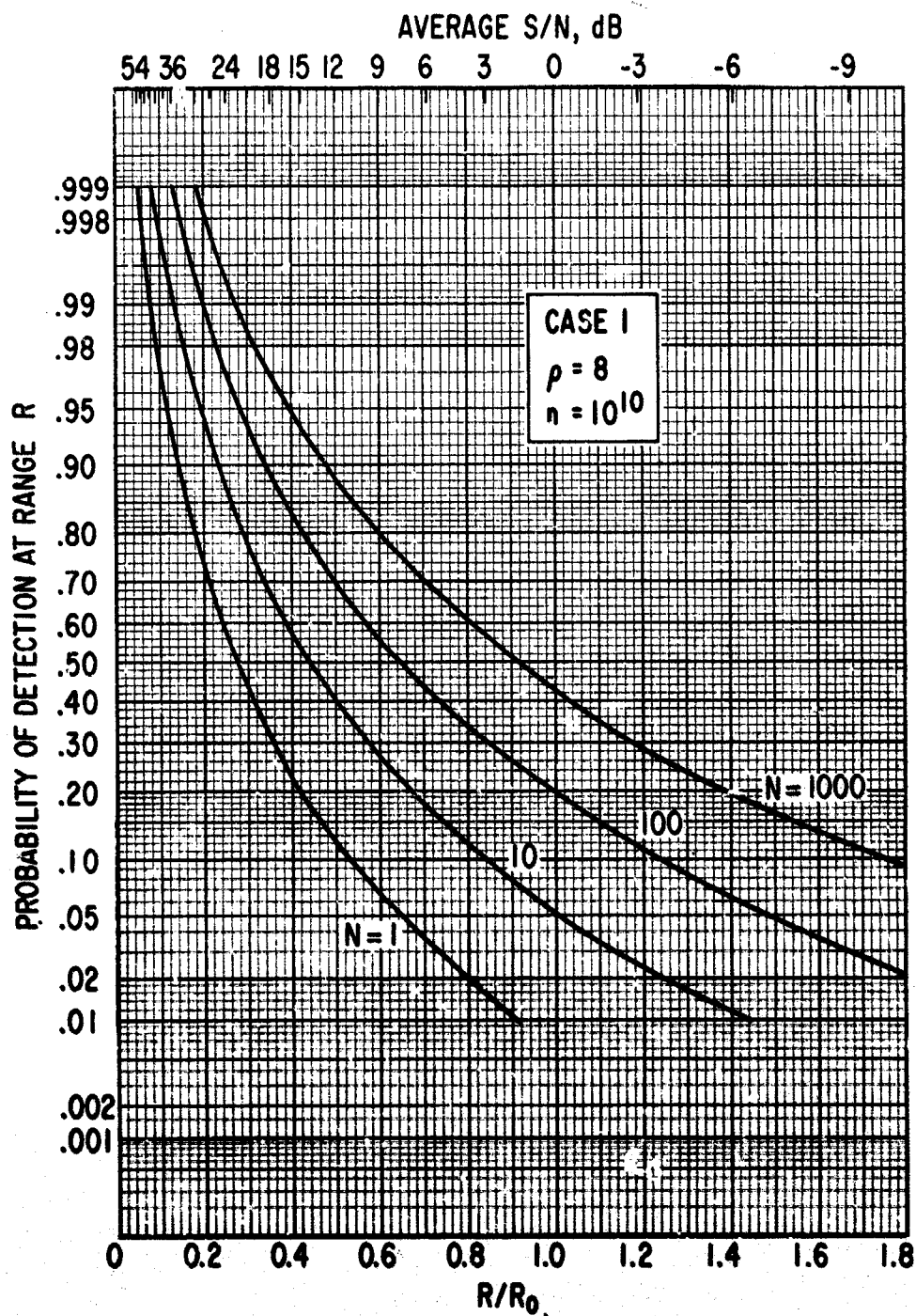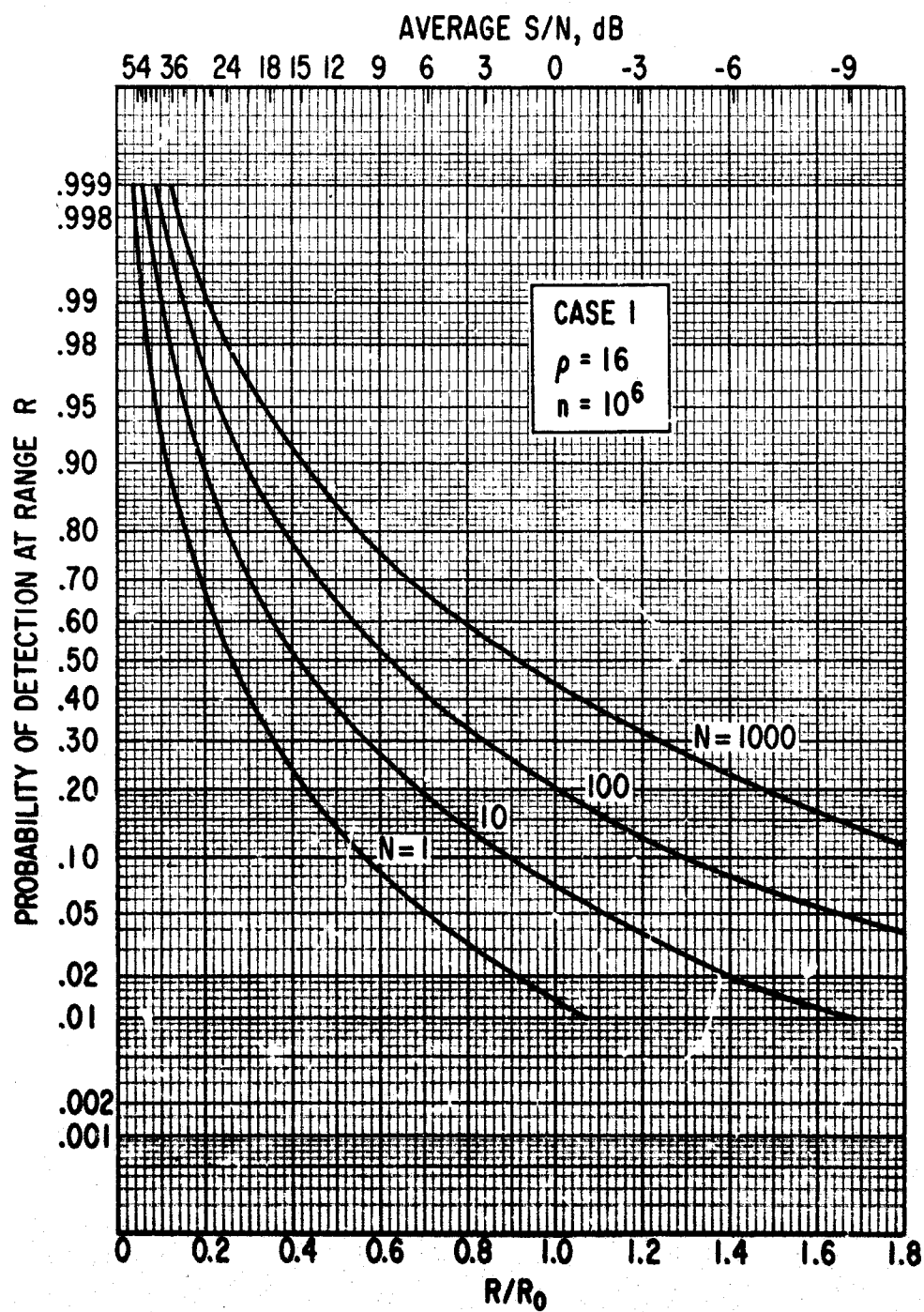Fig. 7. Case 1, $\rho = 2$, $n = 10^{10}$, with N as a Parameter
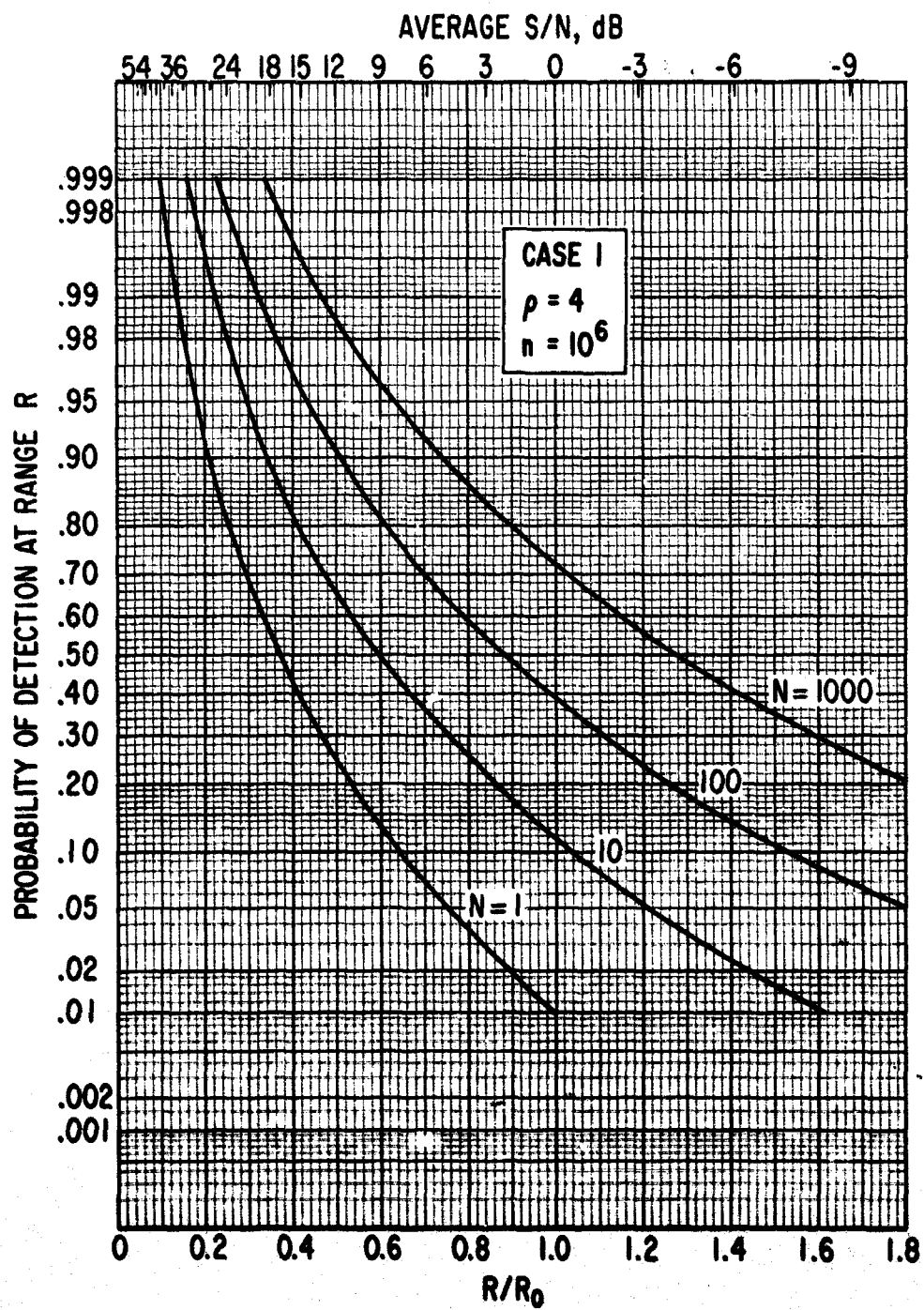
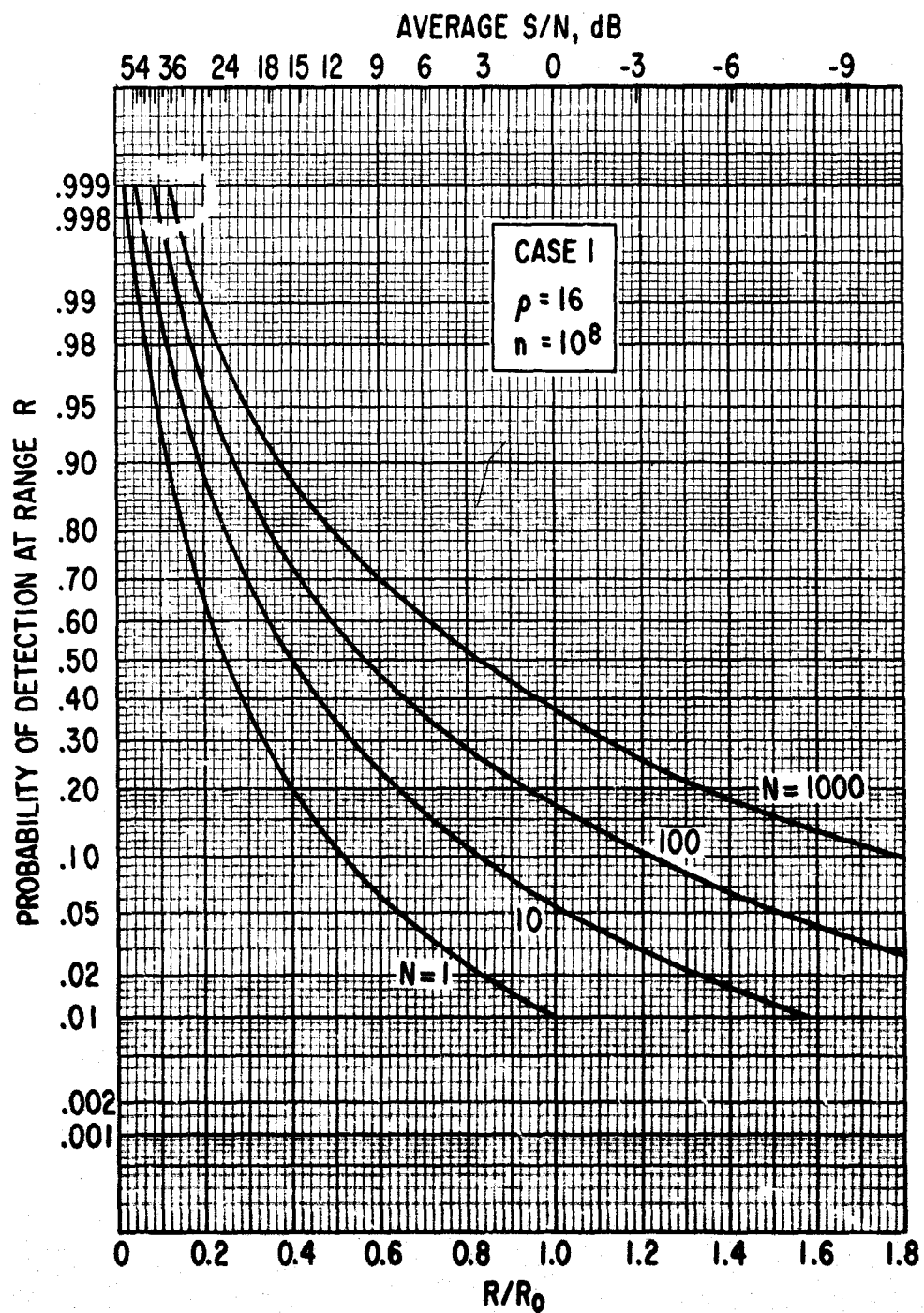Fig. 8. Case 1, $\rho = 4$, $n = 10^6$, with N as a Parameter
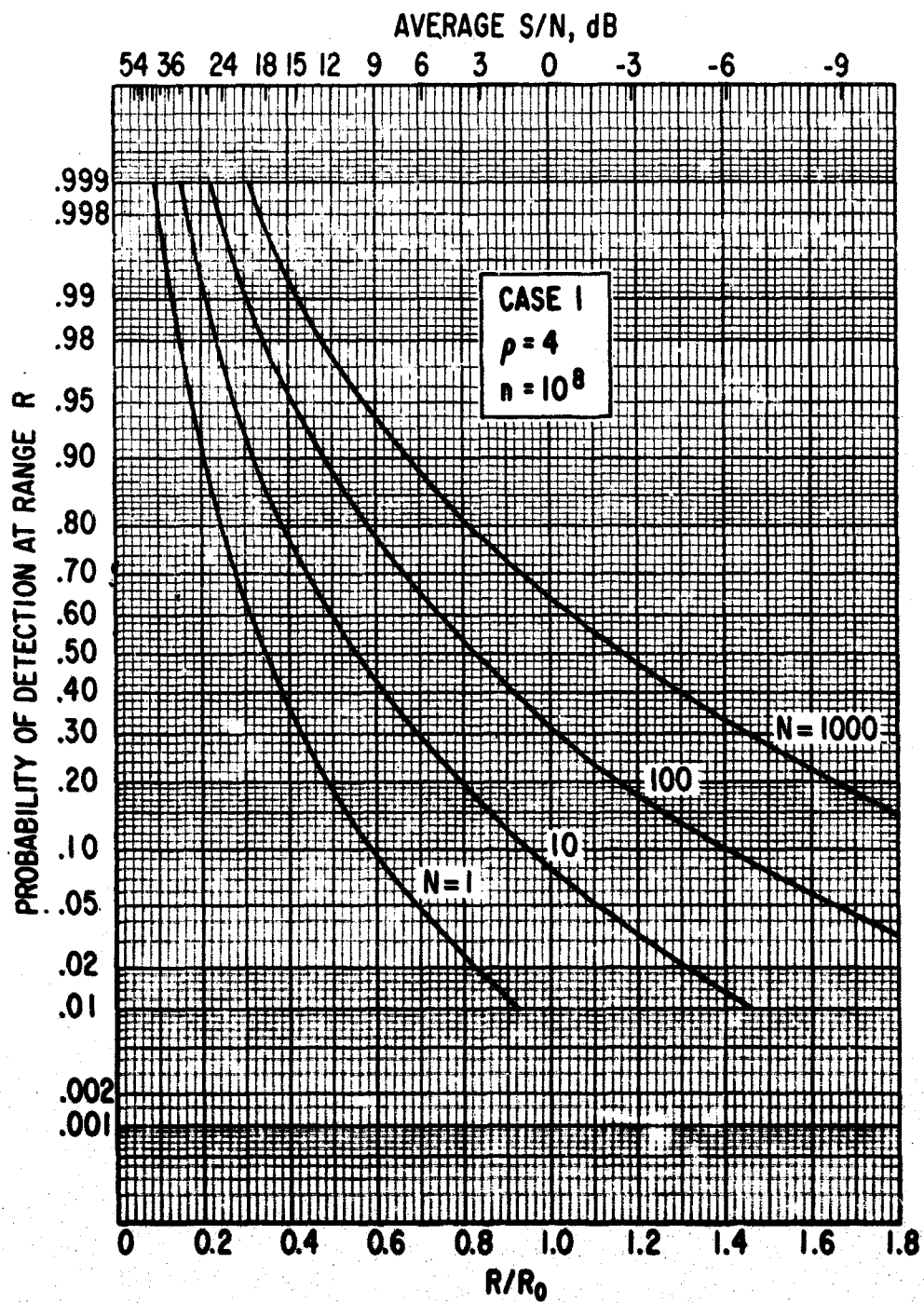
Fig. 9. Case 1, $\rho = 4$, $n = 10^8$, with N as a Parameter
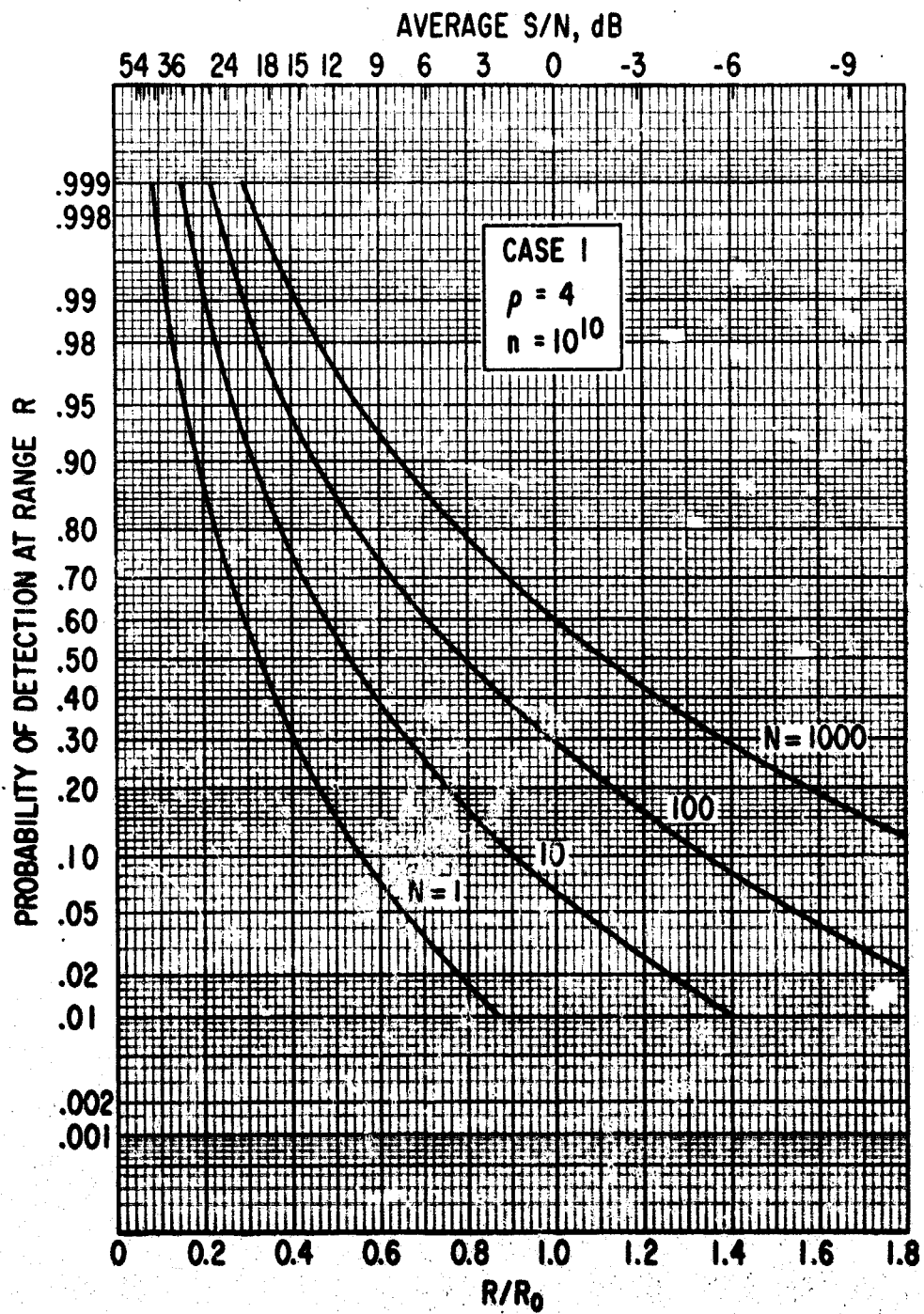
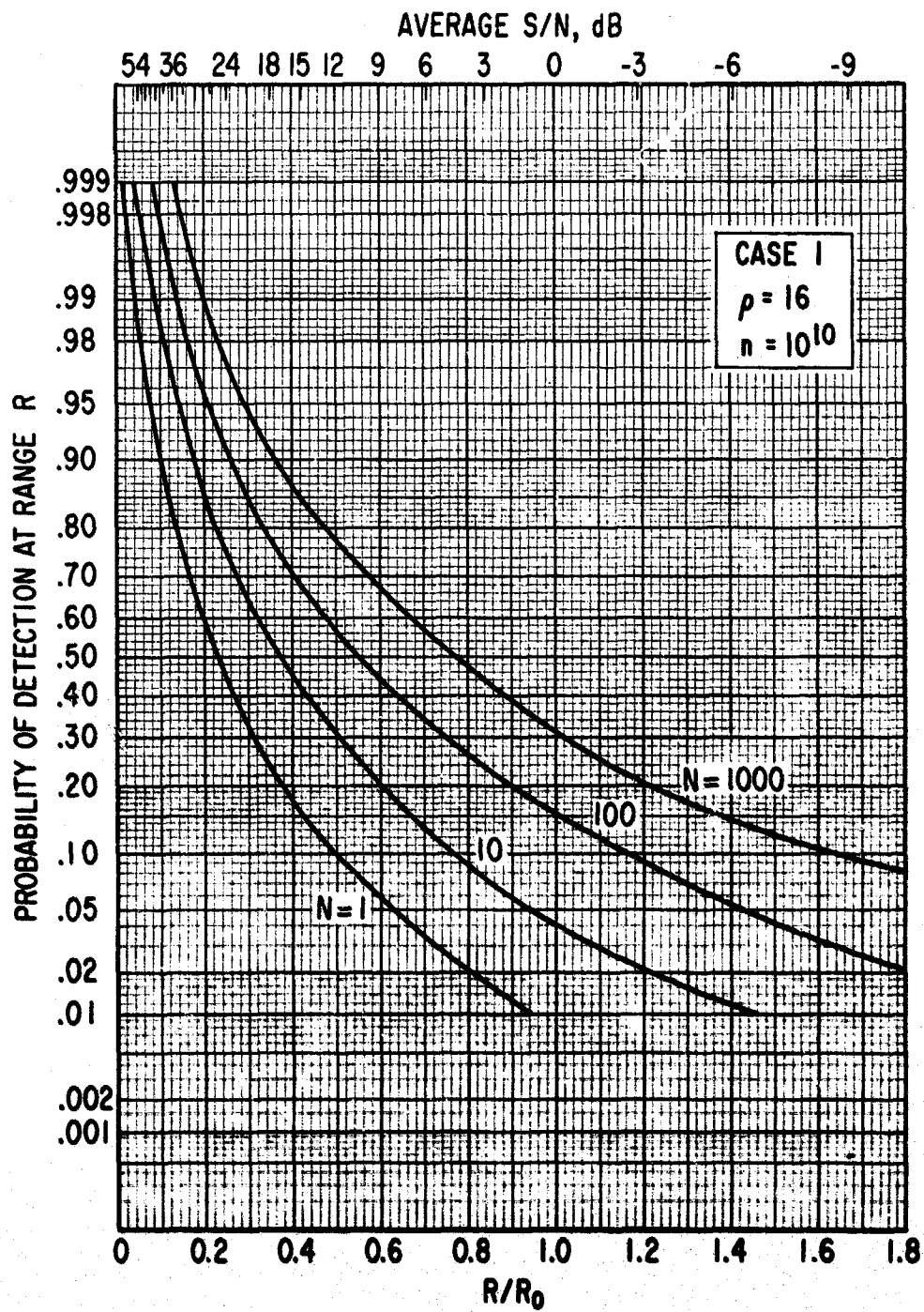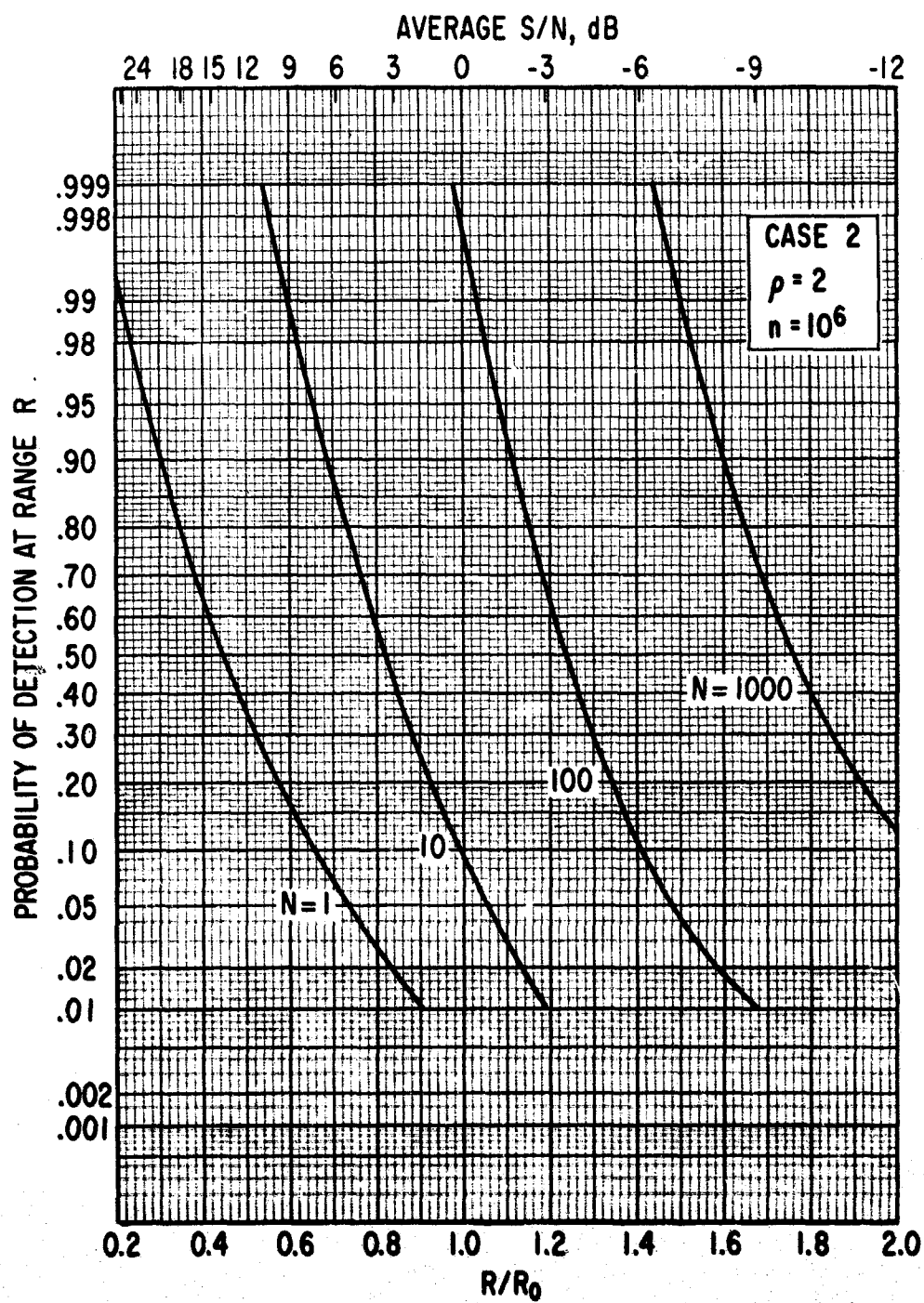Fig. 10. Case 1, $\rho = 4$, $n = 10^{10}$, with N as a Parameter

Fig. 11. Case 1, $\rho = 8$, $n = 10^6$, with N as a Parameter

Fig. 12. Case 1, $\rho = 8$, $n = 10^8$, with N as a Parameter

Fig. 13. Case 1, $\rho = 8$, $n = 10^{10}$, with N as a Parameter

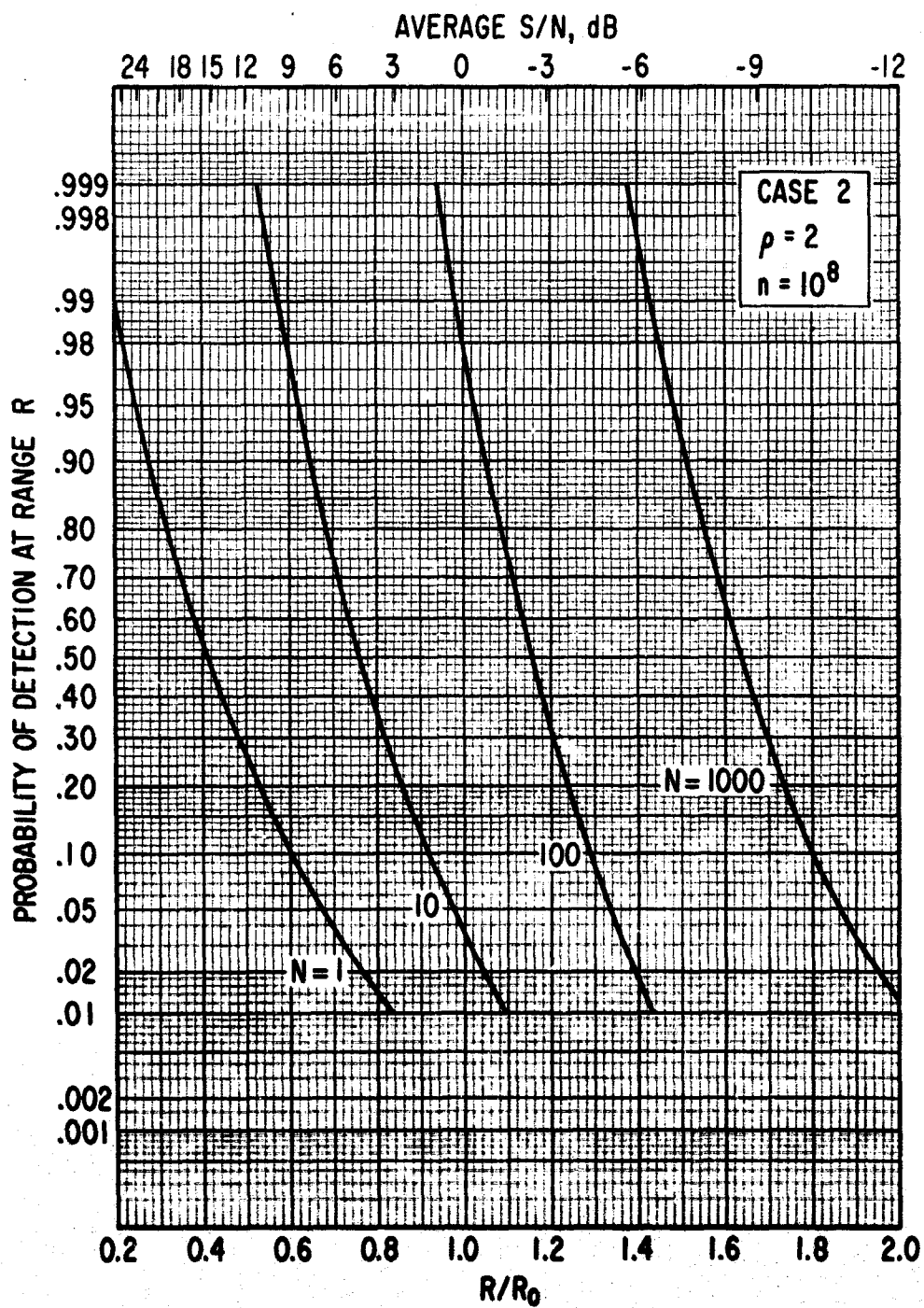Fig. 14. Case 1, $\rho = 16$, $n = 10^6$, with N as a Parameter

Fig. 15. Case 1, $\rho = 16$, $n = 10^8$, with N as a Parameter

Fig. 16. Case 1, $\rho = 16$, $n = 10^{10}$, with N as a Parameter

Fig. 17. Case 2, ρ = 2, n = 10^6, with N as a Parameter

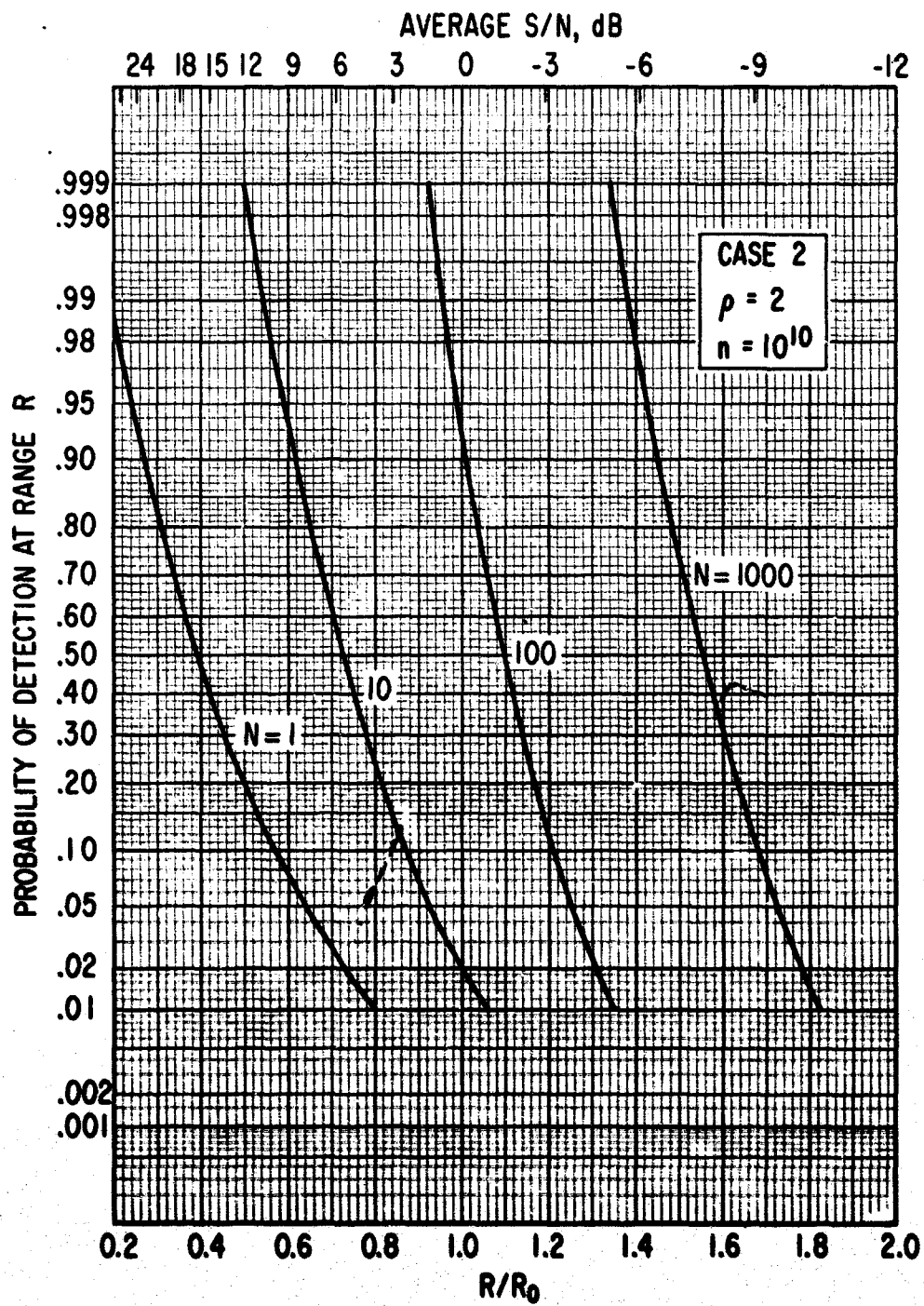Fig. 18. Case 2, $\rho = 2$, $n = 10^8$, with N as a Parameter

Fig. 19. Case 2, $\rho = 2$, $n = 10^{10}$, with N as a Parameter
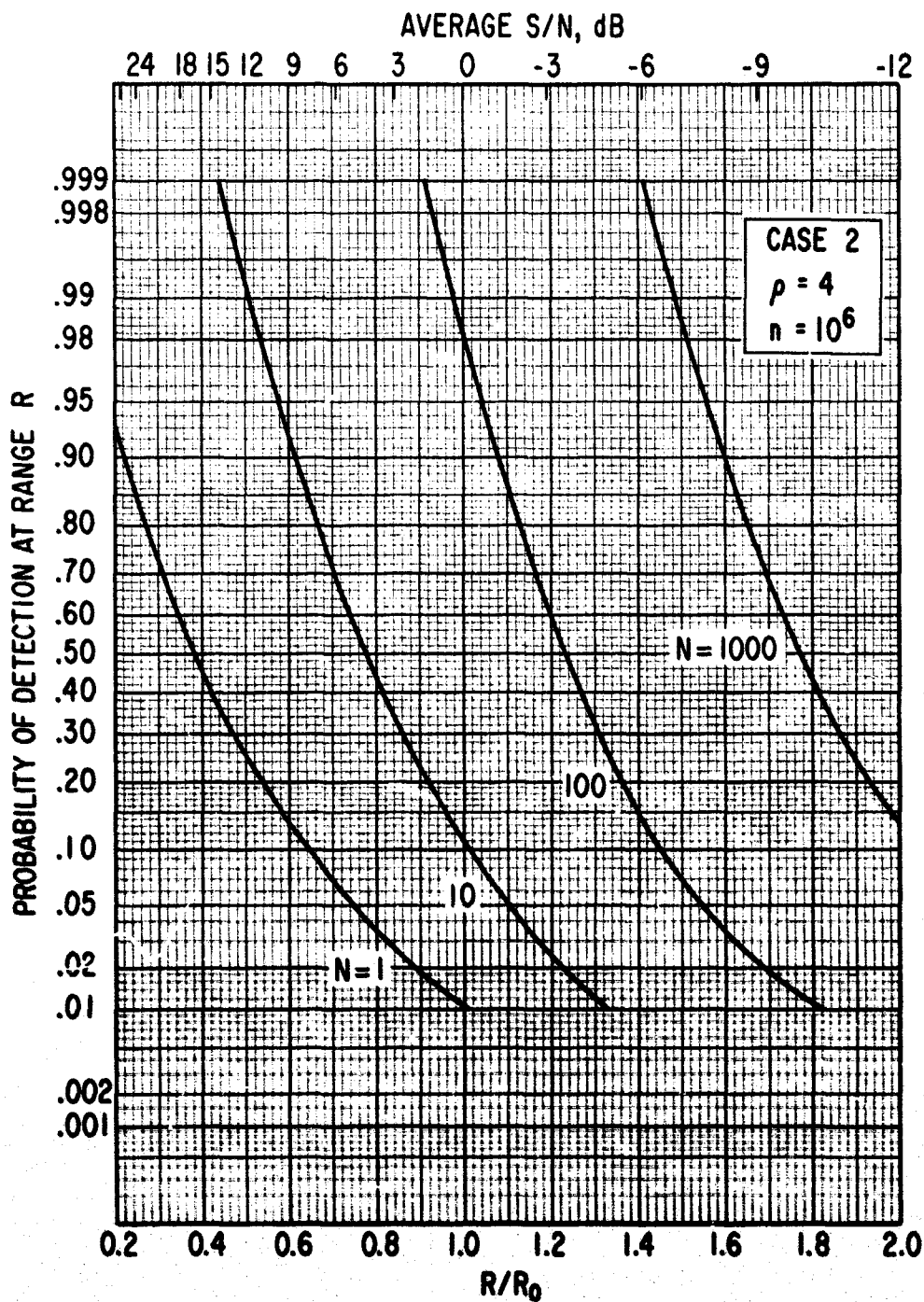
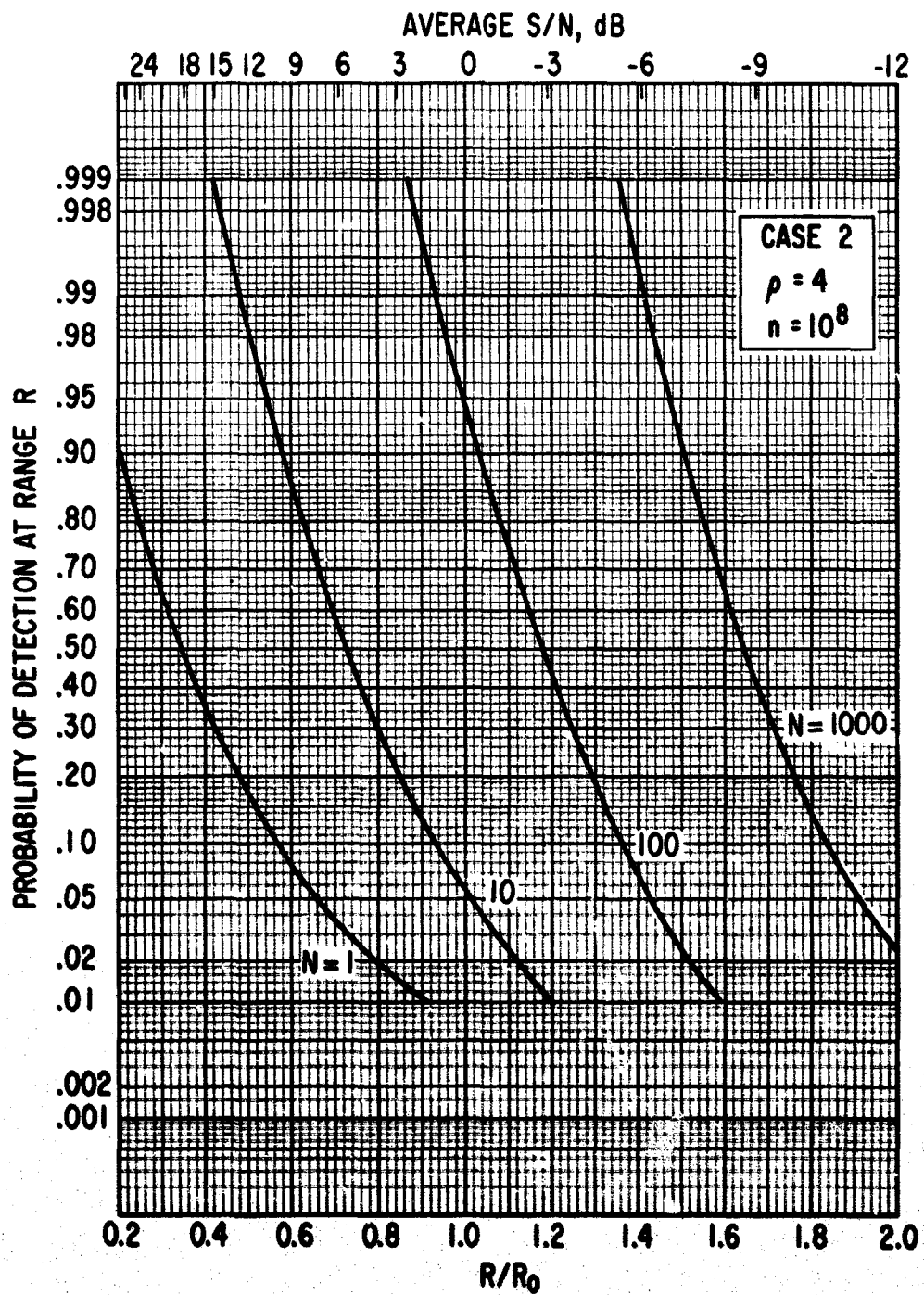Fig. 20. Case 2, $\rho = 4$, $n = 10^6$, with N as a Parameter

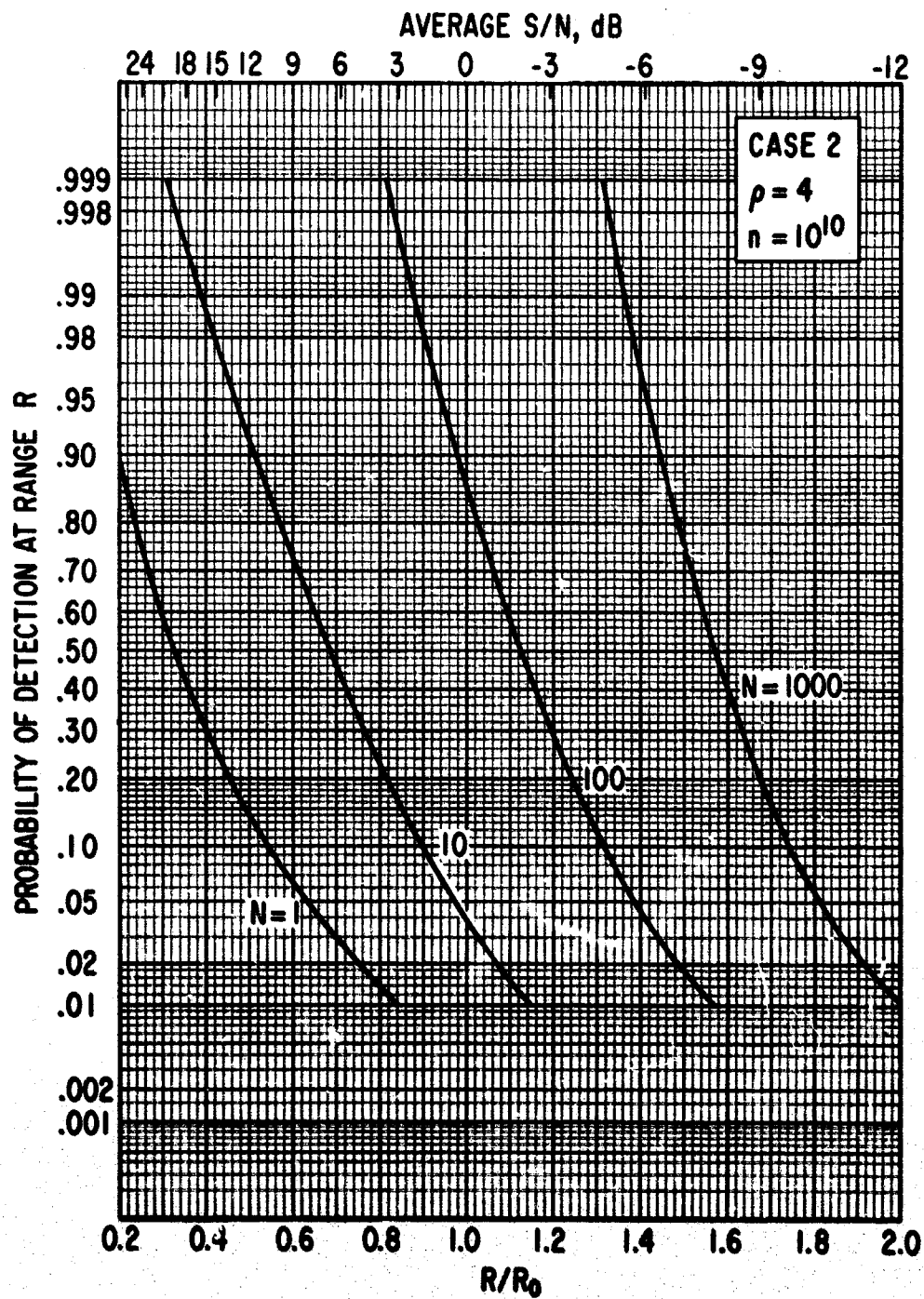Fig. 21. Case 2, $\rho = 4$, $n = 10^9$, with N as a Parameter

Fig. 22. Case 2, $\rho = 4$, $n = 10^{10}$, with N as a Parameter

Fig. 23. Case 2, $\rho = 8$, $n = 10^6$, with N as a Parameter

Fig. 21. Case 2, ρ = 8, n = 10^8, with N as a Parameter

Fig. 25. Case 2, $\rho = 8$, $n = 10^{10}$, with N as a Parameter

Fig. 26. Case 2, $\rho = 16$, $n = 10^6$, with N as a Parameter

Fig. 27. Case 2, $\rho = 16$, $n = 10^8$, with N as a Parameter

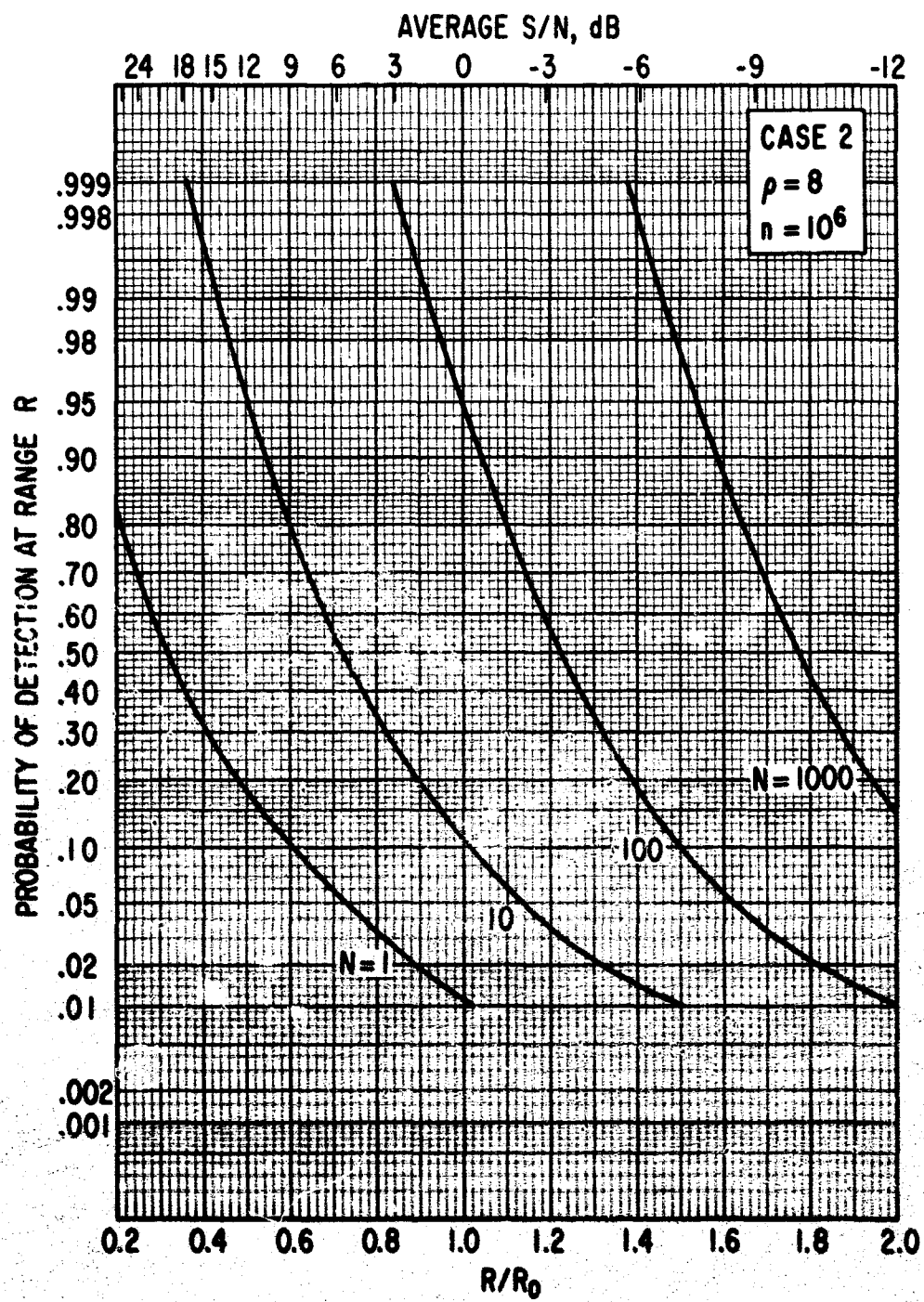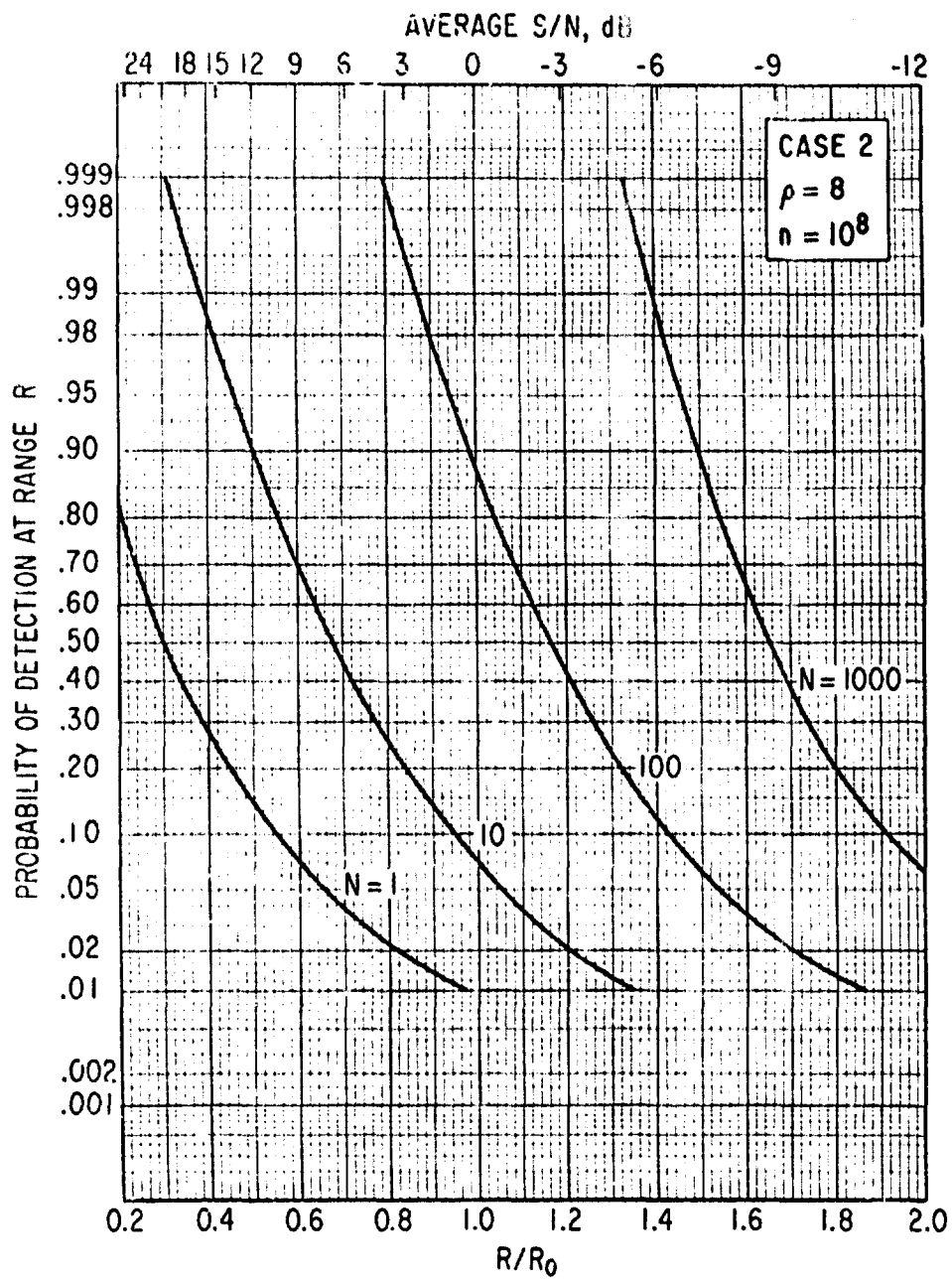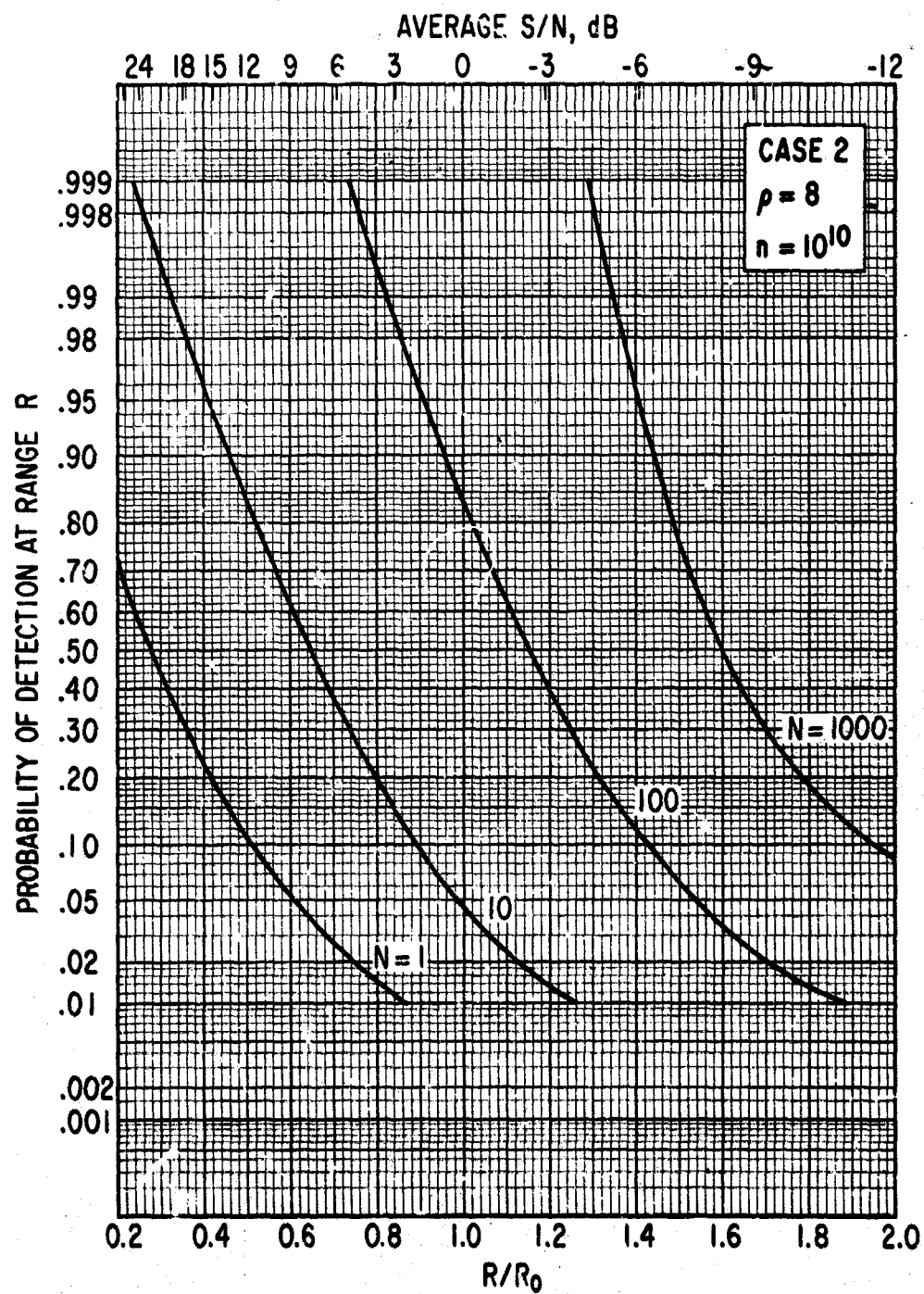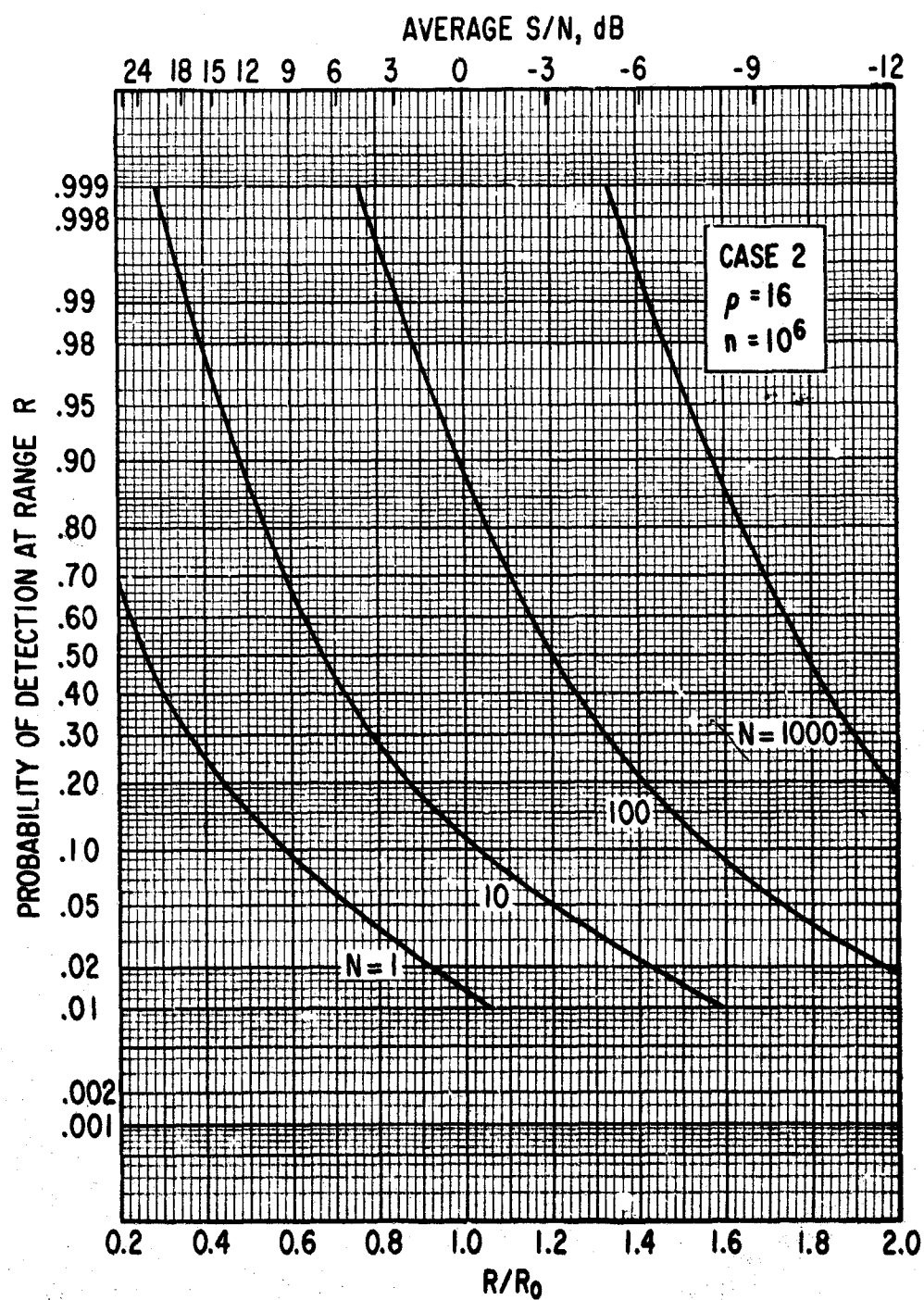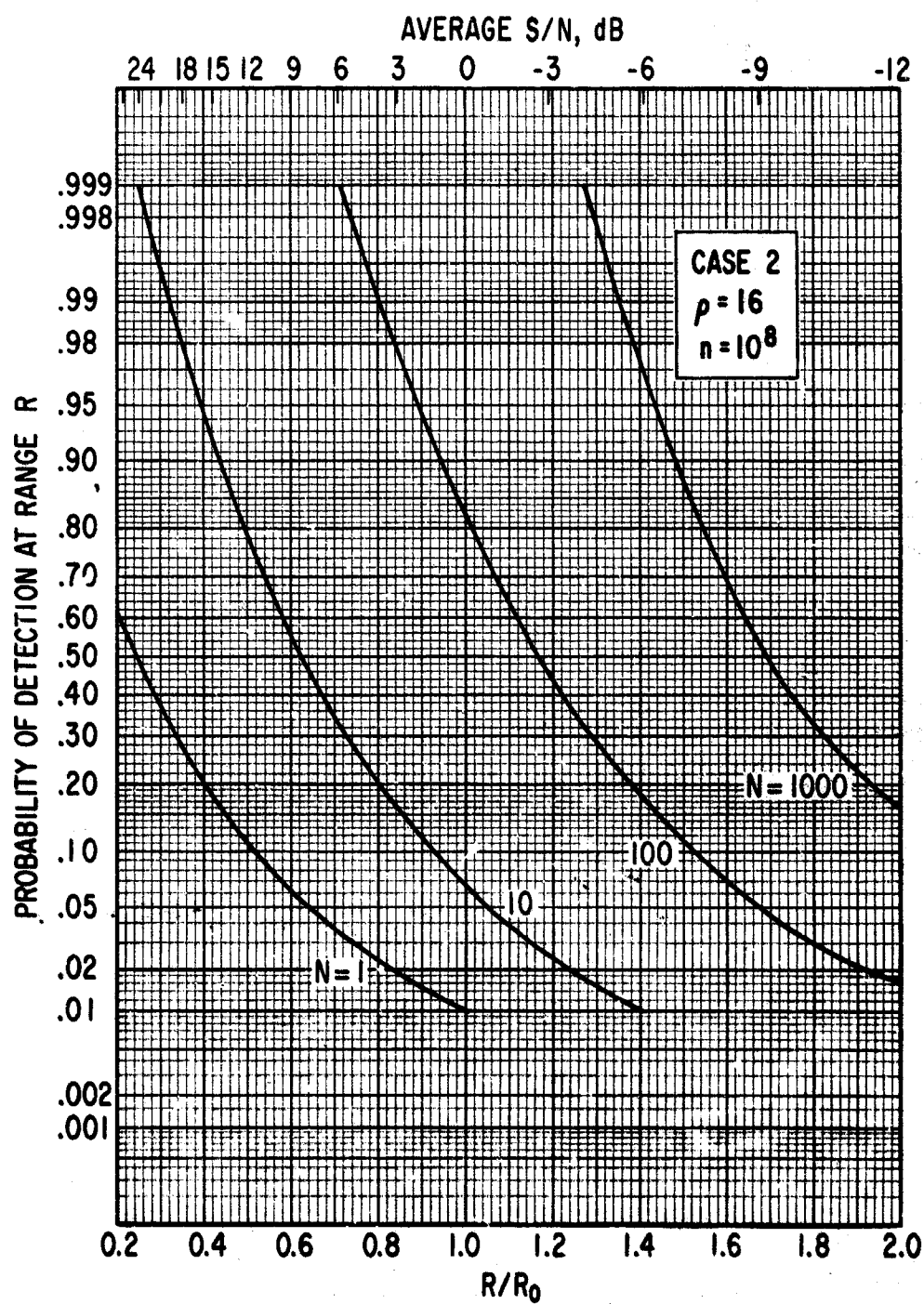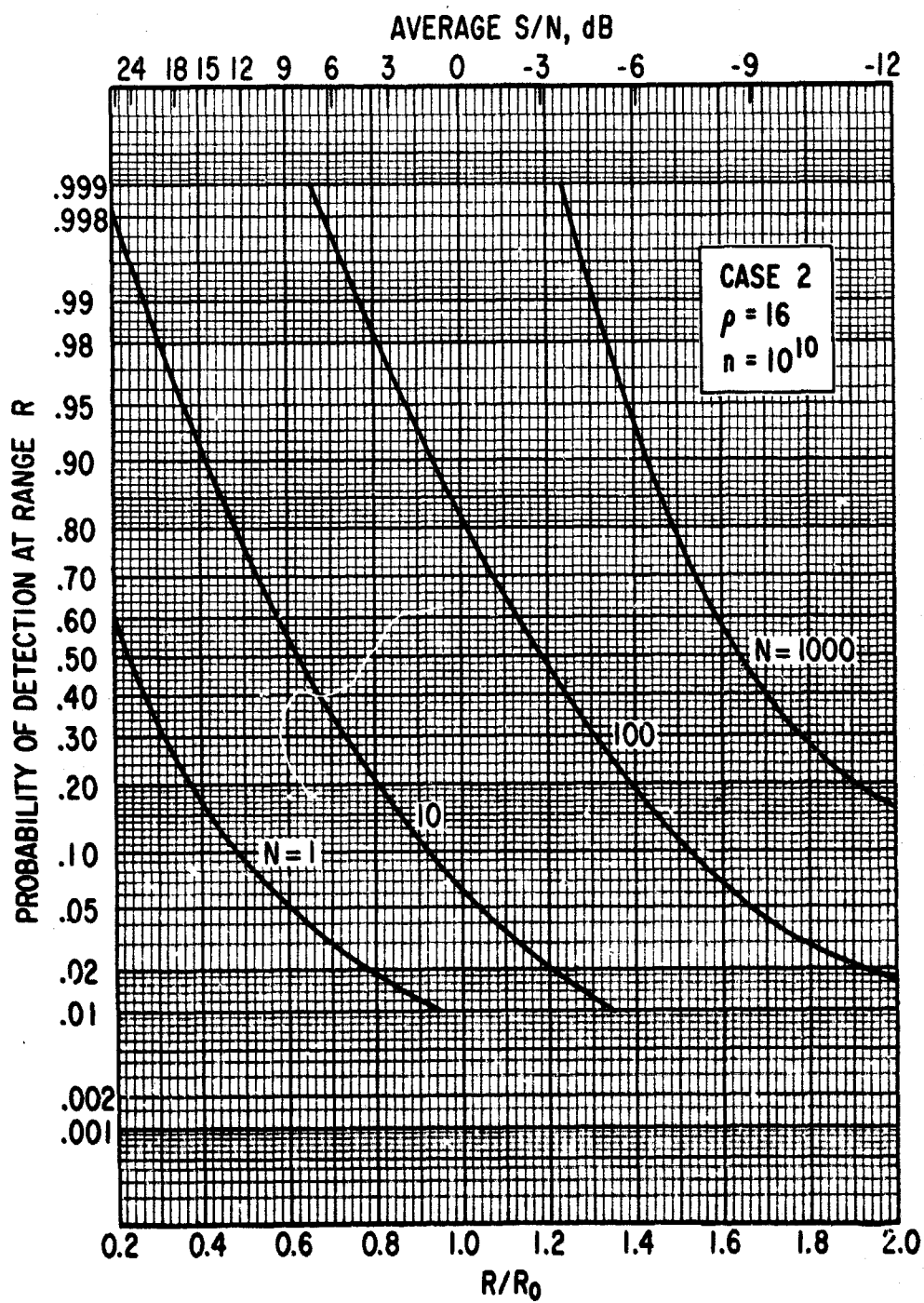Fig. 28. Case 2, $\rho = 16$, $n = 10^{10}$, with N as a Parameter

Fig. 29.   Cases 1 and 2, $n = 10^6$, $N = 1$, with
ρ as a Parameter

-43-
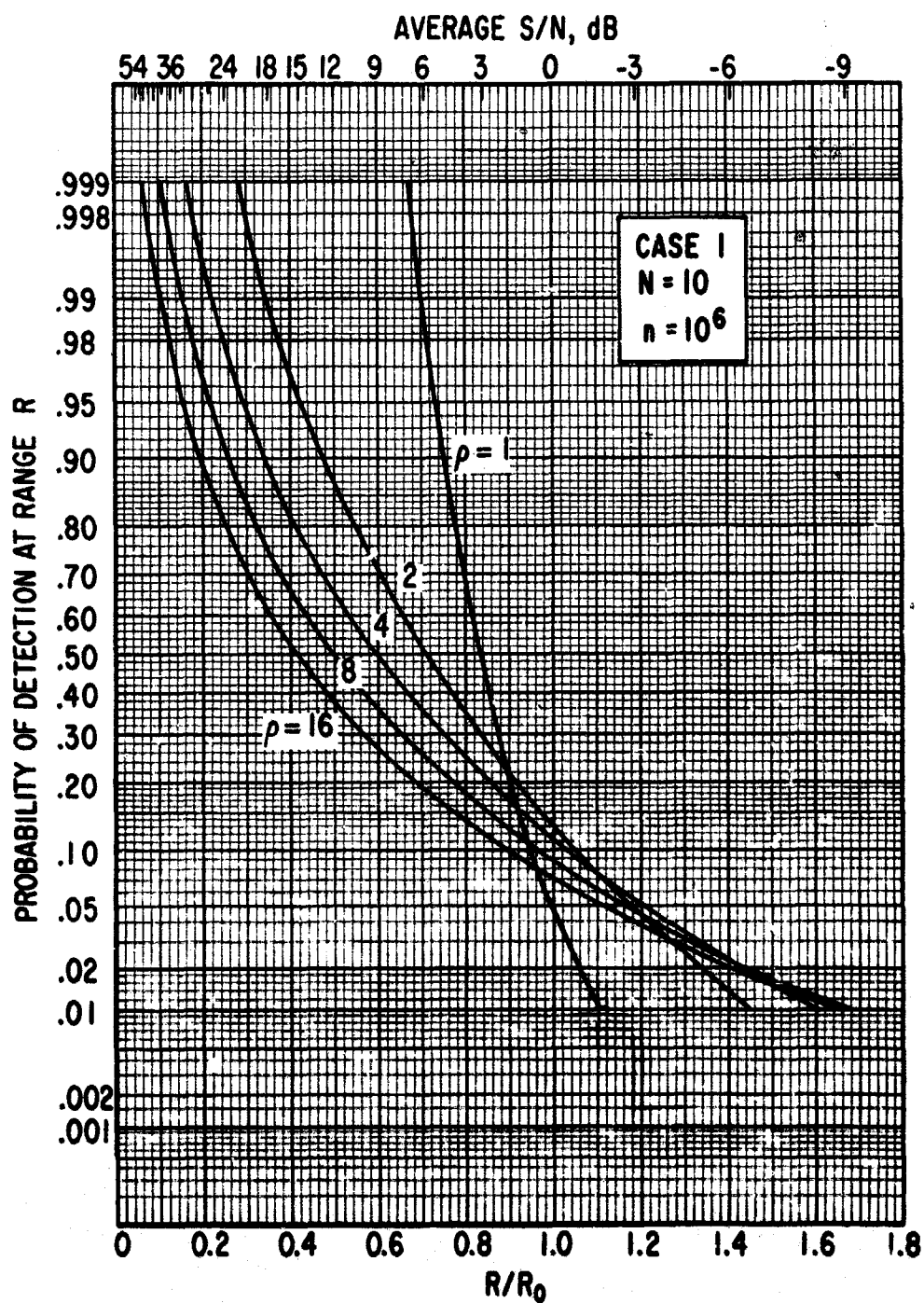
Fig. 30. Case 1, $n = 10^6$, $N = 10$, with ρ as a Parameter
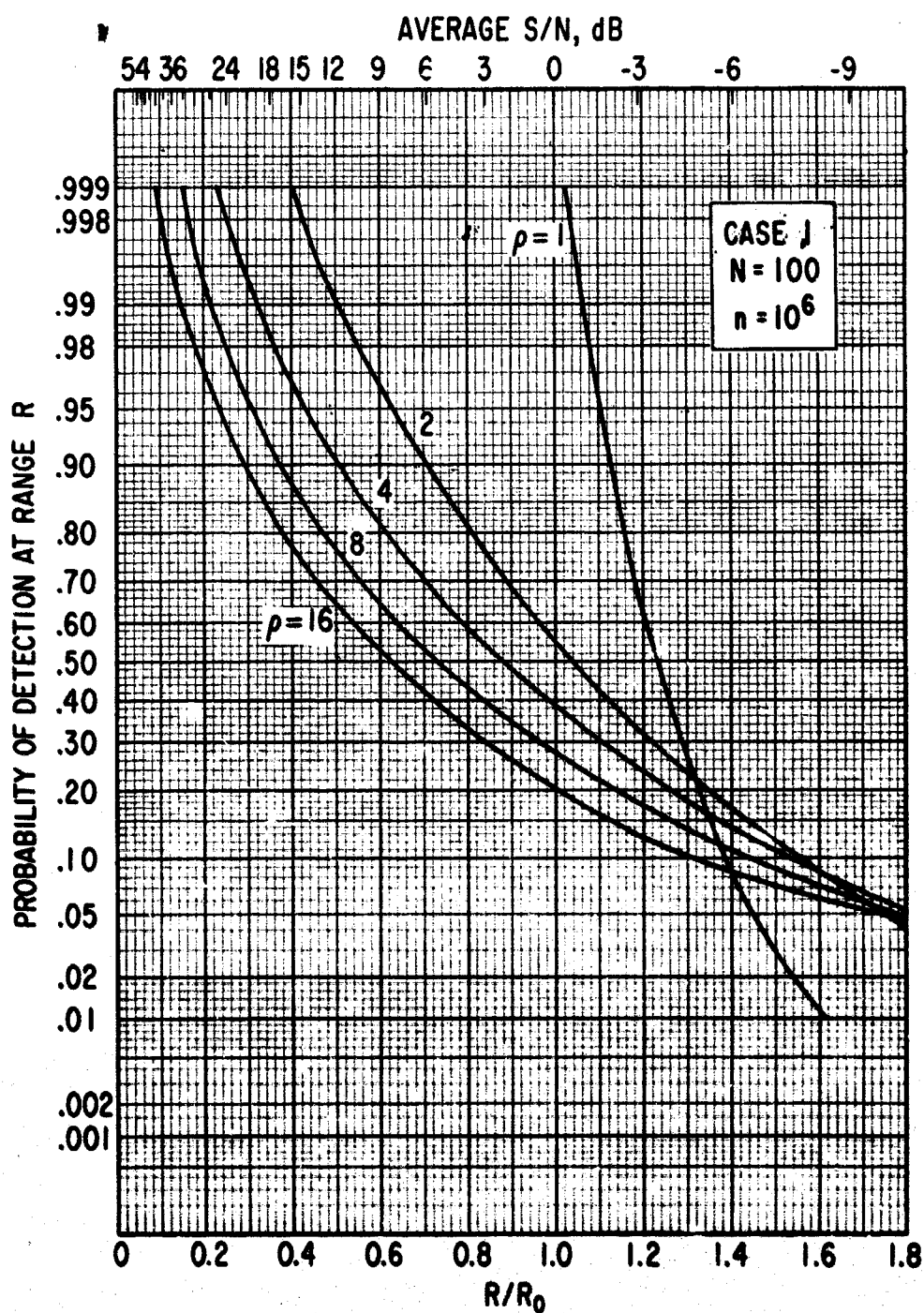
Fig. 31. Case 1, $n = 10^6$, $N = 100$, with ρ as a Parameter
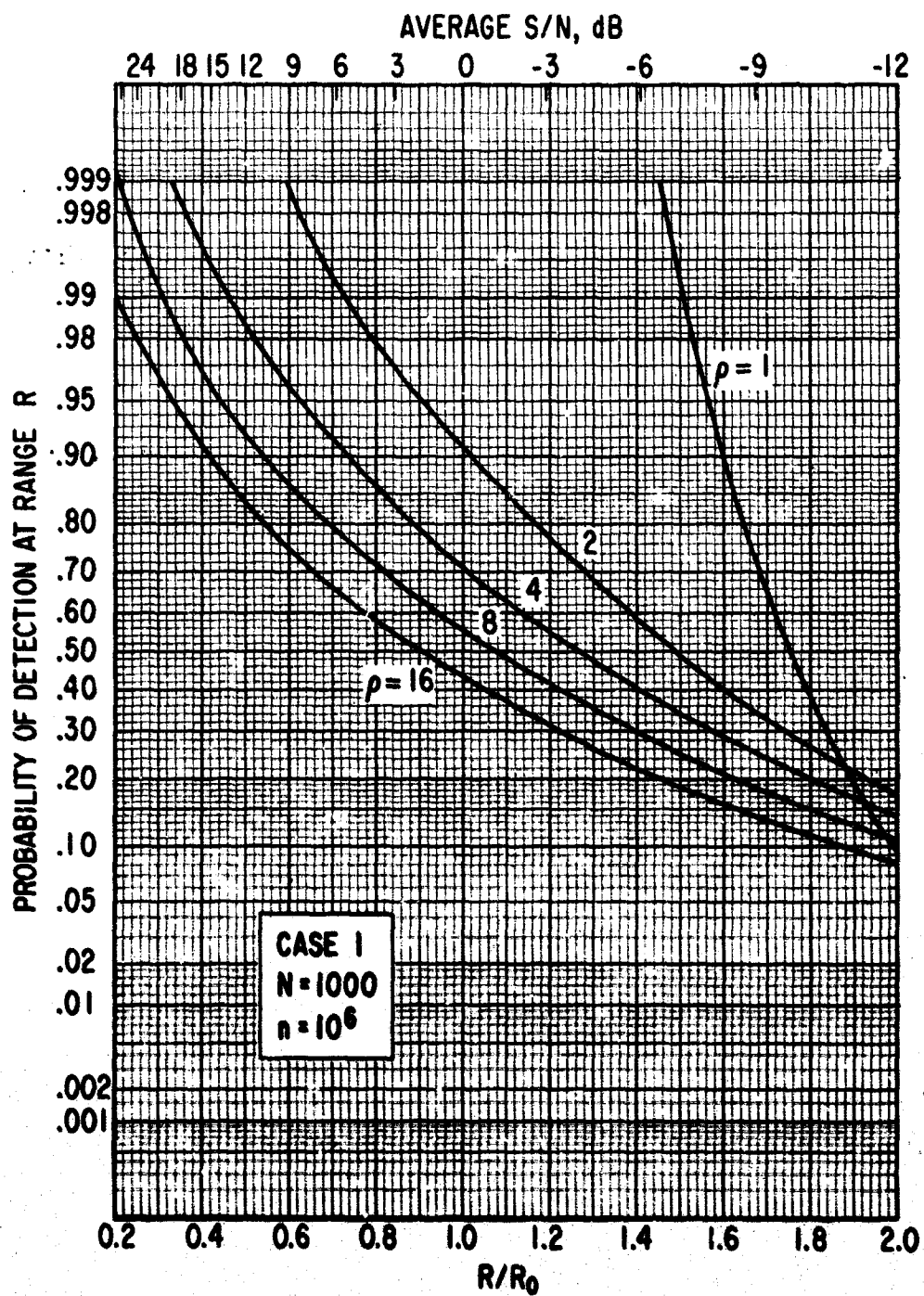
Fig. 32. Case 1, $n = 10^6$, $N = 1000$, with ρ as a Parameter
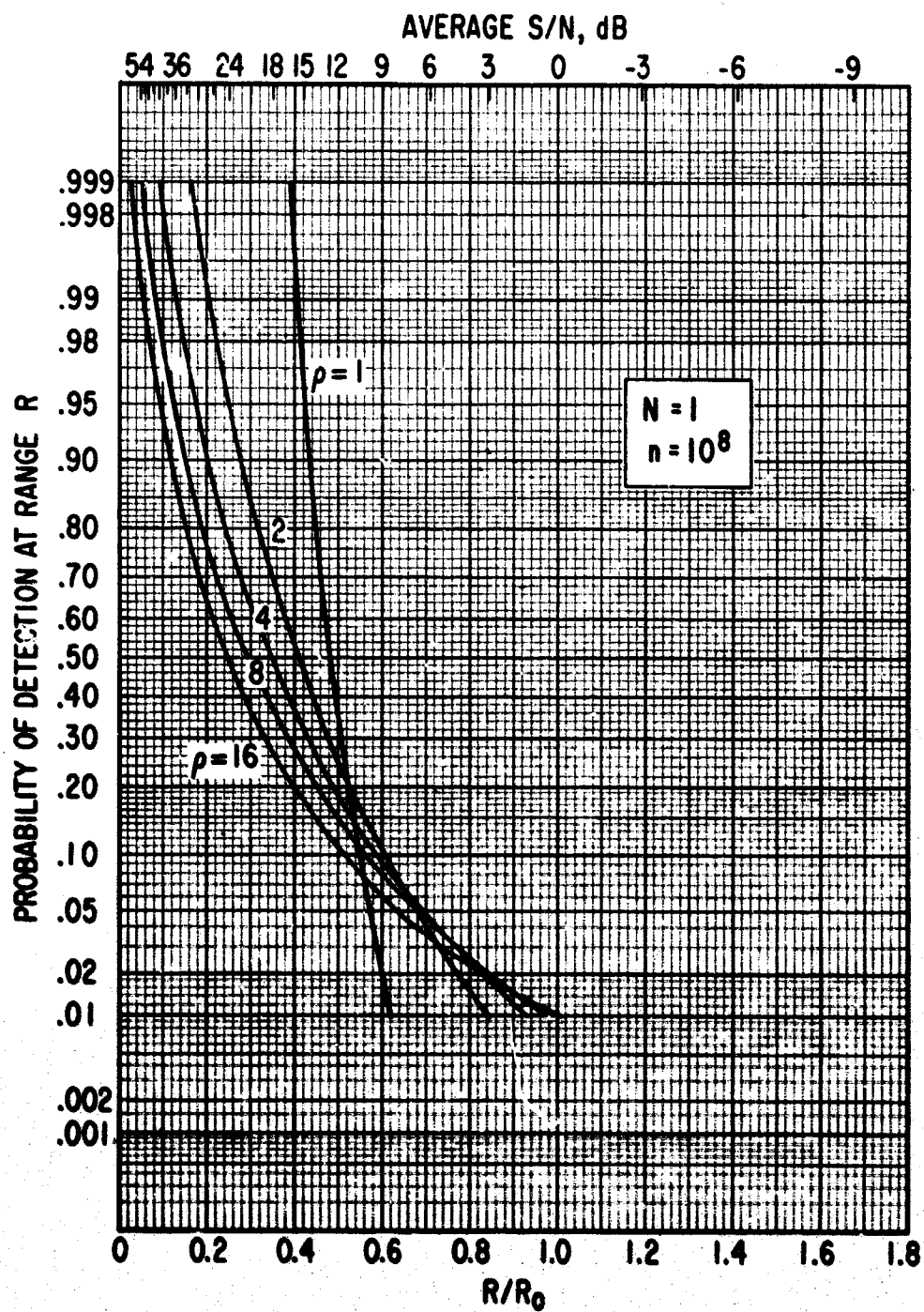
Fig. 33. Cases 1 and 2, $n = 10^8$, $N = 1$, with ρ as a Parameter
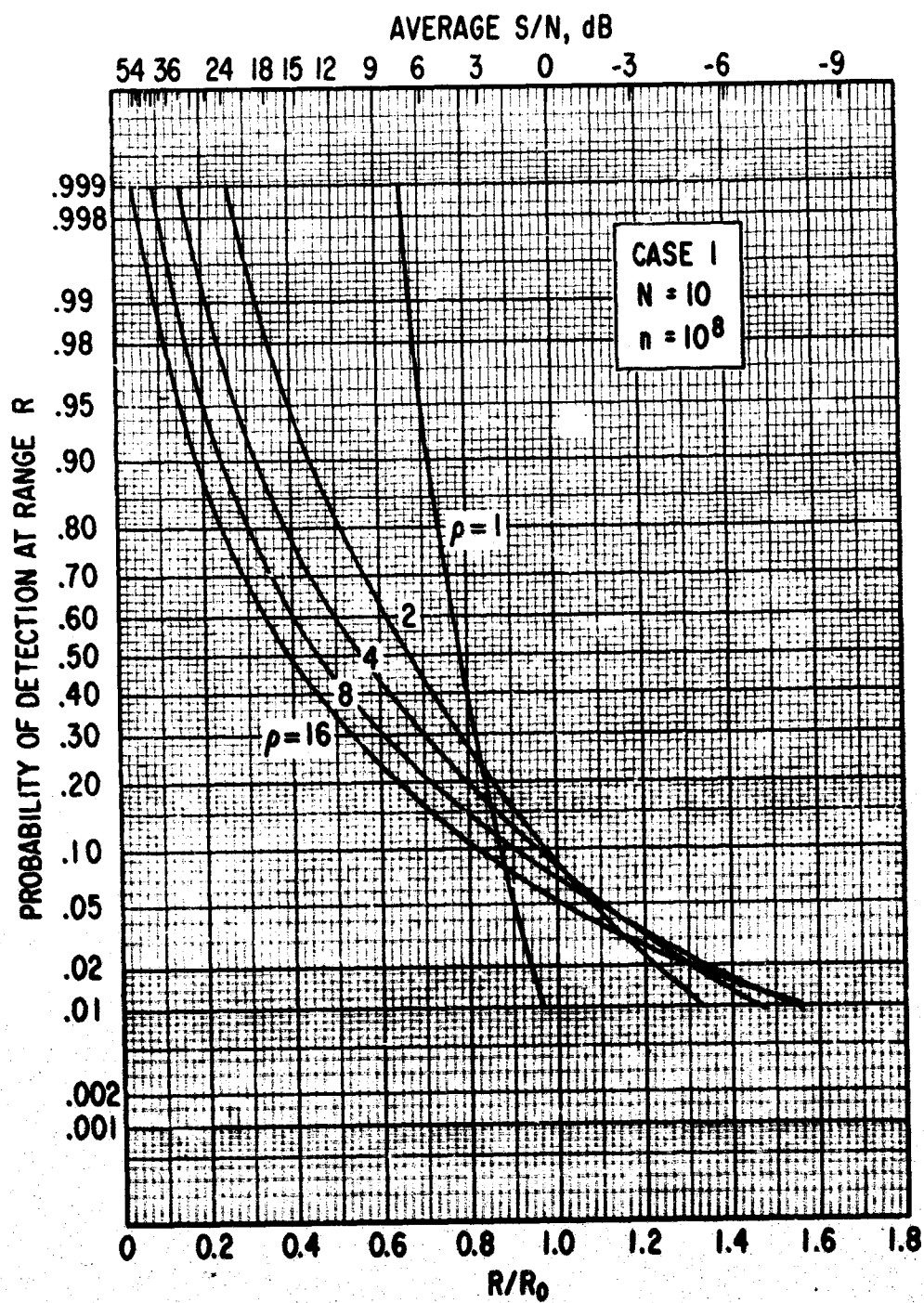
Fig. 34. Case 1, n = 10^8, N = 10, with ρ as a Parameter
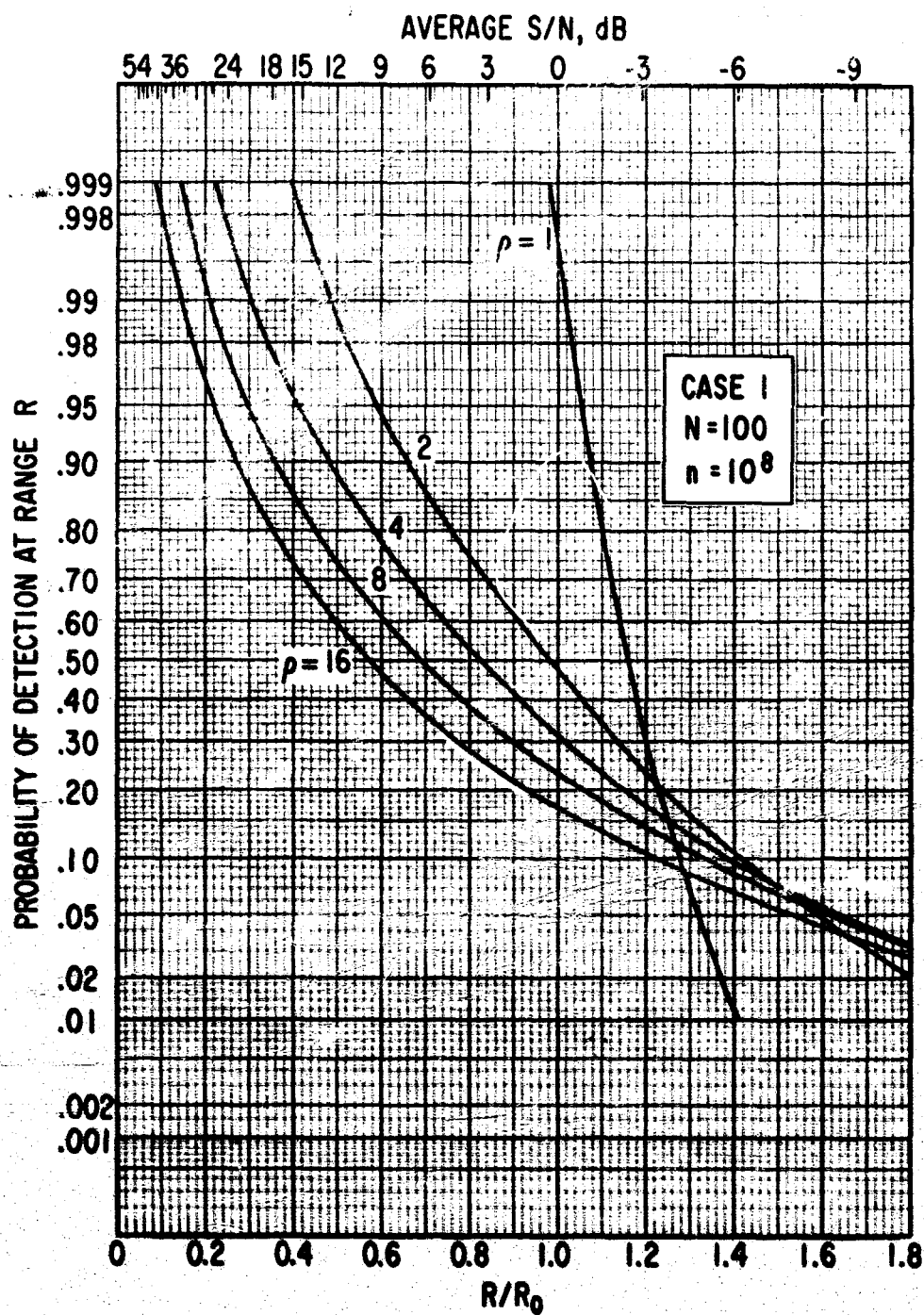
Fig. 35. Case 1, $n = 10^8$, $N = 100$, with ρ as a Parameter
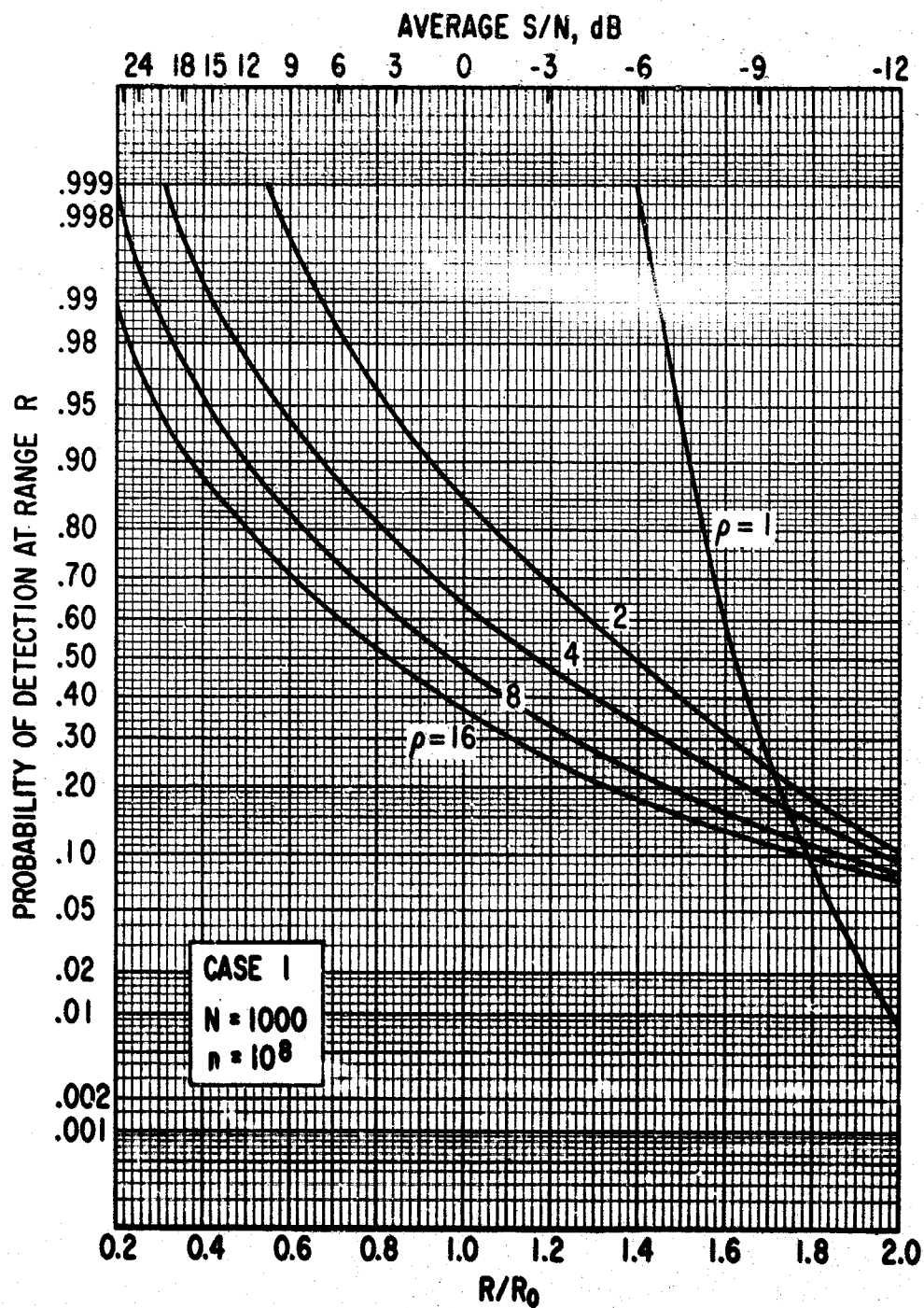
Fig. 36. Case 1, $n = 10^8$, $N = 1000$, with ρ as a Parameter
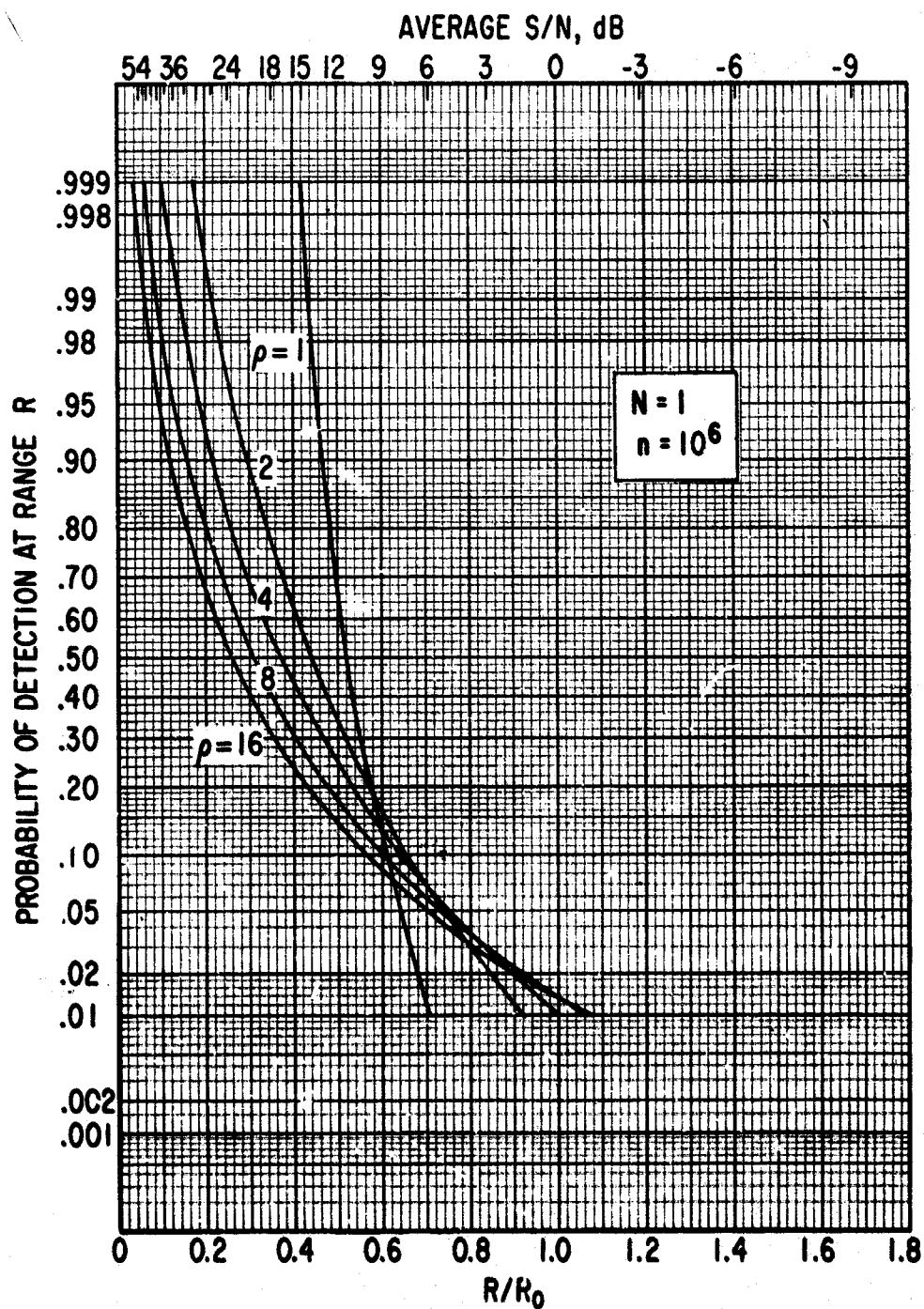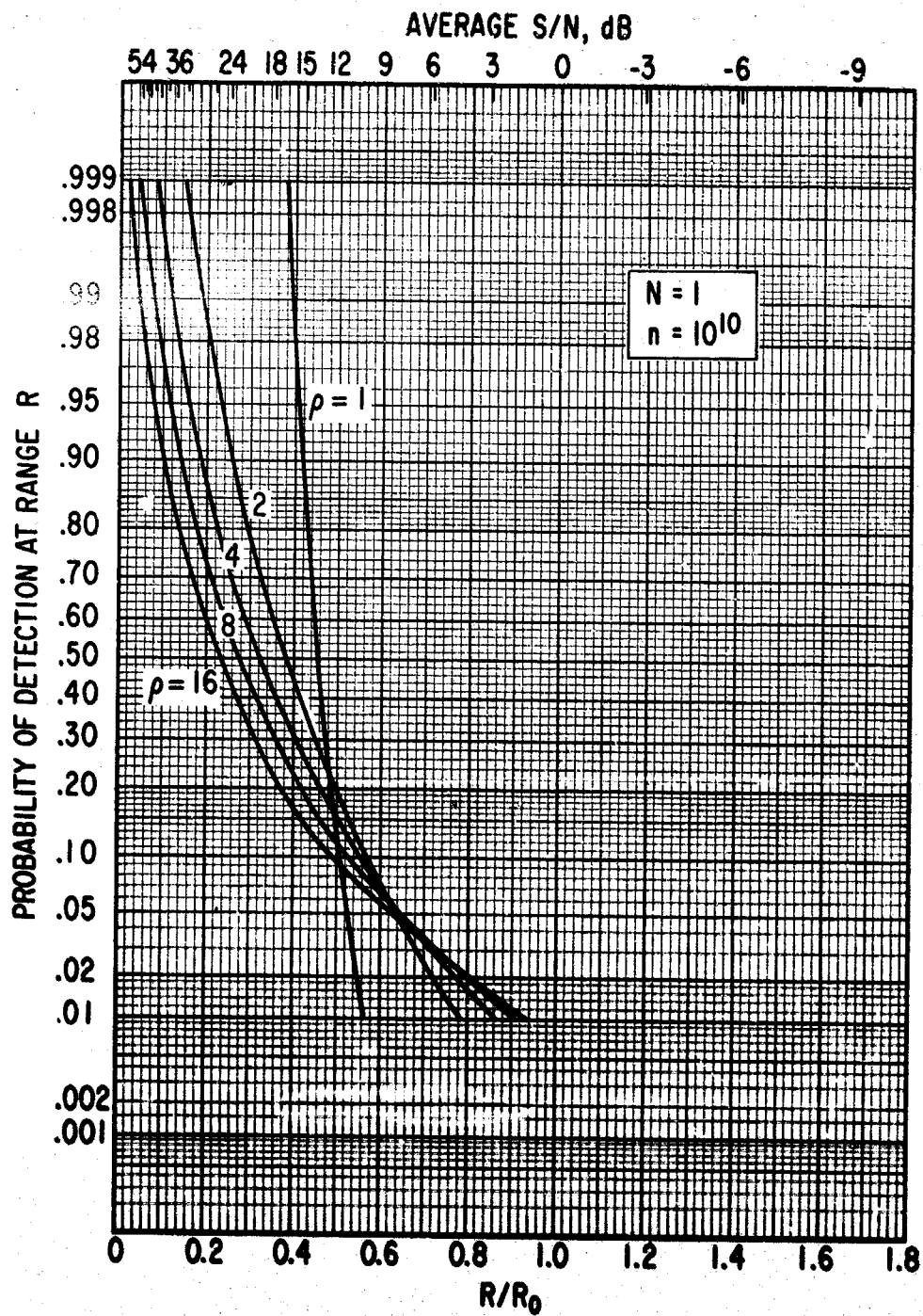
Fig. 37. Cases 1 and 2, $n = 10^{10}$, $N = 1$, with ρ as a Parameter
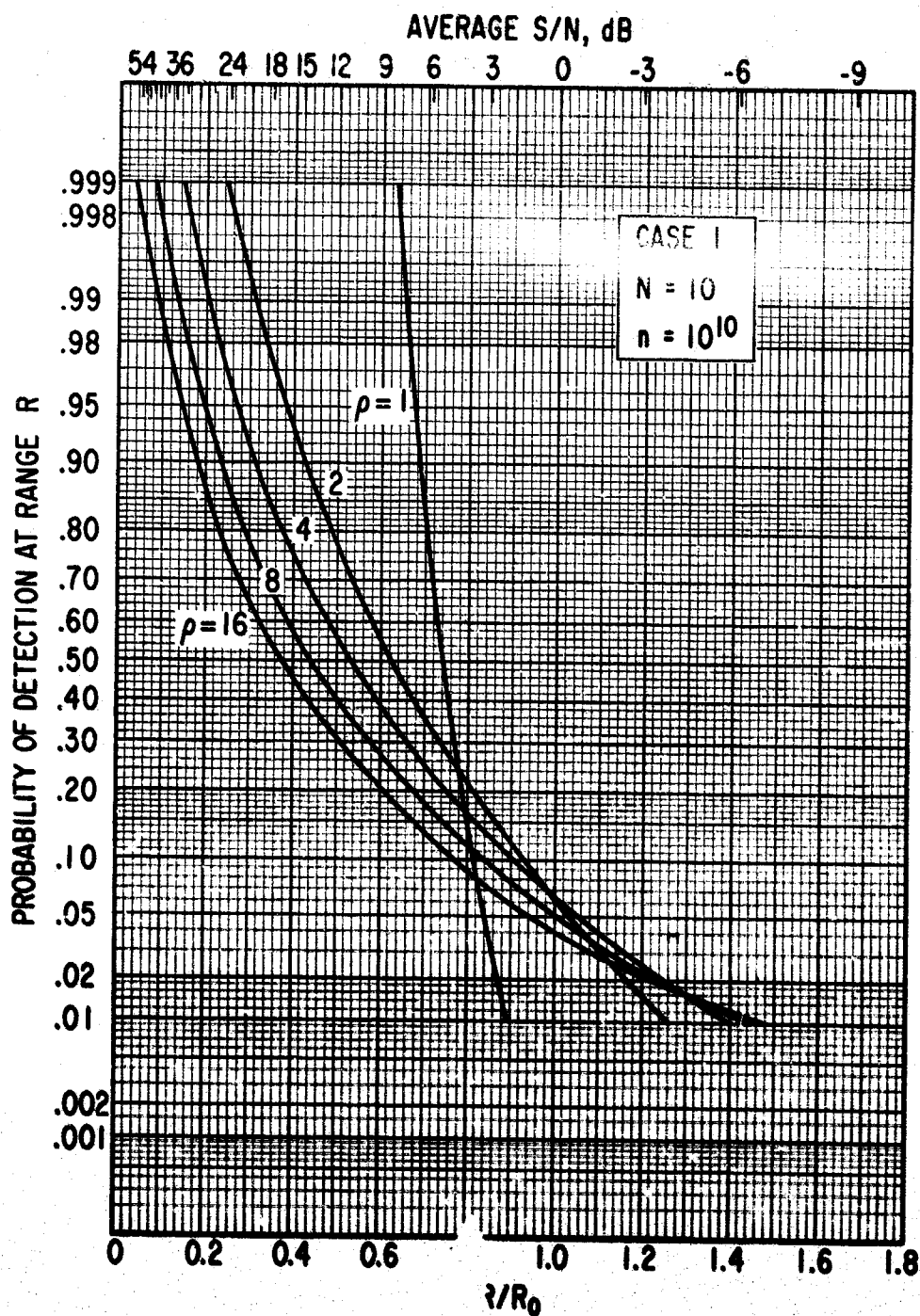
Fig. 38. Case 1, $n = 10^{10}$, $N = 10$, with ρ as a Parameter
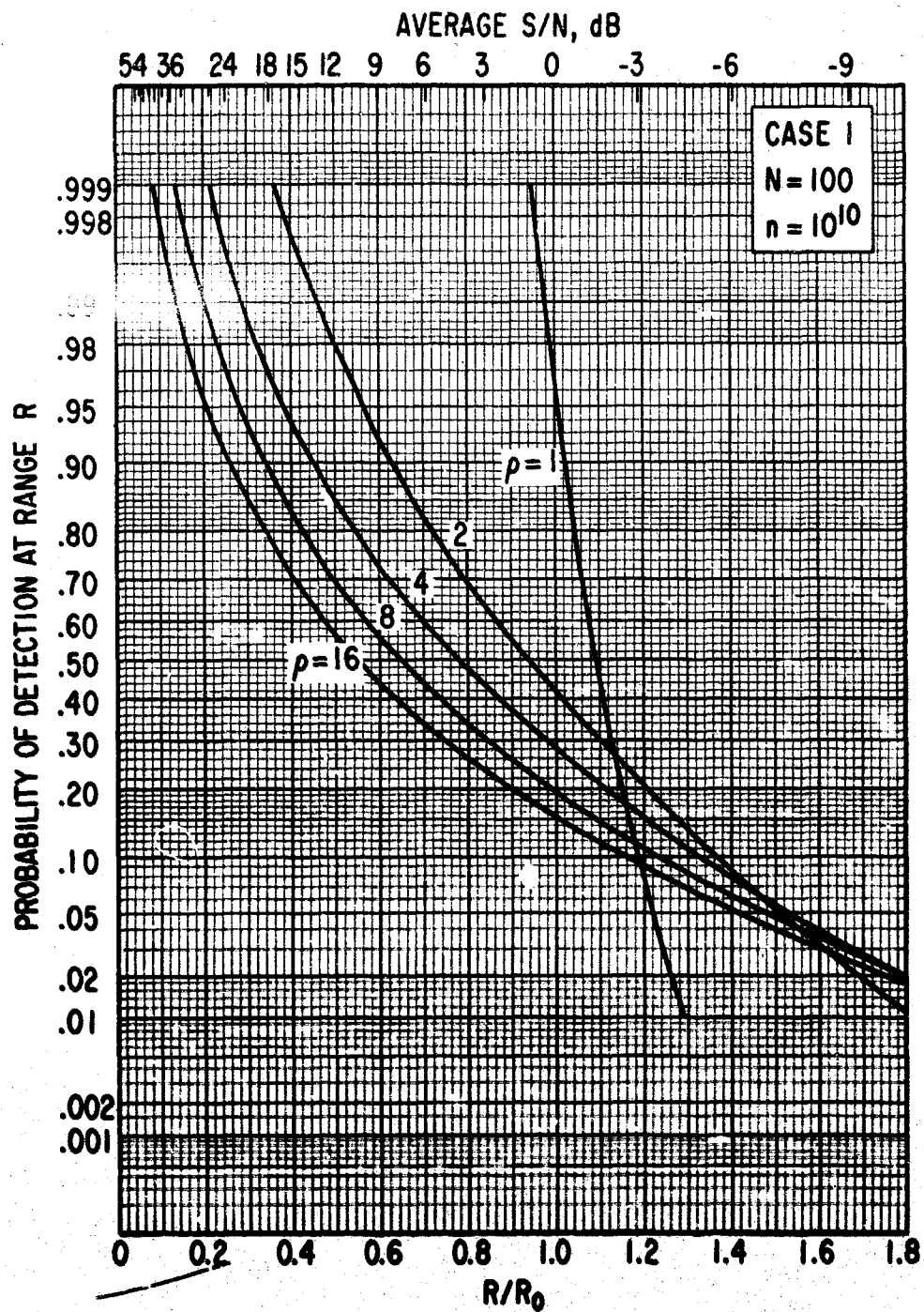
Fig. 39. Case 1, $n = 10^{10}$, $N = 100$, with ρ as a Parameter
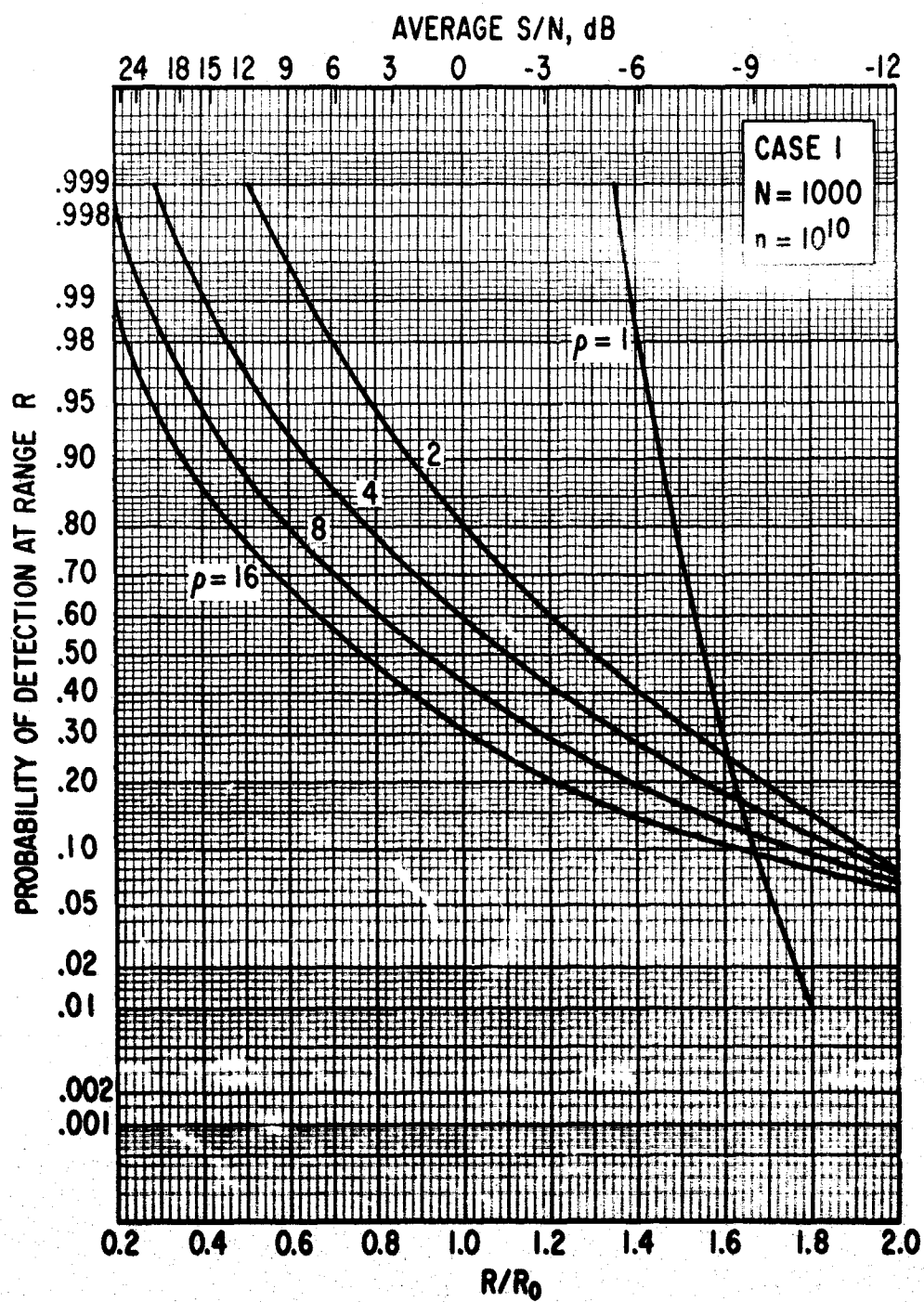
Fig. 40. Case 1, $n = 10^{10}$, $N = 1000$, with ρ as a Parameter

-54-
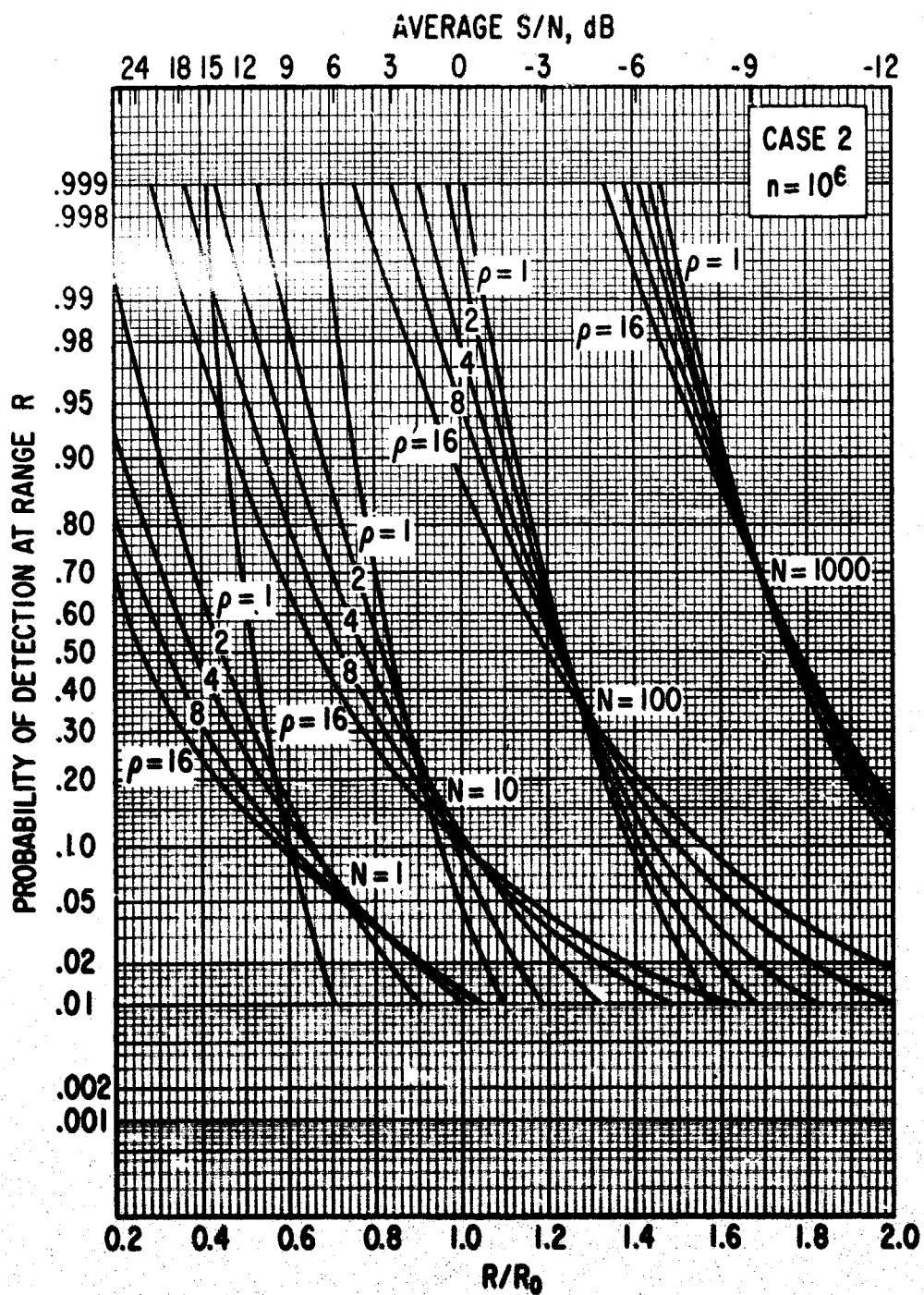
Fig. 41.   Case 2, $n = 10^6$, with ρ and N as Parameters
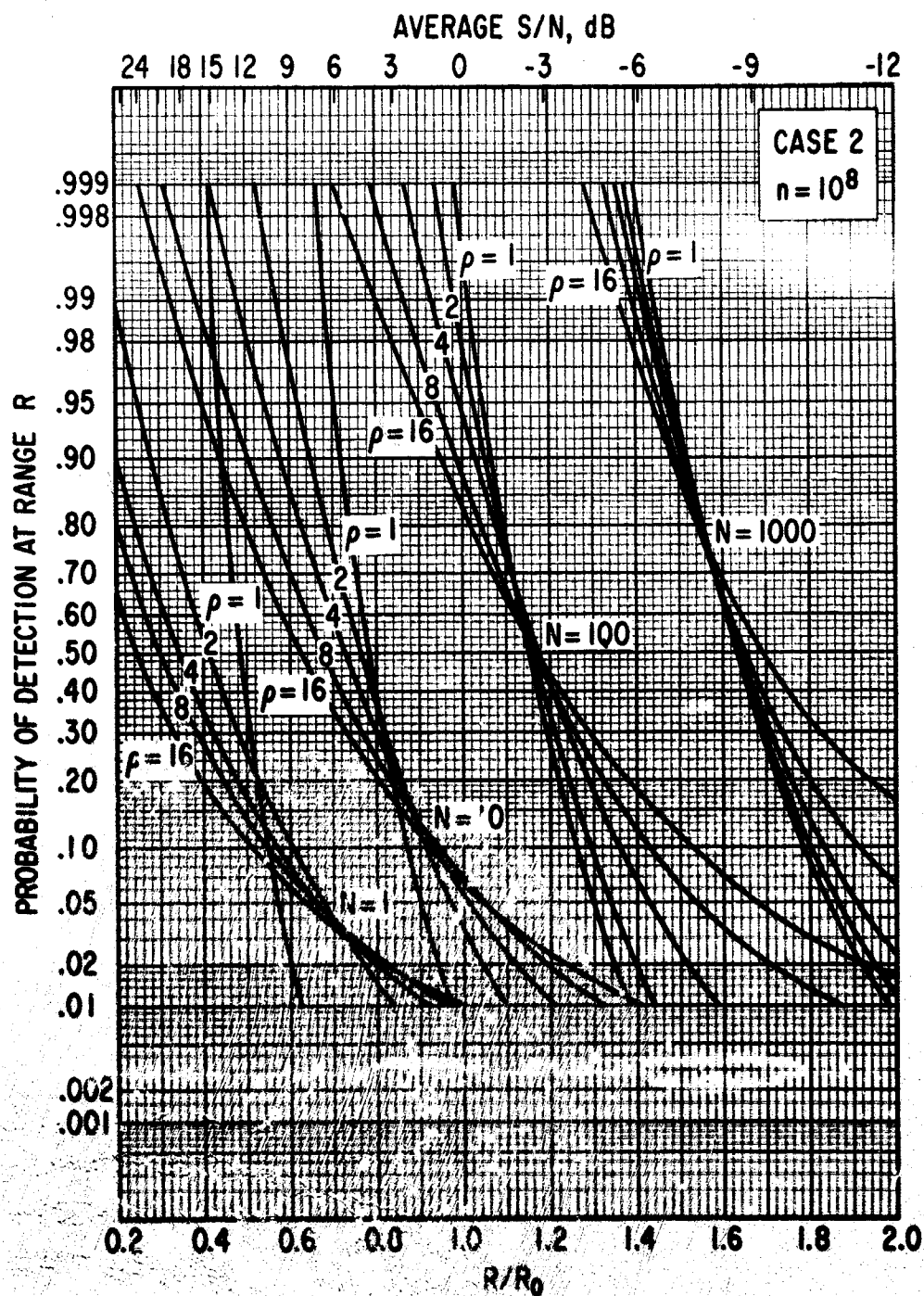
Fig. 42. Case 2, n = 10^8, with ρ and N as Parameters
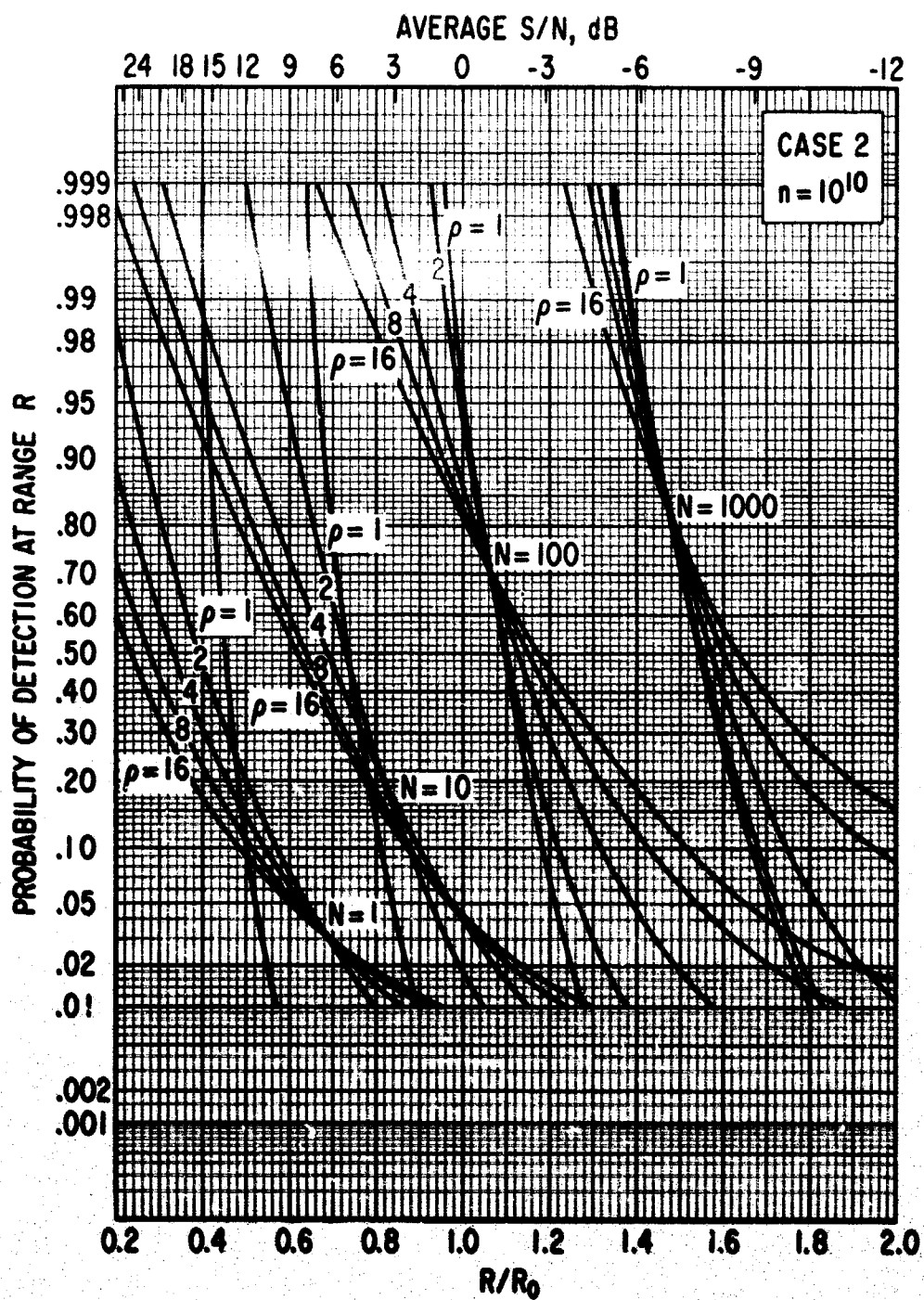
Fig. 43. Case 2, $n = 10^{10}$, with ρ and N as Parameters

MEDIAN S/N, dB
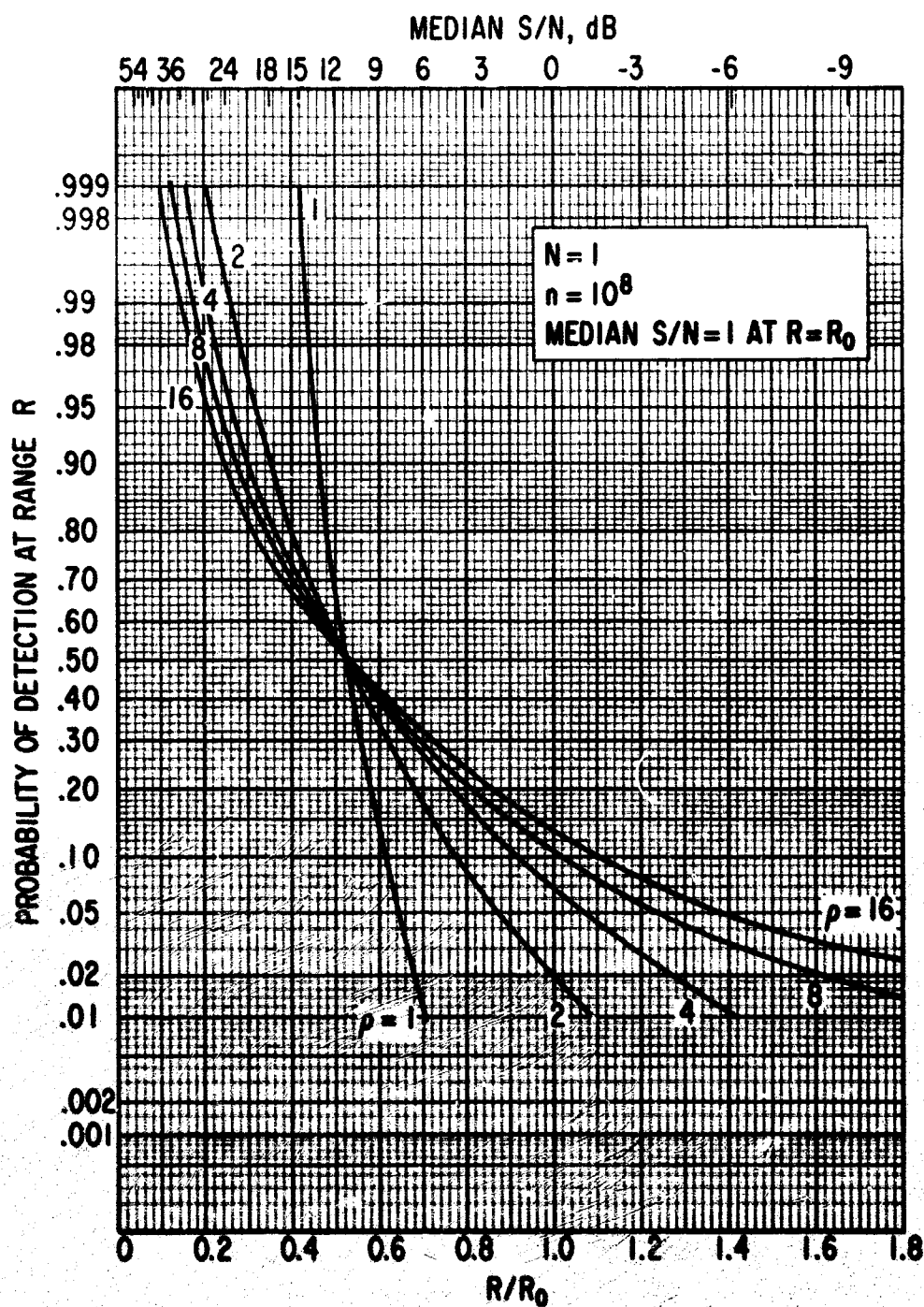
Fig. 44. Cases 1 and 2, $n = 10^8$, $N = 1$, with ρ as a Parameter Versus Median Signal-to-Noise Ratio
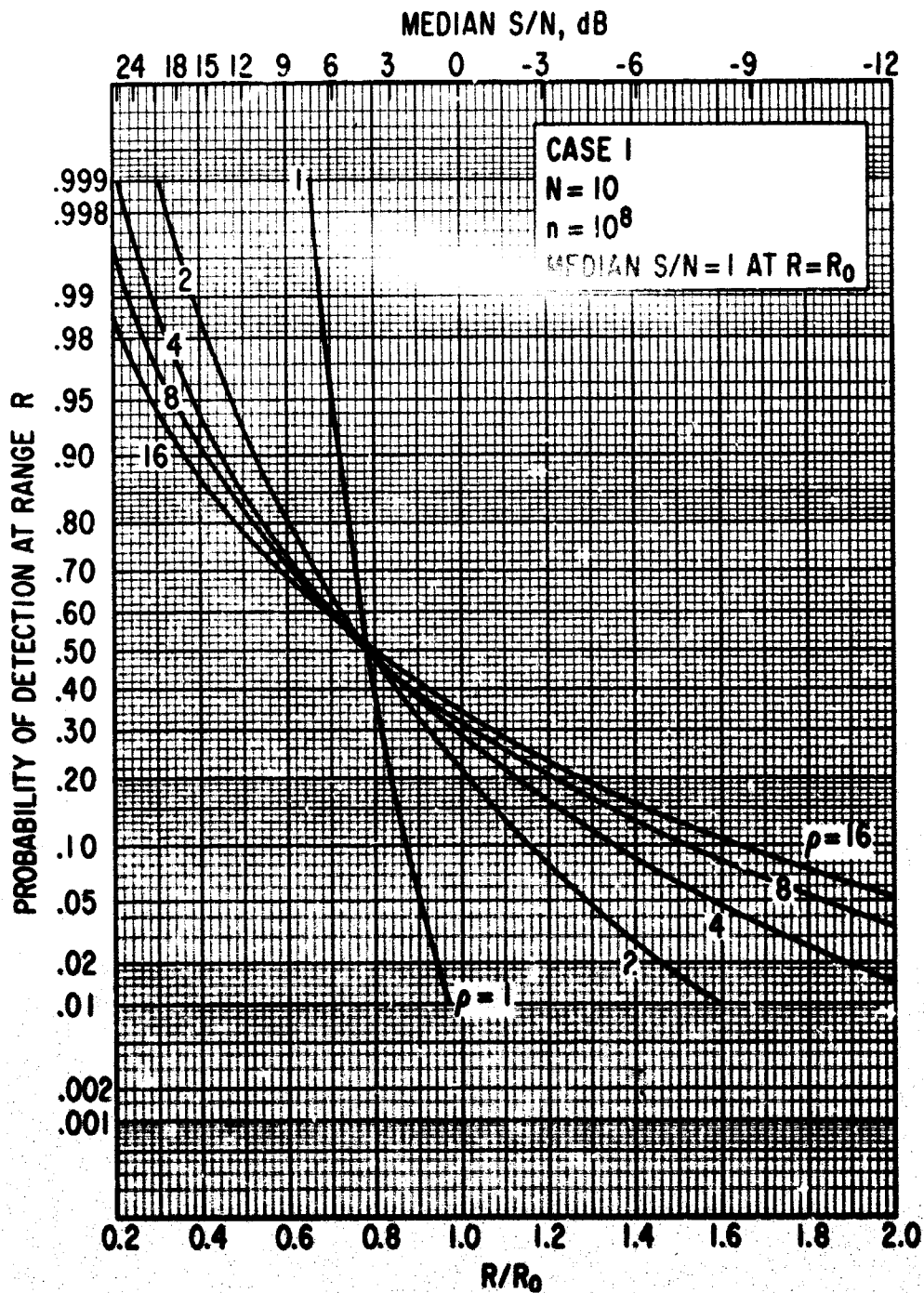
Fig. 45. Case 1, $n = 10^8$, $N = 10$, with ρ as a Parameter Versus Median Signal-to-Noise Ratio
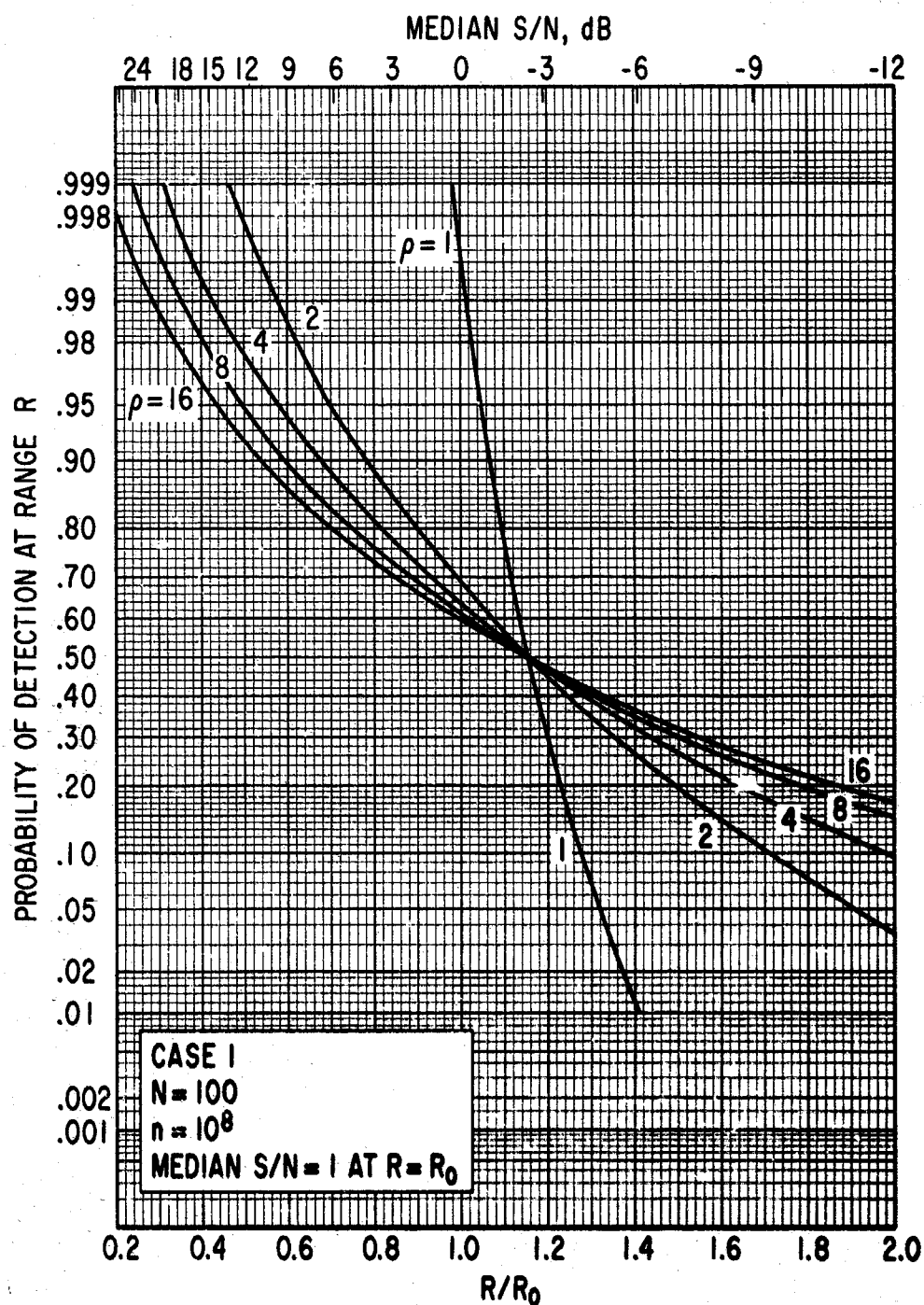
Fig. 46. Case 1, $n = 10^8$, $N = 100$, with ρ as a Parameter Versus Median Signal-to-Noise Ratio
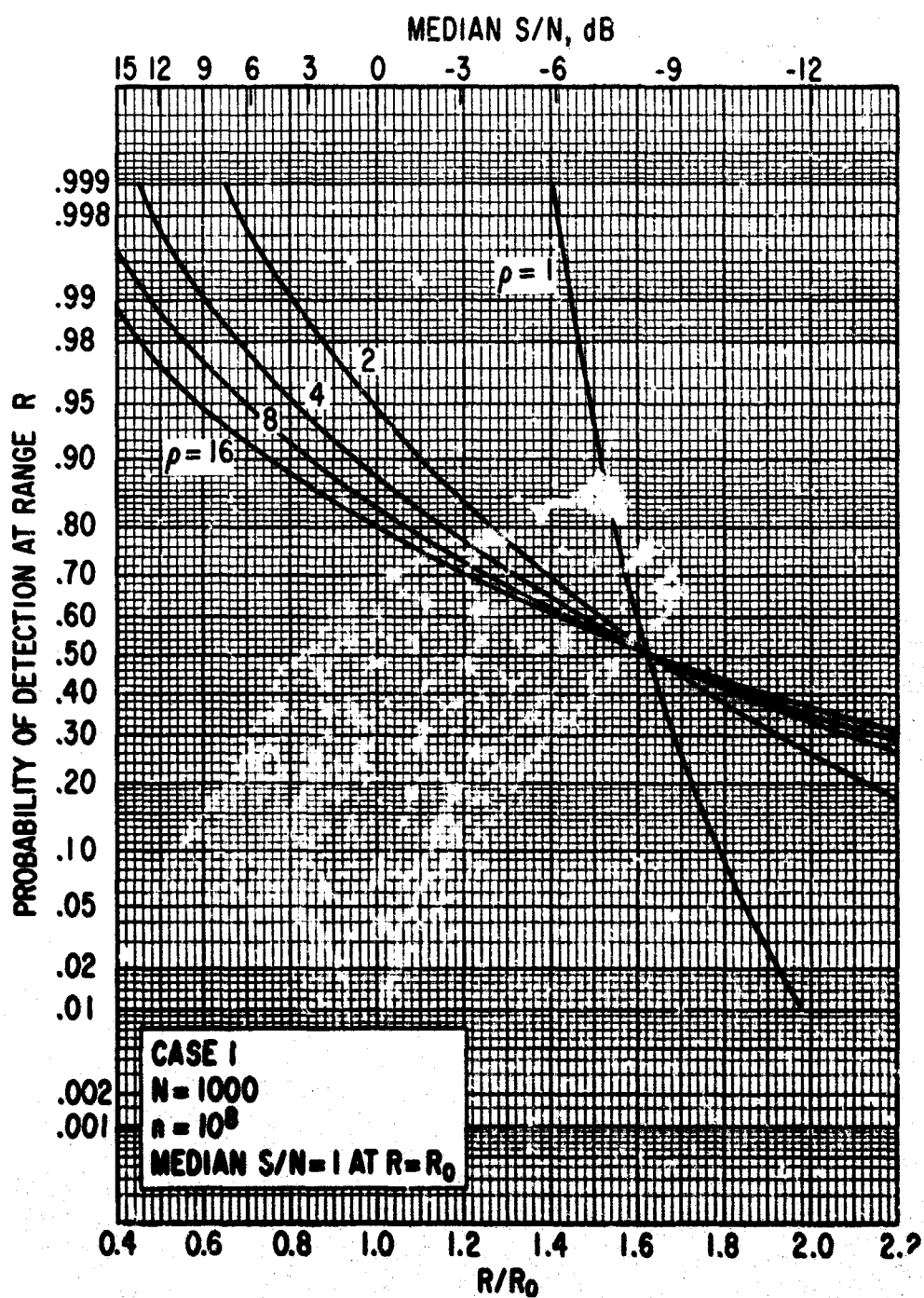
Fig. 47. Case 1, $n = 10^8$, $N = 1000$, with ρ as a Parameter Versus Median Signal-to-Noise Ratio
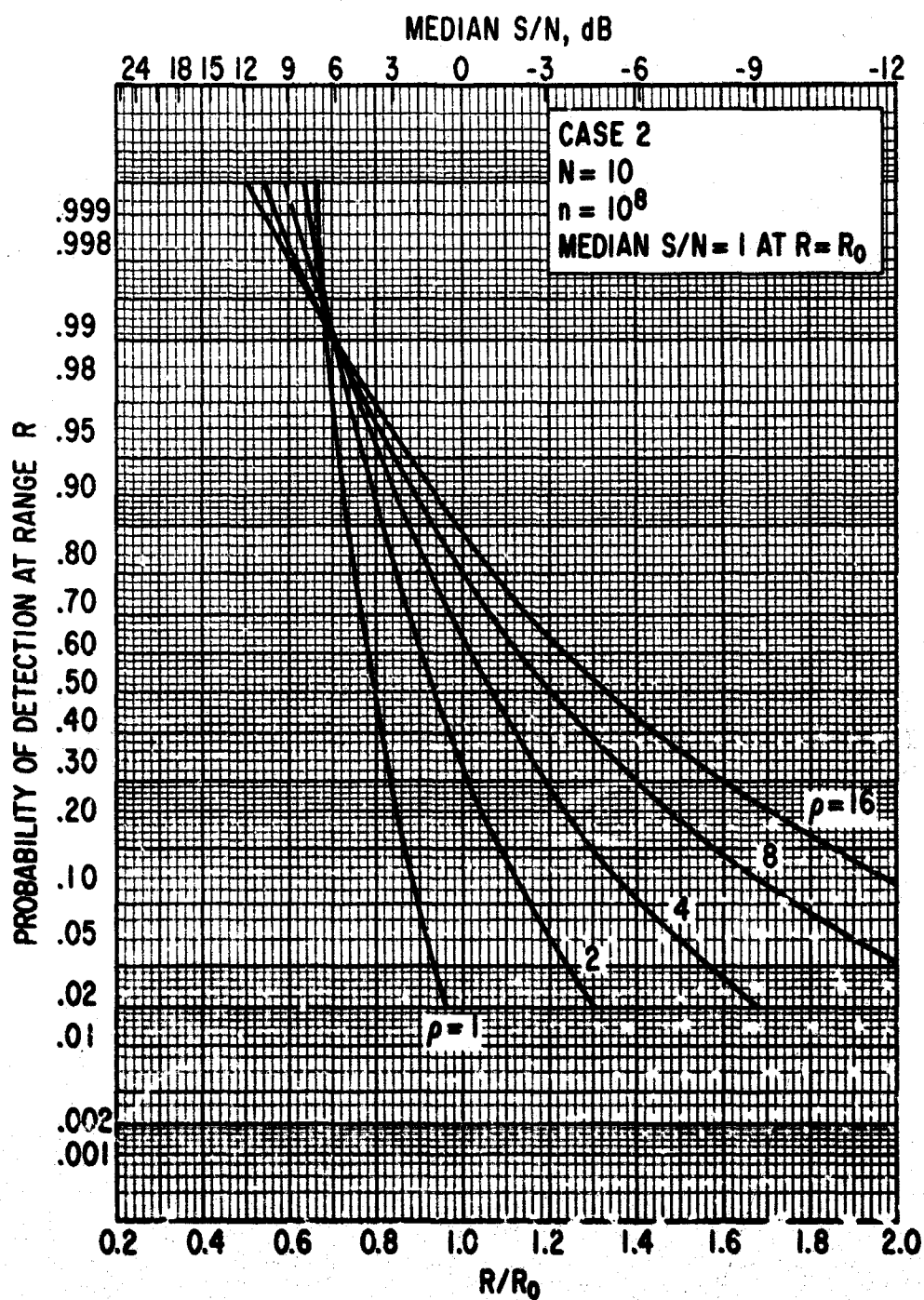
Fig. 48. Case 2, $n = 10^8$, $N = 10$, with ρ as a Parameter
Versus Median Signal-to-Noise Ratio
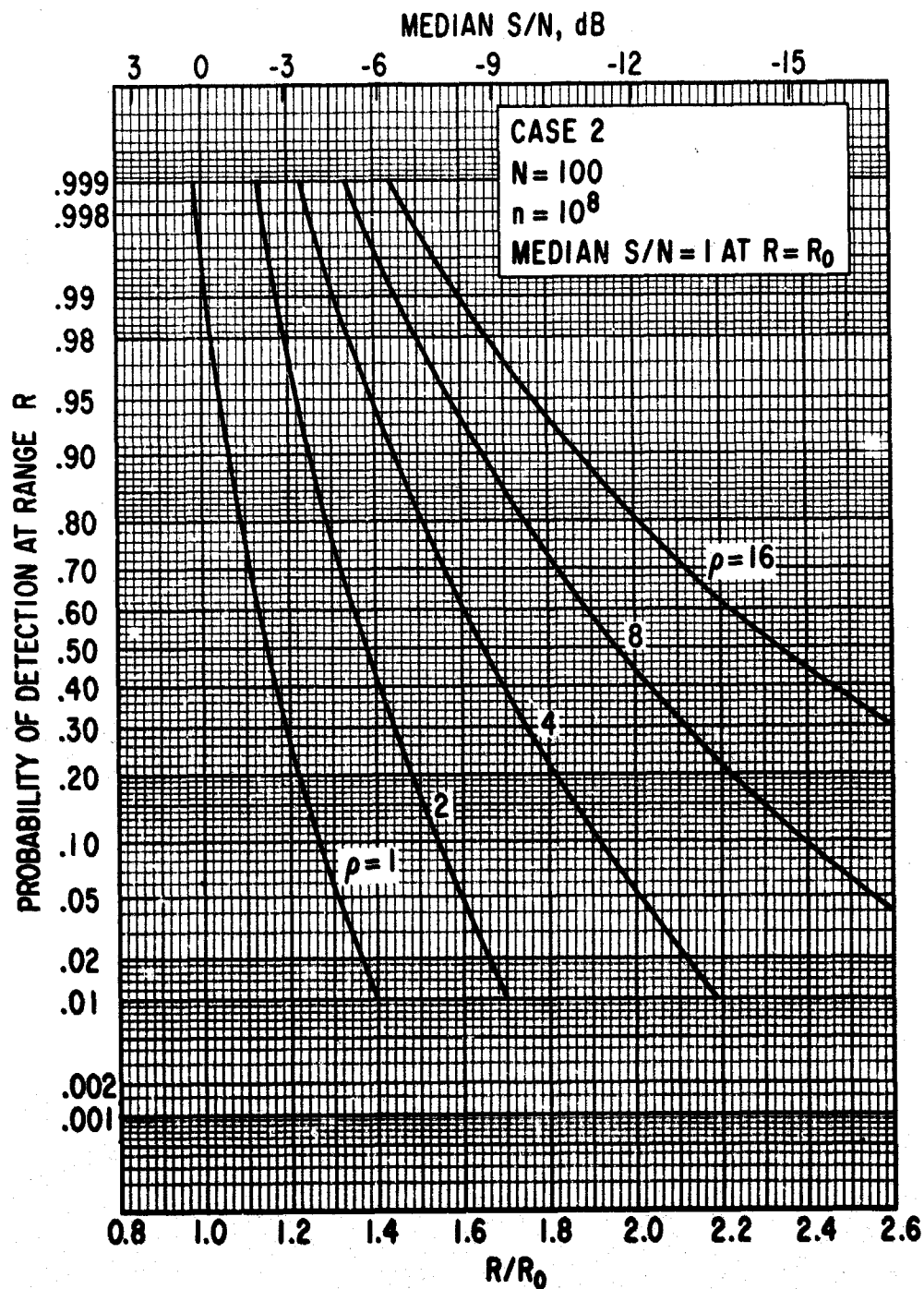
Fig. 49. Case 2, $n = 10^8$, $N = 100$, with ρ as a Parameter Versus Median Signal-to-Noise Ratio
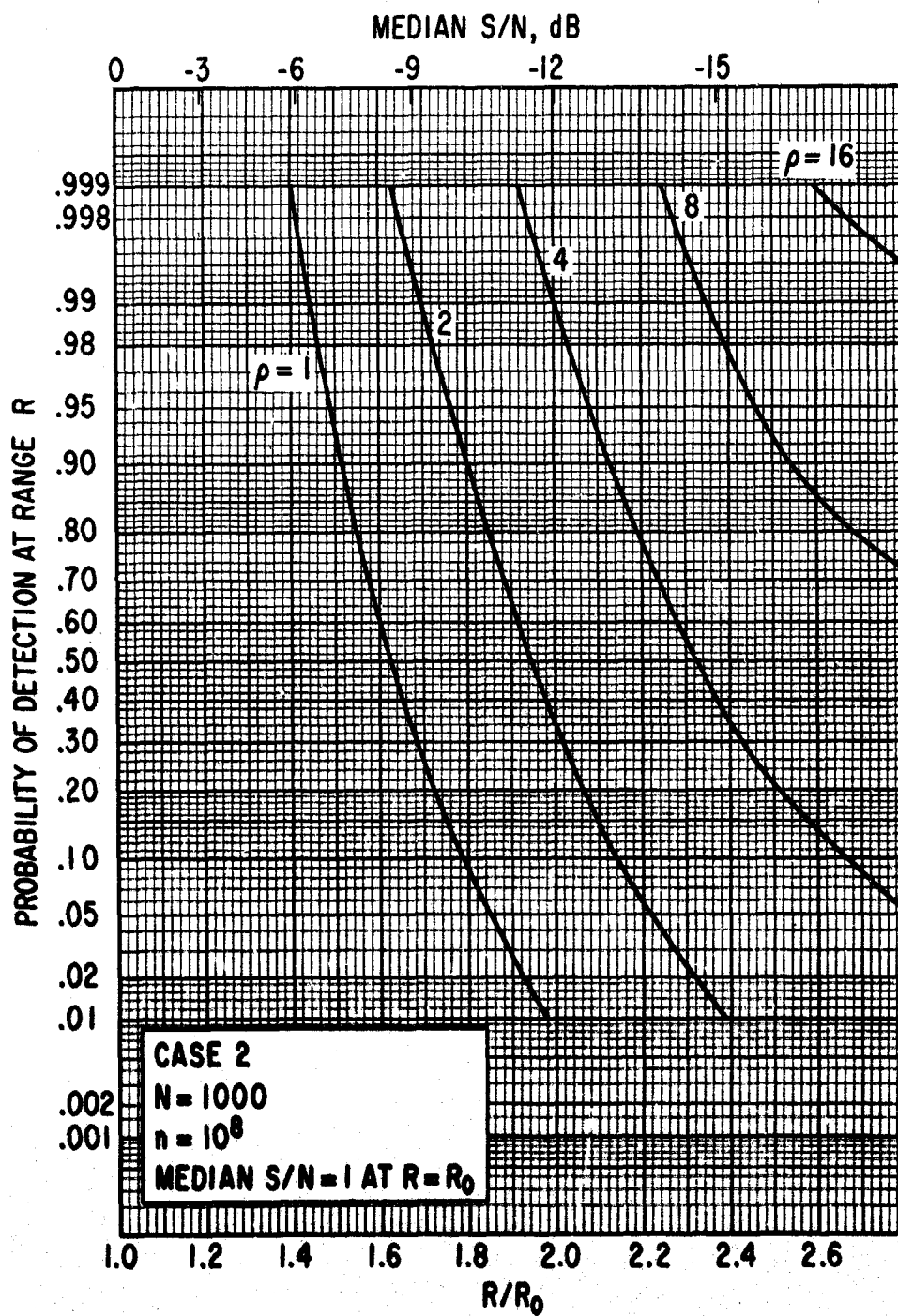
Fig. 50. Case 2, $n = 10^8$, $N = 1000$, with ρ as a Parameter Versus Median Signal-to-Noise Ratio
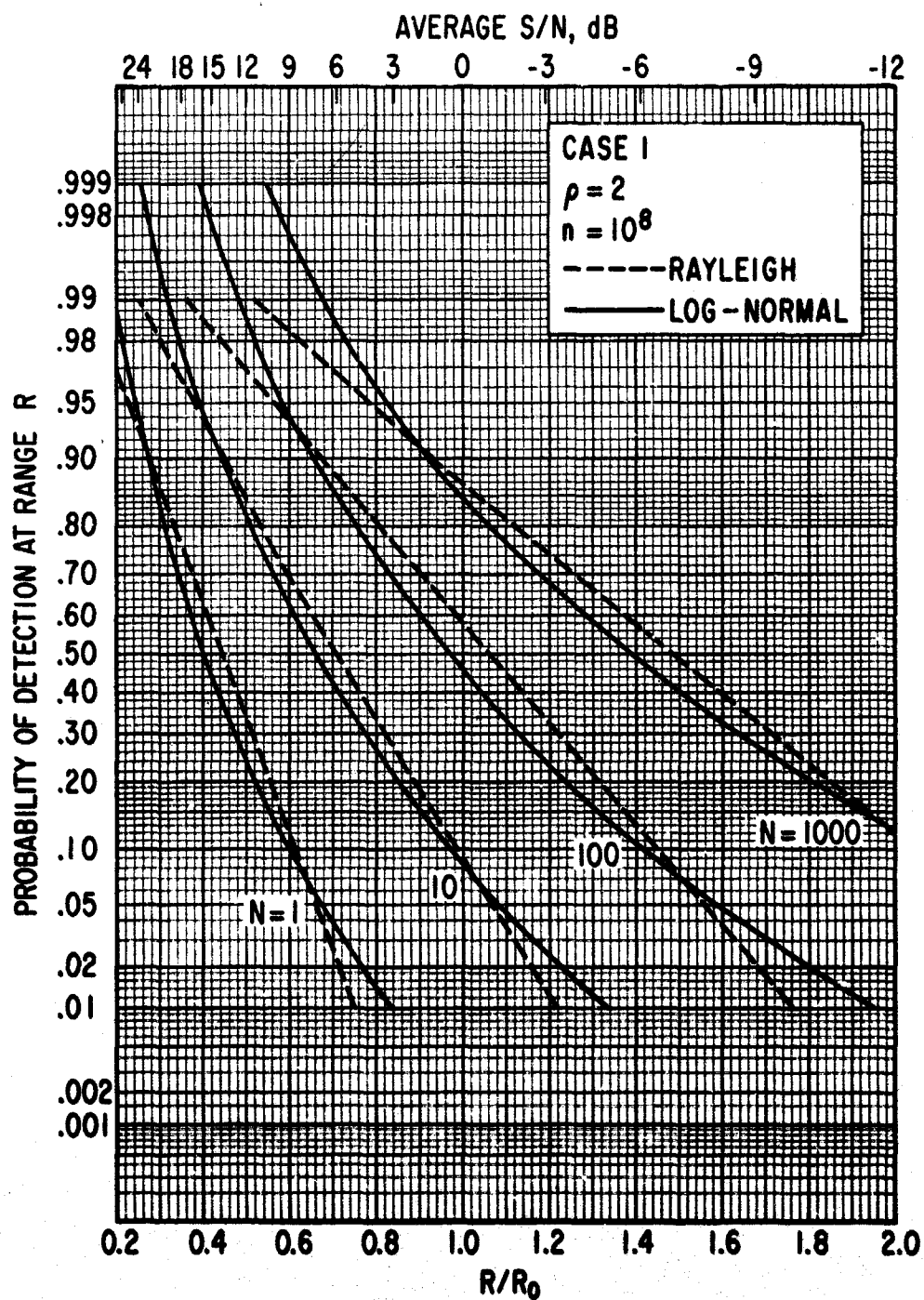
Fig. 51.   Case 1, $\rho = 2$, $n = 10^8$, Comparison to
Swerling Curves
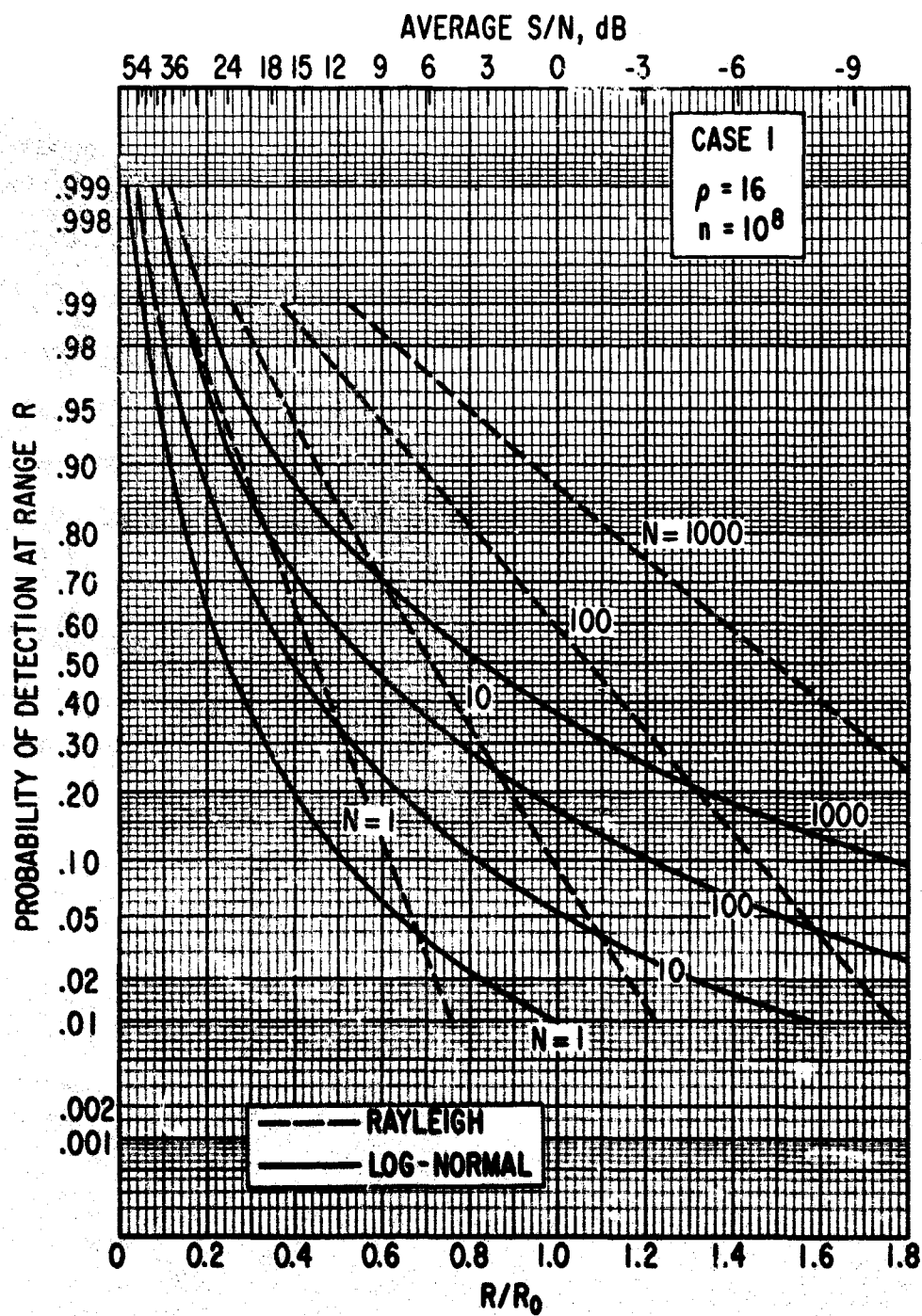
Fig. 52. Case 1, $\rho = 16$, $n = 10^8$, Comparison to Swerling Curves
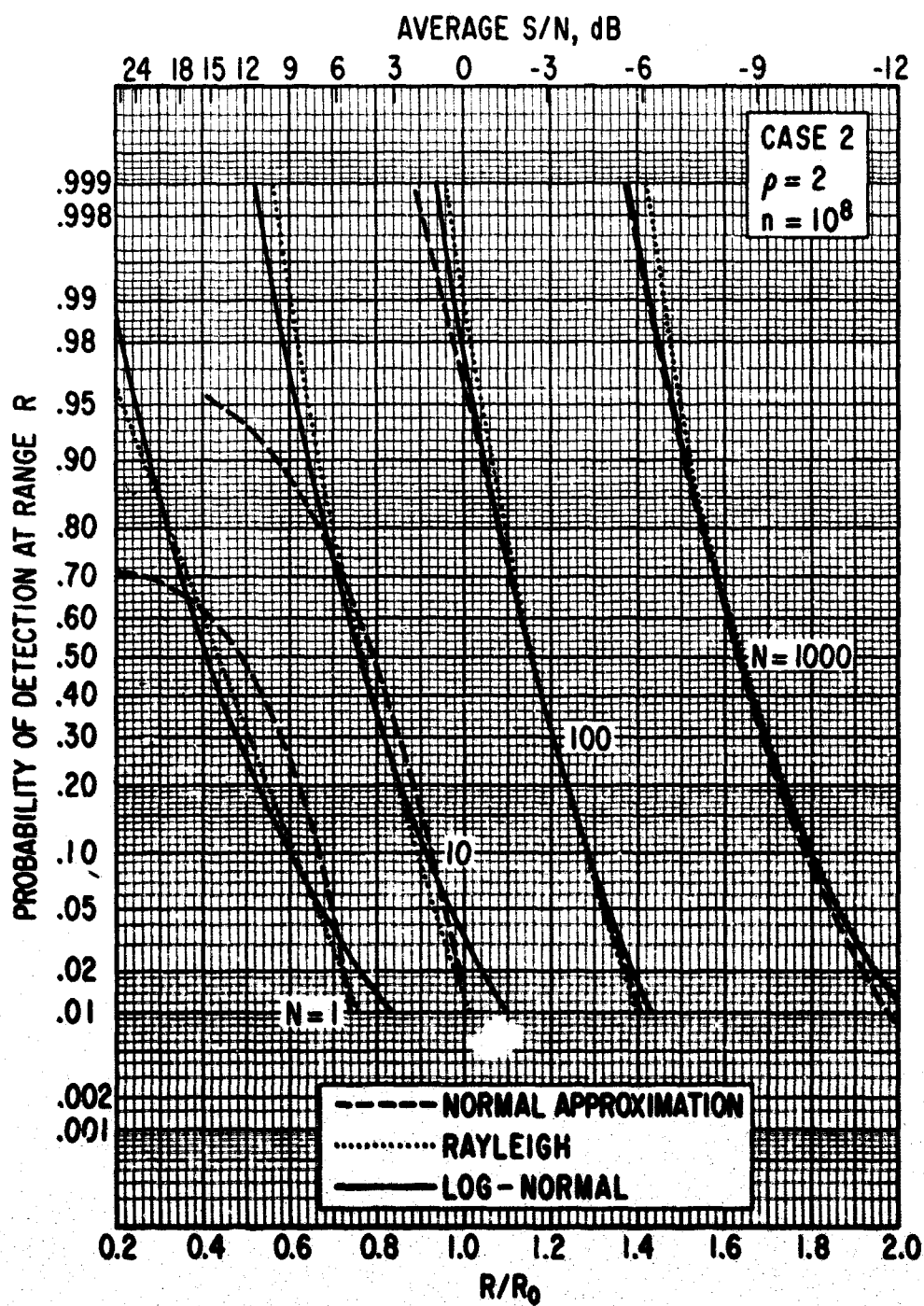
Fig. 53. Case 2, $\rho = 2$, $n = 10^8$, Comparison to Swerling Curves and Normal Approximation
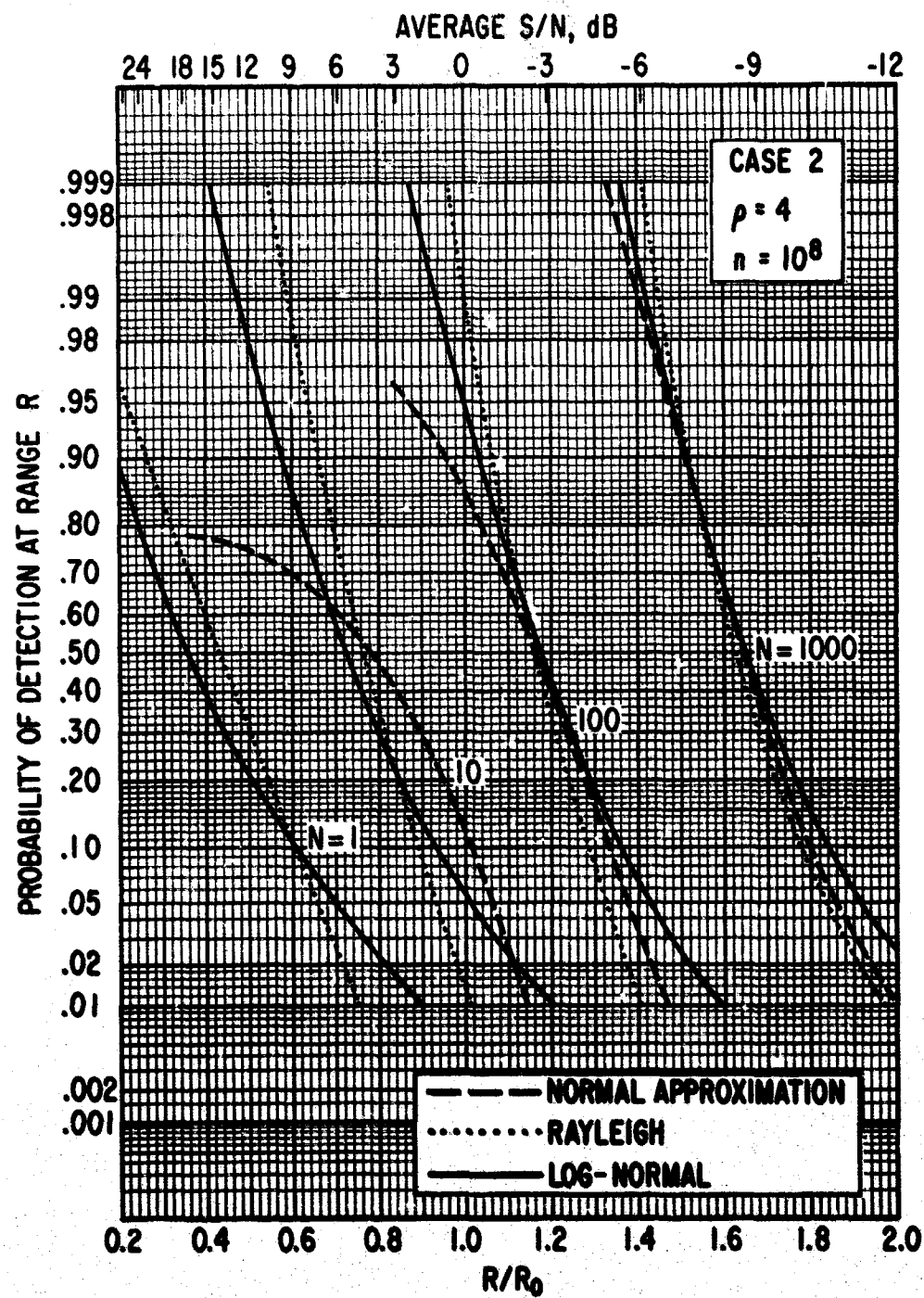
Fig. 54. Case 2, $\rho = 4$, $n = 10^8$, Comparison to Swerling Curves and Normal Approximation
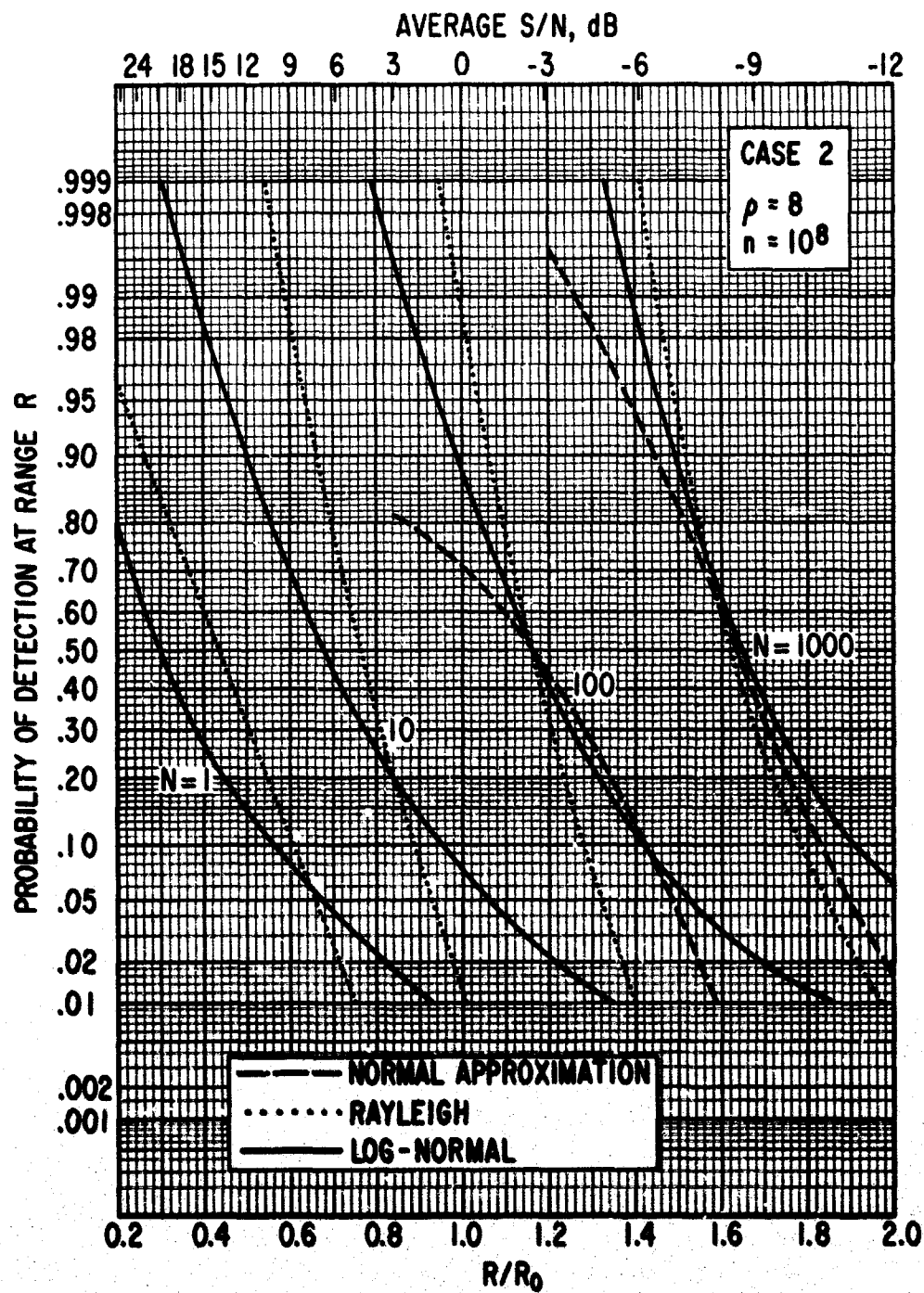
Fig. 55. Case 2, $\rho = 8$, $n = 10^8$, Comparison to Swerling Curves and Normal Approximation
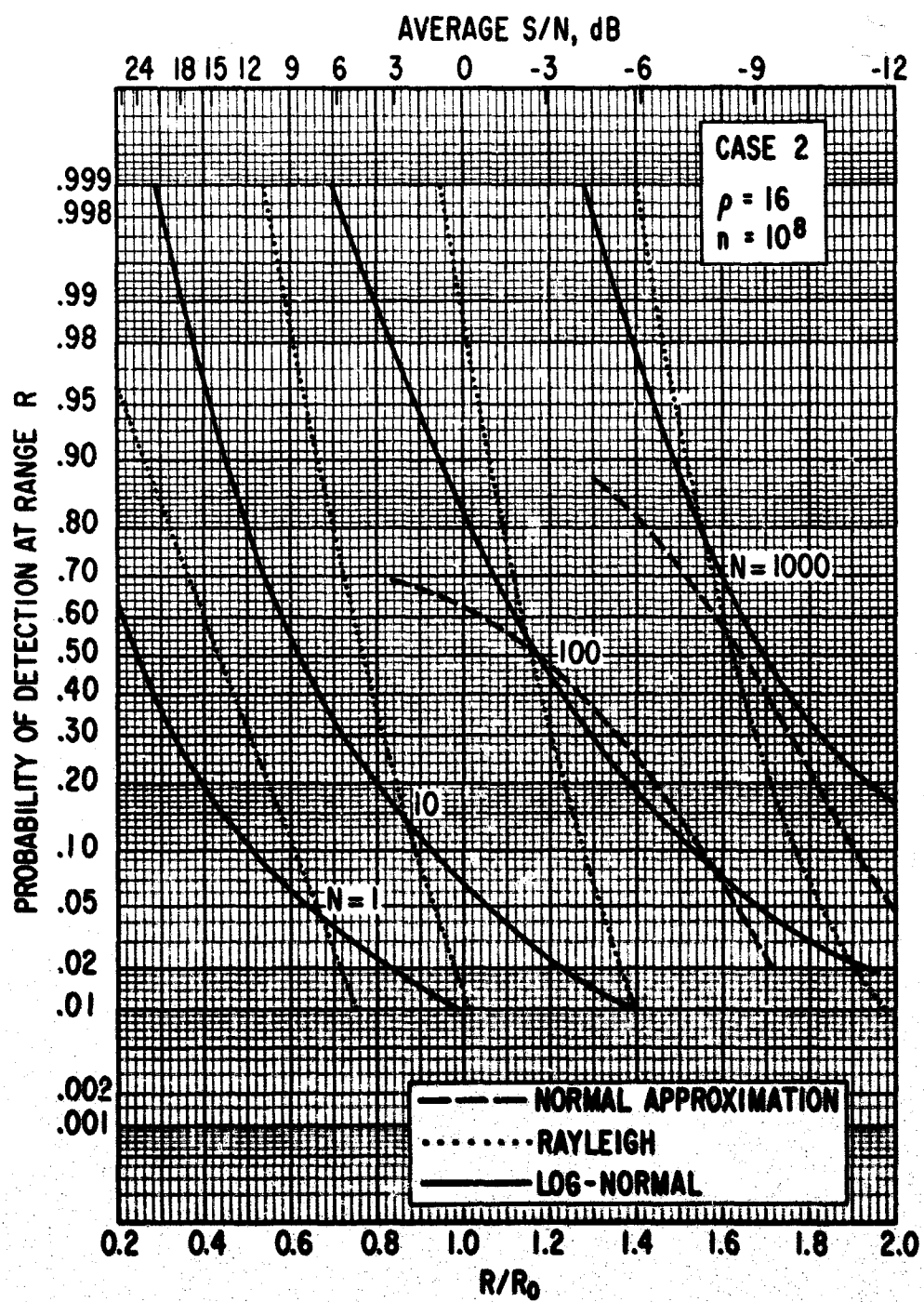
Fig. 56. Case 2, $\rho = 16$, $n = 10^8$, Comparison to Swerling Curves and Normal Approximation
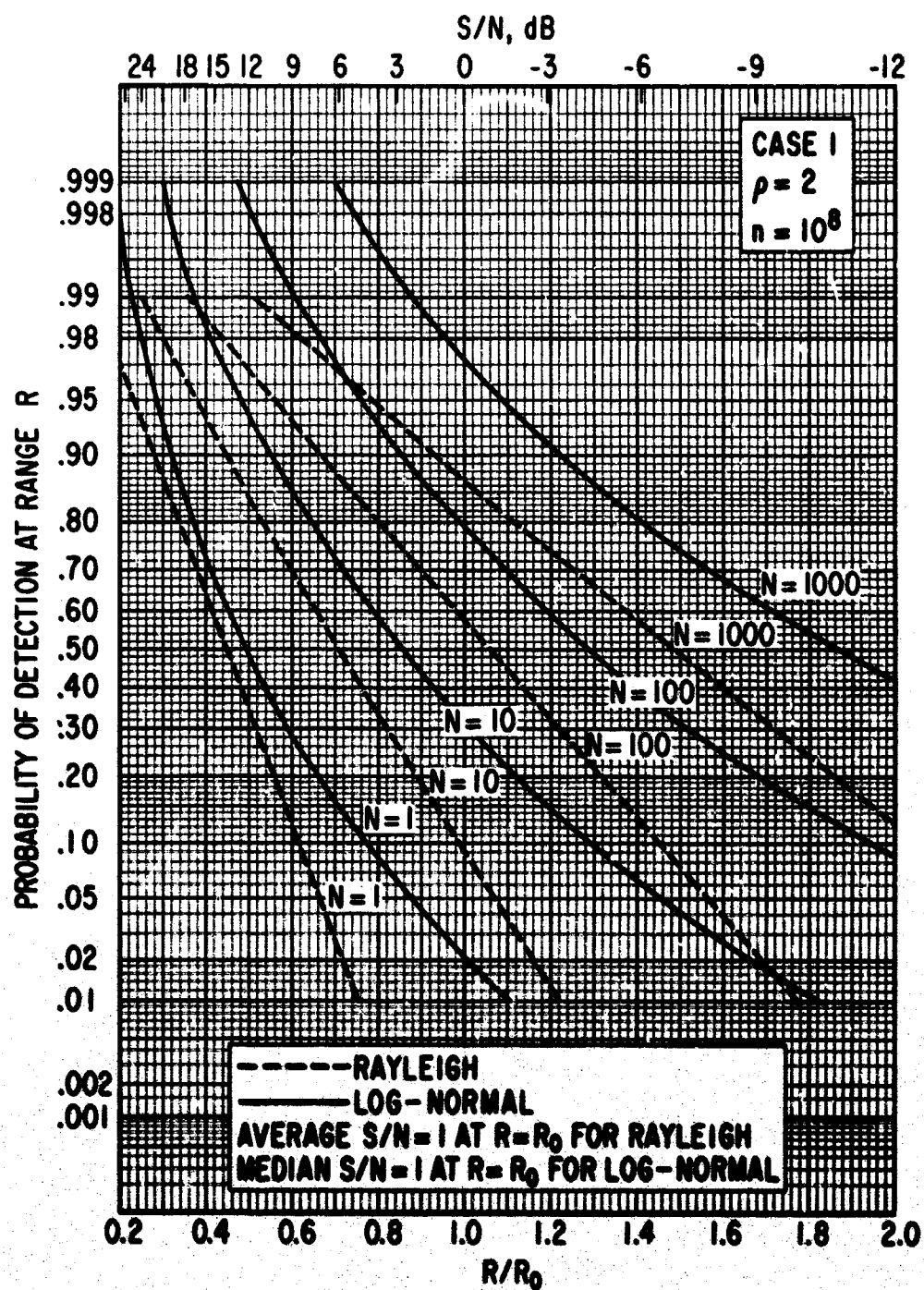
Fig. 57.   Case 1, $\rho = 2$, $n = 10^8$, Versus Median
Signal-to-Noise Ratio
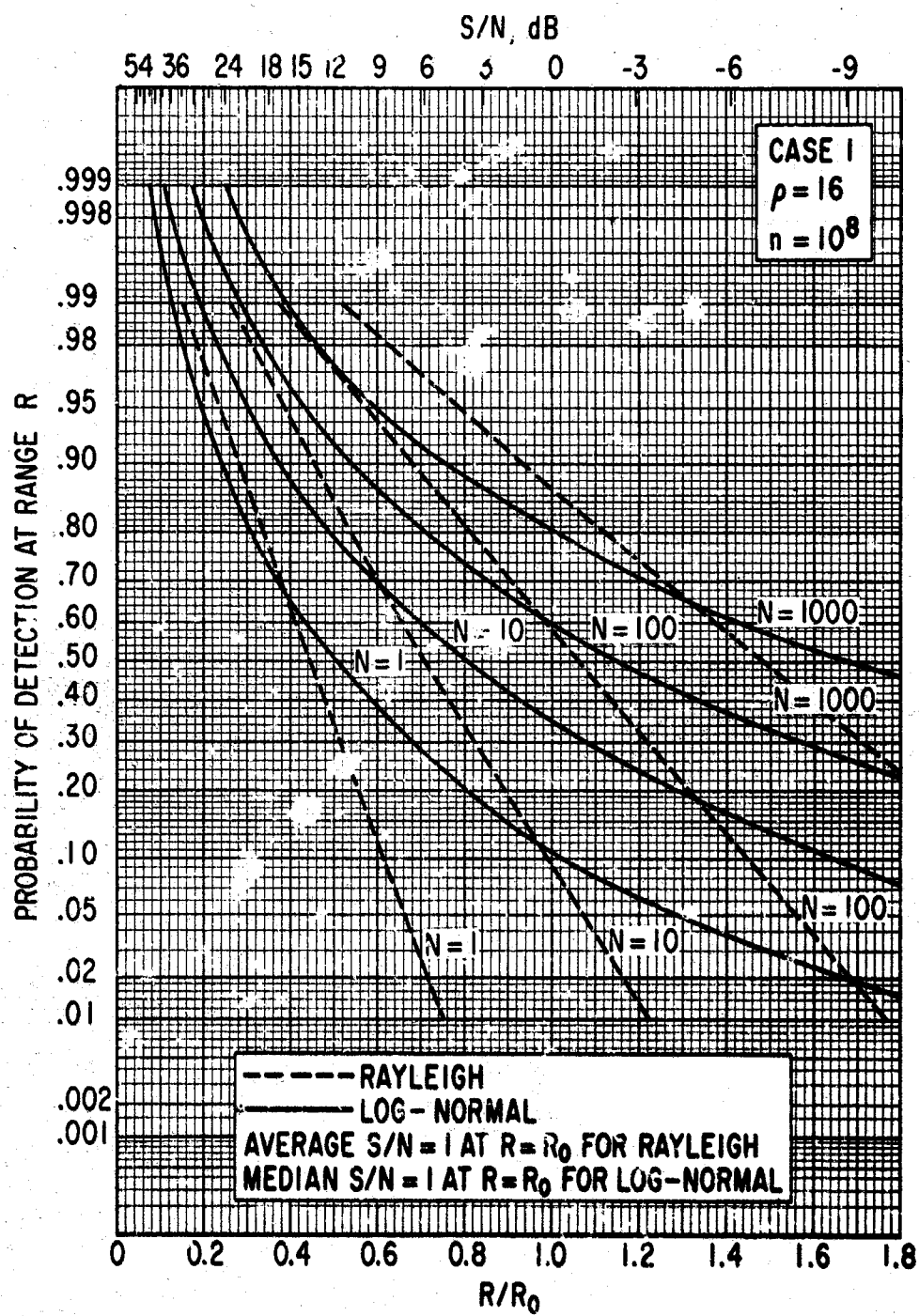
Fig. 58. Case 1, $\rho = 16$, $n = 10^8$, Versus Median
Signal-to-Noise Ratio
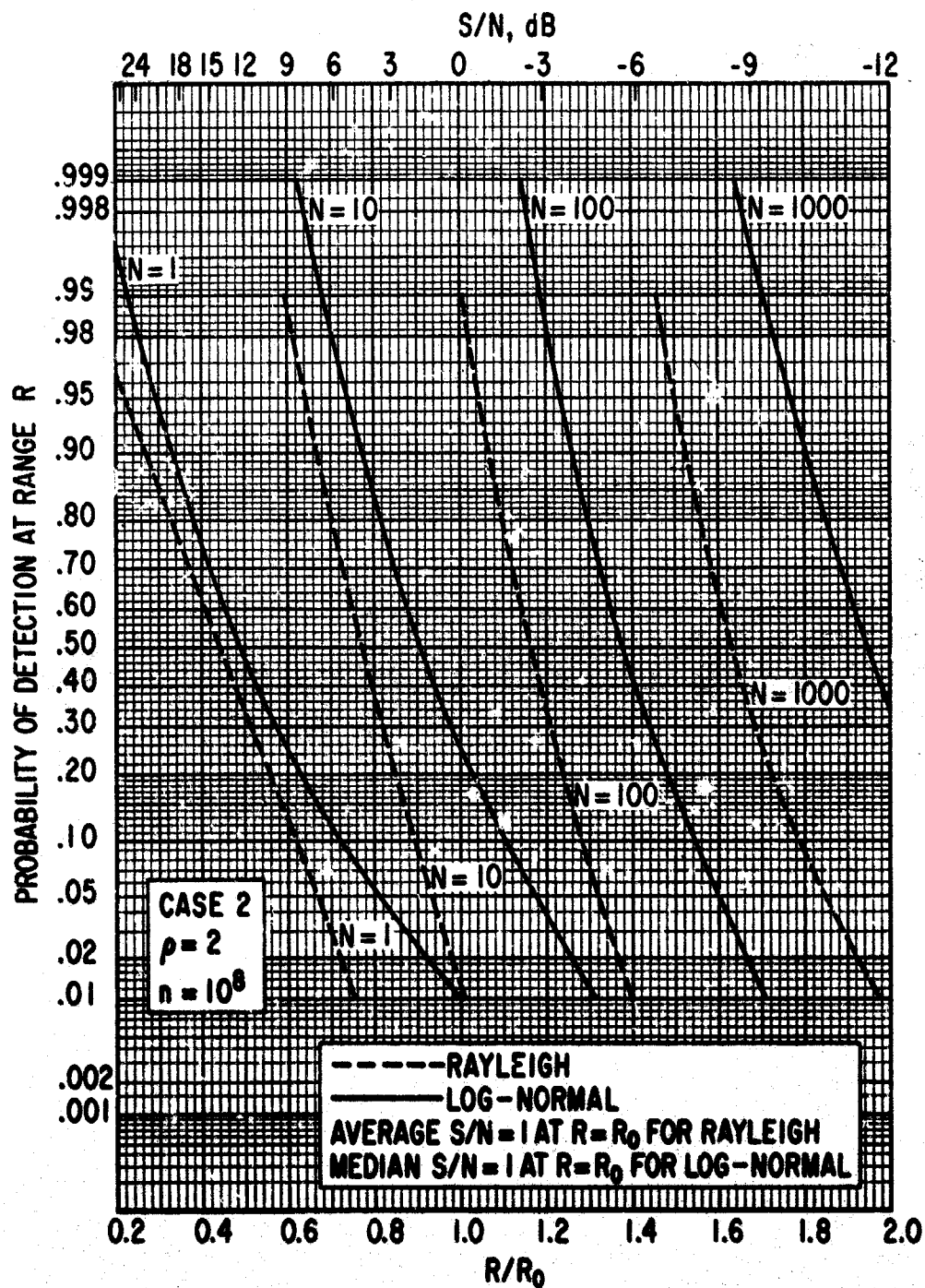
Fig. 59. Case 2, $\rho = 2$, $n = 10^8$, Versus Median
Signal-to-Noise Ratio

-73-
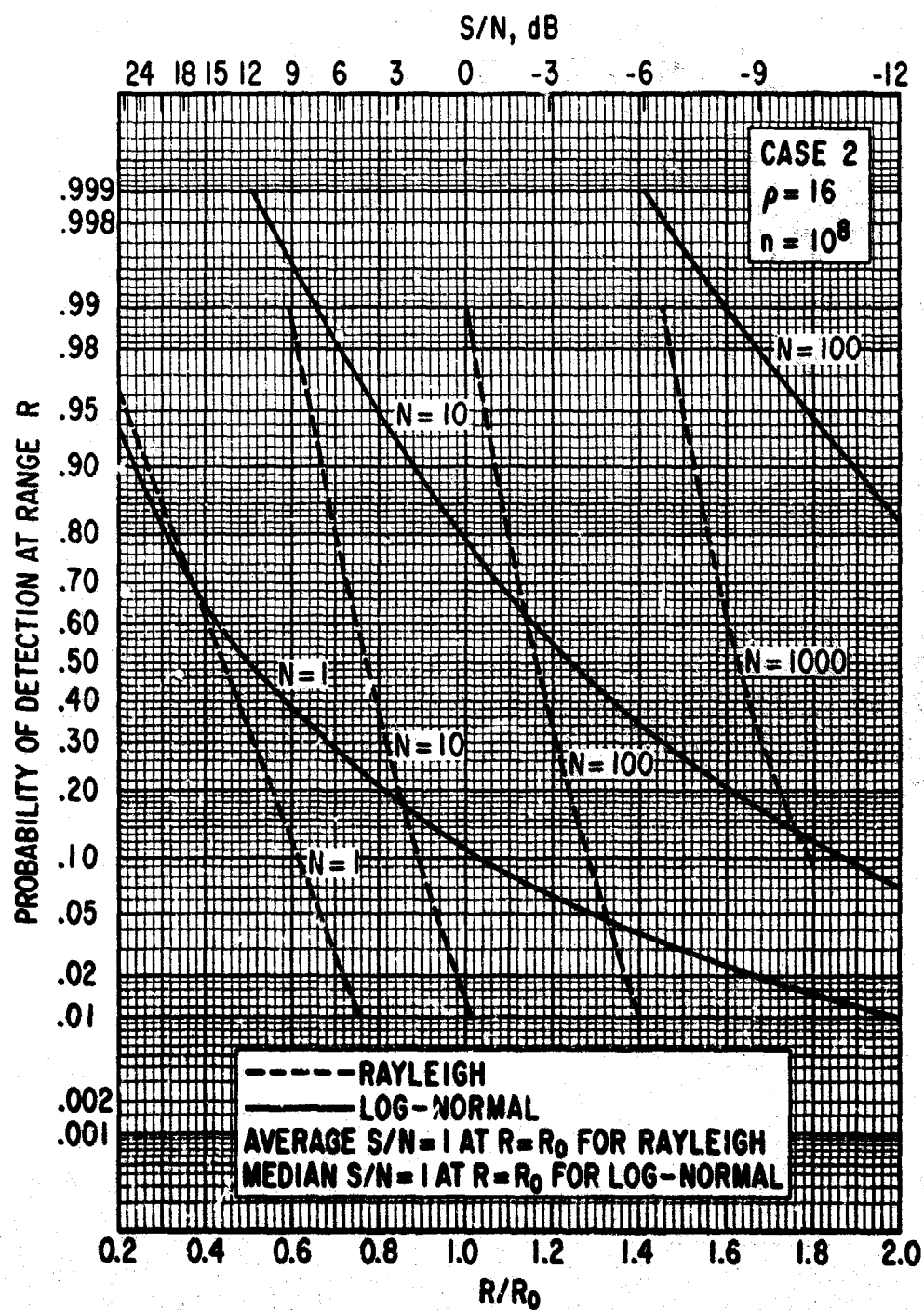
Fig. 60. Case 2, $\rho = 16$, $n = 10^8$, Versus Median
Signal-to-Noise Ratio
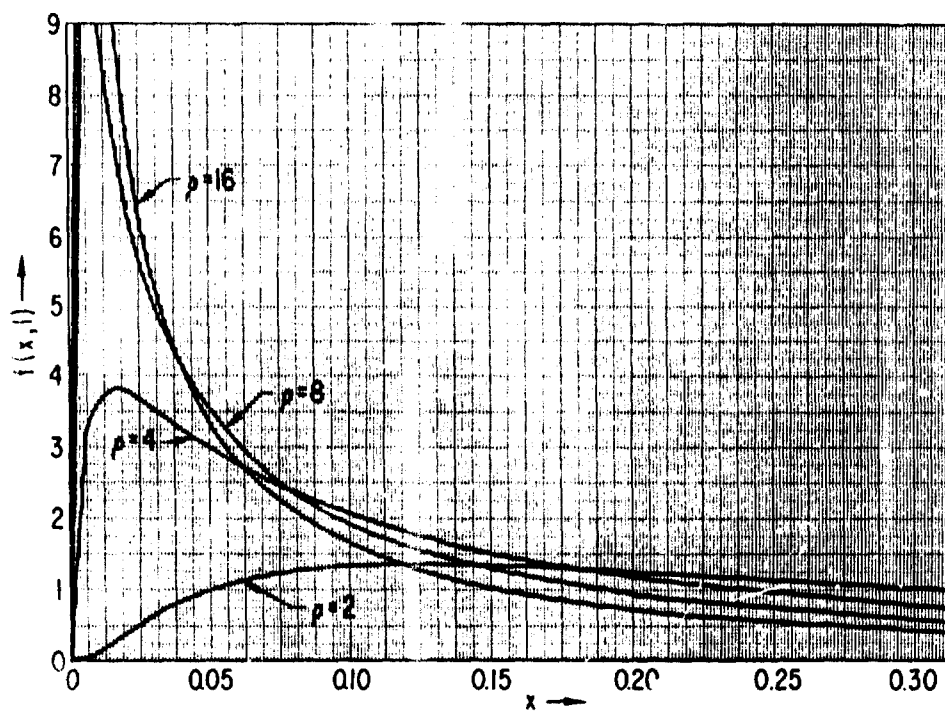
Fig. 61. Log-Normal Probability Density Function, $\bar{x} = 1$,
ρ as a Parameter
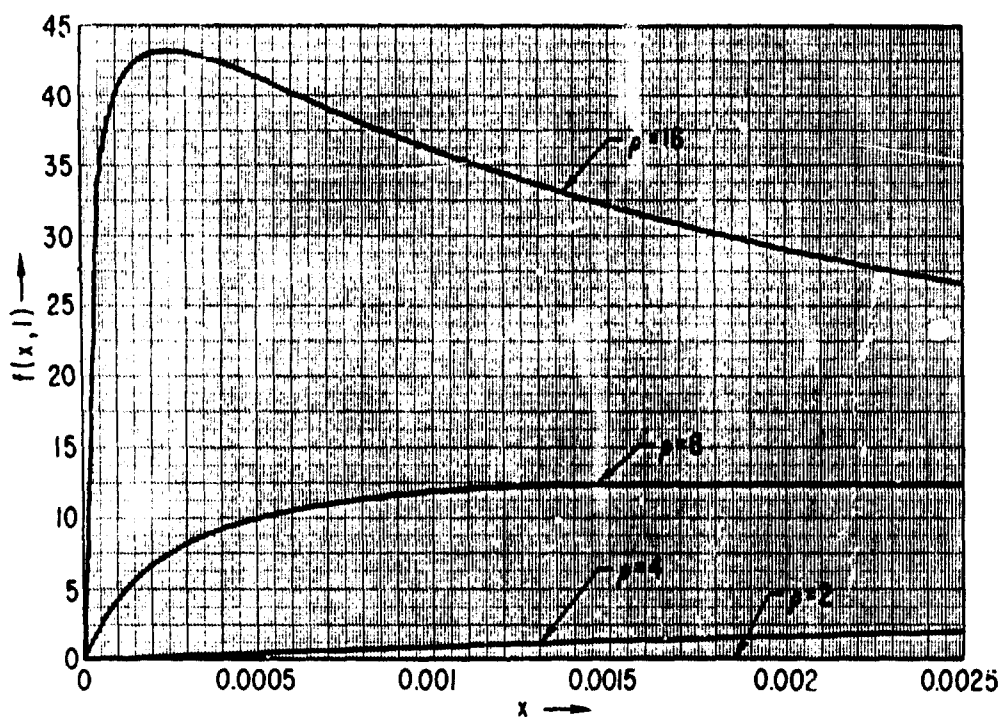
Fig. 62. Log-Normal Probability Density Function, $\overline{x} = 1$, ρ as a Parameter
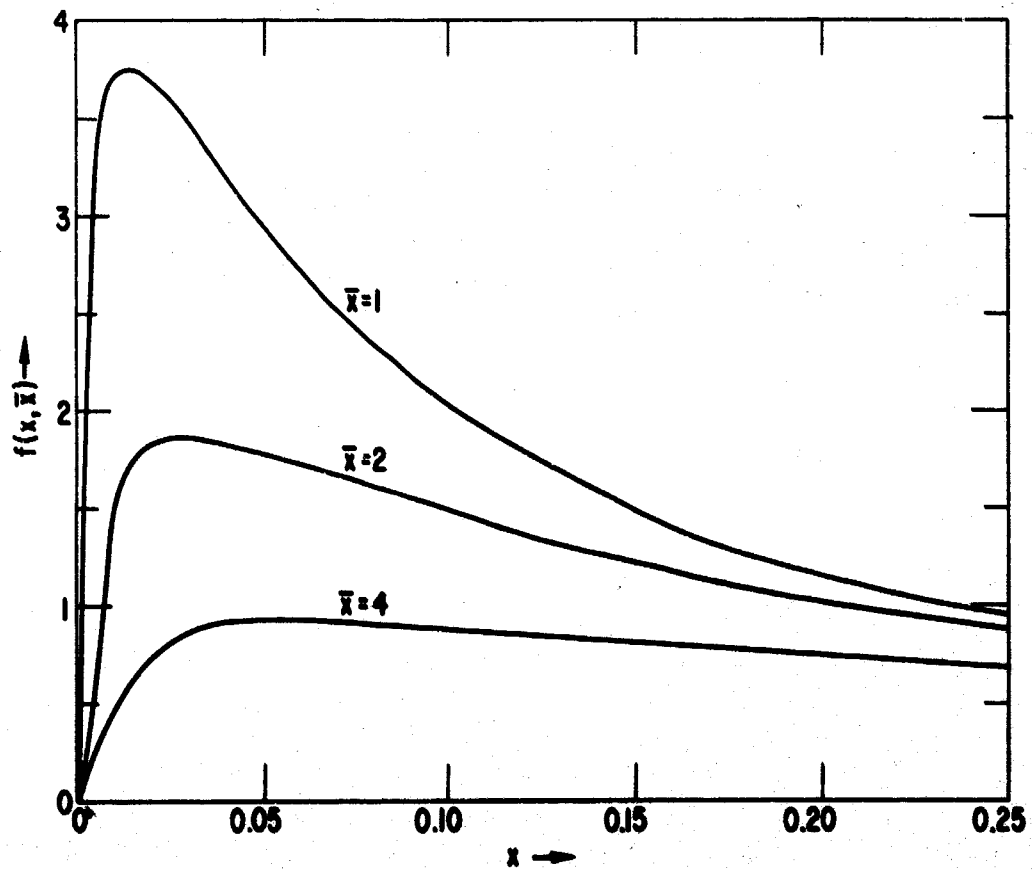
Fig. 63. Log-Normal Probability Density Function,
$\rho = 4$, $\bar{x}$ as a Parameter

APPENDIX

Computational Procedures

A.   CASE 1

The required result is, from Eqs. (1) and (3),

$$P_D(\overline{x}) = \int_{Y_b}^{\infty} f_N(y, \overline{x})\, dy$$

$$= \int_{Y_b}^{\infty} dy \int_0^{\infty} f_N(y/x)\, f(x, \overline{x})\, dx$$

Interchanging the order of integration yields

$$P_D(\overline{x}) = \int_0^{\infty} dx\, f(x, \overline{x}) \int_{Y_b}^{\infty} f_N(y/x)\, dy$$

The inner integral is seen to be precisely the probability of detection obtained by Marcum. Denoting this by $P'(x)$, we have

$$P_D(\overline{x}) = \int_0^{\infty} P'(x)\, f(x, \overline{x})\, dx$$

The integration is made numerically tractable, taking advantage of the normal distribution of ln x, by means of the substitution

$$z = \frac{\ln x - \overline{\ln x}}{\sqrt{2}\ \sigma} \tag{A-1}$$

Then

$$P_D(\bar{x}) = \int_{-\infty}^{\infty} e^{-z^2} P_1(z) \, dz \qquad (A-2)$$

where $P_1(z)$ is $P'(x)$ under the transformation of Eq. (A-1). The integration in Eq. (A-2) is readily performed by means of a numerical quadrature integration formula based on the Hermite polynomials [17]. As in Marcum [5], $P'(x)$ is computed using a Gram-Charlier series with the Edgeworth grouping of terms to represent $f_N(y/x)$. Thus,

$$f_N(y/x) = \sum_{i=0}^{\infty} \frac{c_i}{\sqrt{\mu_2}} \, \phi^i(t) = g(t) \qquad (A-3)$$

where $t = (y - \bar{y})/\sqrt{\mu_2}$ [μ_i is the ith central moment of $f_N(y/x)$],

$$\phi^i(t) = \frac{(-1)^i}{\sqrt{2\pi}} \, e^{-t^2/2} \, H_i(t)$$

and $H_i(t)$ is the Hermite polynomial of degree i. The coefficients c_i are given by

$$c_i = \frac{(-1)^i \sqrt{\mu_2}}{i!} \int_{-\infty}^{\infty} H_i(t) \, g(t) \, dt$$

$$= \frac{(-1)^i}{i!} \int_{-\infty}^{\infty} H_i\left(\frac{y - \bar{y}}{\sqrt{\mu_2}}\right) f_N(y/x) \, dy$$

Substituting

$$H_i(t) = i! \sum_{m=0}^{[i/2]} \frac{(-1)^m t^{i-2m}}{2^m m! (i - 2m)!}$$

yields

$$c_i = \sum_{m=0}^{[i/2]} \frac{(-1)^{i+m}}{2^m m! (i - 2m)!} \int_{-\infty}^{\infty} \left(\frac{y - \bar{y}}{\sqrt{\mu_2}}\right)^{i-2m} f_N(y/x)\, dy$$

$$= \sum_{m=0}^{[i/2]} \frac{(-1)^{i+m}}{2^m m! (i - 2m)!} \frac{\mu_{i-2m}}{\mu_2^{i/2-m}}$$

The μ_i are expressed in terms of the moments about the origin ν_i by

$$\mu_i = \sum_{n=0}^{i} \binom{i}{n}(-1)^{i-n} \nu_1^{i-n} \nu_n \qquad \text{(A-4)}$$

The moments ν_i are, in turn, obtained using the characteristic function as a moment generating function. Thus,

$$\nu_i = (-1)^i \left(\frac{d^i C(p)}{dp^i}\right)\Bigg|_{p=0} \qquad \text{(A-5)}$$

From the results

$$f_N(y/x) = \left(\frac{y}{Nx}\right)^{(N-1)/2} e^{-y-Nx} I_{N-1}(2\sqrt{Nxy}) \qquad \text{(A-6)}$$

and

$$C(p) = \frac{e^{-Nx}}{(p+1)^N} e^{Nx/(p+1)}$$

Marcum obtains

$$\nu_i = \frac{(N+i-1)!}{(N-1)!} {}_1F_1(-i, N, -Nx) \qquad \text{(A-7)}$$

where ${}_1F_1$ is the confluent hypergeometric function. The coefficients c_i are computed from Eqs. (A-7), (A-5), and (A-4) using the recursion relationship

$${}_1F_1(-i, N, Nx) = \frac{Nx + N + 2i - 2}{N + i - 1} {}_1F_1(-i+1, N, Nx)$$

$$- \frac{i-1}{N+i-1} {}_1F_1(-i+2, N, Nx)$$

Finally, $P'(x)$ is obtained as

$$P'(x) = \int_{Y_b}^{\infty} f_N(y/x) \, dy$$

$$= \sqrt{\mu_2} \int_T^{\infty} g(t) \, dt$$

where

$$T = \frac{Y_b - \nu_1}{\sqrt{\mu_2}}$$

The function $f_N(y/x)$ is given by Eq. (A-3), so that

$$P'(x) = \sum_{i=0}^{\infty} c_i \int_T^{\infty} \phi^i(t)\, dt$$

The result of the integration is

$$P'(x) = \left[\frac{1}{2} - \frac{1}{2}\phi^{-1}(T)\right] - \left[c_3\phi^2(T)\right] - \left[c_4\phi^3(T) + c_6\phi^5(T)\right]$$

$$- \left[c_5\phi^4(T) + c_7\phi^6(T) + c_9\phi^7(T)\right] - \dots$$

The brackets indicate the Edgeworth grouping of terms ($c_0 = 1$ and $c_1 = c_2 = 0$). Following Marcum, all of the curves except those for $N = 1$ were computed using only the first three Edgeworth groupings to approximate $P'(x)$.

The accuracy of the calculation is limited by the number of ordinates used in the quadrature integration formula. A total of 20 were used, i.e.,

$$\int_{-\infty}^{\infty} e^{-z^2} P_1(z)\, dz \sim \sum_{i=1}^{20} w(z_i)\, P_1(z_i) \qquad \text{(A-8)}$$

where the z_i are zeros of the 20$^{\text{th}}$ degree Hermite polynomial and the $w(z_i)$ are the quadrature formula weighting factors [17]. The effect of using a small number of ordinates is to introduce error in the points on the probability of detection curves. In general, with 20 ordinates, the computed points generate a smooth curve, although some spread is noticeable for the larger

-83-

values of ρ. The manner in which the spread decreases is shown in Fig. A-1 which gives points for $N = 1$, $n = 10^{10}$, and $\rho = 16$ obtained using 10, 16, and 20 ordinates. It appears from the manner in which the points converge as the number of ordinates increases that the maximum error in probability is of the order of 0.01 and occurs for low detection probabilities. The curves of $P'(x)$ obtained for $N = 1$ and $\rho = 1$ are quite smooth and agree remarkably well with Marcum's curve except at very low probabilities. The curves of $P_D(\bar{x})$ for $N = 1$ were obtained as discussed under Case 2. Cases 1 and 2 are the same for $N = 1$.

B.   CASE 2

The probability density function of N integrated signal plus noise variates at the detector output where the fluctuations are independent from pulse to pulse is given by the N-fold self-convolution of $f_1(y, \bar{x})$. For numerical computation, the Hermite quadrature integration formula in Eq. (A-8) is a convenient method to calculate $f_1(y, \bar{x})$. But, for this case, the integrand is equal to $f_1(y/x)/\sqrt{\pi}$ under the transformation of Eq. (A-1). The function $f_1(y, \bar{x})$ was computed for 621 points over the interval 0(0.06)37.2[1] for each combination of ρ and $\bar{x}$ (values of $\bar{x}$ were chosen at 3-dB increments). The function $f_2(y, \bar{x})$ is obtained by convolving $f_1(y, \bar{x})$ with itself. At this point, the increment in y was doubled so that the 311 points on the interval 0(0.12)37.2 correspond to every other point on the previous interval. The function over the interval 37.32(0.12)74.4 was assumed to be zero. Similarly, $f_4(y, \bar{x})$ was obtained

---

[1] The interval (0, 37.2) was divided into increments of 0.06.

-84-

from $f_2(y, \bar{x})$, $f_6(y, \bar{x})$ from $f_4(y, \bar{x})$, and $f_{10}(y, \bar{x})$ from both $f_2(y, \bar{x})$ and $f_8(y, \bar{x})$. This procedure is continued to obtain $f_N(y, \bar{x})$ for $N = 20$, 40, 80, 100, 200, 400, 800, and 1000. The increment in y was doubled (in the same manner as before) after 10, 20, 100, and 200. The probability of detection,

$$P_D(\bar{x}) = 1 - \int_0^{Y_b} f_N(y, \bar{x}) \, dy$$

was computed by Simpson's rule for numerical integration. Simpson's rule was also used in the convolution integrals.

The question of accuracy is difficult to answer because of the difficulty in obtaining the maximum value of high order derivatives of $f_1(y/x)$ and $f_N(y, \bar{x})$ either analytically or numerically. These derivatives are needed to fix a bound on the numerical integration errors [17]. However, by doubling the initial increment in y and using only half as many points for $f_1(y, \bar{x})$, the resulting computed probability of detection seldom changed by as much as 0.01 (the greatest differences usually occurred at low detection probabilities). About 1 hour of computing time on the SDS 920 computer was required to find $f_{1000}(y, \bar{x})$. At first glance, it would seem possible to shorten the computation time by an approximation method. This is discussed next.

As the number of integrated pulses, N, is increased, it is expected that $f_N(y, \bar{x})$ will approach a normal density function with mean and variance equal to N times the mean and variance of $f_1(y, \bar{x})$. It is also possible to include a first-order correction term [18] as

$$f_N(\xi, \bar{x}) \simeq \frac{1}{\sqrt{2\pi}} e^{-\xi^2/2} \left[1 + \frac{m_{3N}}{6\sigma_N^3} (\xi^3 - 3\xi) \right] \tag{A-9}$$

where $\xi = (y - \mu_N)/\sigma_N$.

The quantities μ_N, σ_N^2, and m_{3N} are the first moment and second and third central moments of $f_N(y, \bar{x})$, respectively. The probability of detection, provided the approximation is valid, is given by

$$P_D(\bar{x}) \simeq \frac{1}{\sqrt{2\pi}} \int_S^\infty e^{-\xi^2/2} \, d\xi + \frac{1}{\sqrt{2\pi}} \frac{m_{3N}}{6\sigma_N^3} e^{-S^2/2}(S^2 - 1) \tag{A-10}$$

where $S = (Y_b - \mu_N)/\sigma_N$.

The general moments of $f_1(y, \bar{x})$ can be calculated in a straightforward manner. The kth moment about the origin of $f_1(y/x)$ as a function of x is given by

$$\nu_k(x) = \int_0^\infty y^k f_1(y/x) \, dy$$

$$= \int_0^\infty y^k e^{-(x+y)} I_0(2\sqrt{xy}) \, dy$$

$$= k! \, L_k(-x)$$

where $L_k(x)$ is the Laguerre polynomial of the kth degree. Hence, the kth moment about the origin of $f_1(y, \bar{x})$ is given by

$$\nu_k = \int_0^\infty \nu_k(x) \, f(x, \bar{x}) \, dx$$

-86-

which can be expressed in terms of the moments of $f(x, \bar{x})$. Thus, the first few moments are given by

$$\nu_1 = 1 + \bar{x}$$

$$\nu_2 = 2 + 4\bar{x} + \overline{x^2}$$

$$\nu_3 = 6 + 18\bar{x} + 9\overline{x^2} + \overline{x^3}$$

$$\nu_4 = 24 + 96\bar{x} + 72\overline{x^2} + 16\overline{x^3} + \overline{x^4}$$

In general, the nth moment of a log-normal distribution is given by

$$\overline{x^n} = \rho^{n(n-1)} \bar{x}^n$$

Hence, the moments of $f_1(y, \bar{x})$ can be expressed in terms of ρ and $\bar{x}$. The central moments can be computed by means of Eq. (A-4). Finally,

$$\mu_N = N[1 + \bar{x}]$$

$$\sigma_N^2 = N[1 + 2\bar{x} + (\rho^2 - 1)\bar{x}^2]$$

$$m_{3N} = N[2 + 6\bar{x} + 6(\rho^2 - 1)\bar{x}^2 + (2 + \rho^6 - 3\rho^2)\bar{x}^3]$$

For large ρ, the coefficient of the correction term in Eq. (A-10) is given approximately by

$$\frac{m_{3N}}{15\sigma_N^3} \simeq \frac{\rho^3}{15\sqrt{N}} \qquad\qquad \text{(A-11)}$$

A necessary, but not sufficient, condition for the convergence of Eq. (A-10) to the true probability of detection is that Eq. (A-11) should be much less than unity. Based on this result, $N \gg 16$ for $\rho = 4$, $N \gg 1000$ for $\rho = 8$, and $N \gg 75,000$ for $\rho = 16$.

The probability of detection based on the normal approximation (one term only) is shown in Figs. 47 - 50 for $\rho = 2$, 4, 8, and 16 and $n = 10^8$. For $\rho = 2$, the normal approximation is accurate for $N = 100$ and 1000. For $\rho = 4$, it is accurate for only $N = 1000$, and, for $\rho > 4$, it is not a suitable representation for the actual probability of detection. The first-order correction term is, in most cases, either negligible or unrealistic (i.e., probabilities larger than unity).
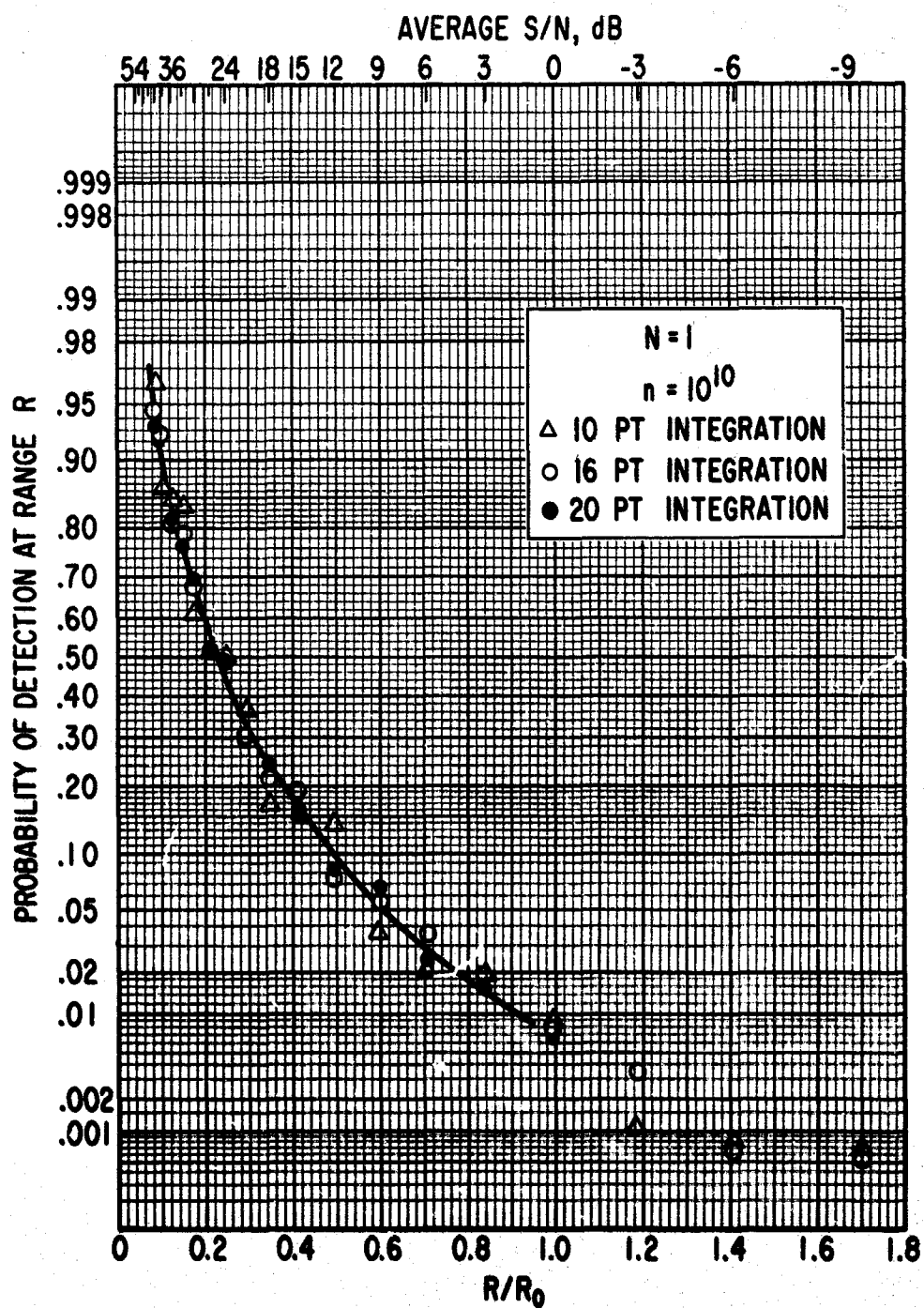
Fig. A-1.   Case 1, n = 10^{10}, N = 1

REFERENCES

[1] P. Swerling, "Probability of detection for fluctuating targets," RAND Corp., Santa Monica, Calif., Research Memo. RM-1217, 17 March 1954; also IRE Trans. Inform. Theory, vol. IT-6, pp. 269-308, April 1960.

[2] P. Swerling, "Detection of fluctuating pulsed signals in the presence of noise," IRE Trans. Inform. Theory, vol. IT-3, pp. 175-178, September 1957.

[3] M. Schwartz, "Effects of signal fluctuation in the detection of pulsed signals in noise," IRE Trans. Inform. Theory, vol. IT-2, pp. 66-71, June 1956.

[4] E. L. Kaplan, "Signal detection with applications," Bell System Tech. J., vol. 34, pp. 403-437, March 1955.

[5] J. I. Marcum, "A statistical theory of target detection by pulsed radar," RAND Corp., Santa Monica, Calif., Research Memos. RM-754, 1 December 1947, and RM-753, 1 July 1948; also IRE Trans. Inform. Theory, vol. IT-6, pp. 59-267, April 1960.

[6] P. Beckmann, "Rayleigh distribution and its generalizations," J. Res. Natl. Bur. Std., vol. 68-D, no. 9, pp. 927-932, September 1965.

[7] H. Goldstein, "The origins of echo fluctuations," in MIT Radiation Laboratory Series, D. E. Kerr, Ed. New York: McGraw-Hill, 1951, vol. 13, p. 546.

[8] L. Peters, Jr., and F. C. Weimer, "Concerning the assumption of random scatters as model of an aircraft for tracking radars," *IRE Trans. Antennas Propagation*, vol. AP-9, p. 110, 1961.

[9] R. B. Muchmore, "Reply to comments by L. Peters, Jr., and F. C. Weimer," *IRE Trans. Antennas Propagation*, vol. AP-9, p. 112, 1961.

[10] R. H. Delano, "Further reply to comments by L. Peters, Jr., and F. C. Weimer," *IRE Trans. Antennas Propagation,* vol. AP-9, p. 110, 1961.

[11] R. E Harrison, "Statistics of ship radar cross-section data," Aerospace Corp., El Segundo, Calif., Rept. No. TR-669(9990)-5 (in preparation).

[12] A. M. Peterson, et al., "Radar echoes obtained from earth satellites 1957 Alpha and 1957 Beta," in *Avionics Research: Satellites and Problems of Long Range Detection and Tracking,* E. V. D. Glazier, E. Rechtin, and V. Voge, Eds. New York: Pergamon Press, 1960, pp. 148-149.

[13] R. W. Kennedy, "The spatial and spectral characteristics of the radar cross section of satellite type targets," Air Force Avionics Lab., Tech. Rept. AFAL-TR-66-17, December 1965.

[14] W. Weinstock, "Target cross section models for radar systems analysis," Ph. D. dissertation, University of Pennsylvania, 1964.

REFERENCES (cont.)

[15] P. Beckmann, "Amplitude probability distribution of atmospheric radio noise," J. Res. Natl. Bur. Std., vol. 68-D, no. 6, pp. 723-836, June 1964.

[16] B. J. DuWaldt, Aerospace Corp., El Segundo, Calif., private communication.

[17] M. Abramowitz and I. A. Stegun, "Handbook of mathematical functions," Natl. Bur. Std. (U.S.) Appl. Math. Series 55, p. 890, June 1964.

[18] A. Papoulis, Probability, Random Variables, and Stochastic Processes. New York: McGraw-Hill, 1965, p. 270.

DOCUMENT CONTROL DATA · R&D

(Security classification of title, body of abstract and indexing annotation must be entered when the overall report is classified)

1. ORIGINATING ACTIVITY (Corporate author)	2a. REPORT SECURITY CLASSIFICATION
Aerospace Corporation El Segundo, California	Unclassified
	2b. GROUP

3. REPORT TITLE

DETECTION PROBABILITIES FOR LOG-NORMALLY DISTRIBUTED SIGNALS

4. DESCRIPTIVE NOTES *(Type of report and inclusive dates)*

5. AUTHOR(S) *(Last name, first name, initial)*

Heidbreder, Glenn R., and Mitchell, Richard L.

6. REPORT DATE	7a. TOTAL NO. OF PAGES	7b. NO. OF REFS
April 1966	99	18

8a. CONTRACT OR GRANT NO.	9a. ORIGINATOR'S REPORT NUMBER(S)
AF 04(695)-669	
b. PROJECT NO.	TR-669(9990)-6
c.	9b. OTHER REPORT NO(S) (Any other numbers that may be assigned this report)
d.	SSD-TR-66-87

10. AVAILABILITY/LIMITATION NOTICES

This document is subject to special export controls, and each transmittal to foreign governments or foreign nationals may be made only with prior approval of SSD (SSTRT).

11. SUPPLEMENTARY NOTES	12. SPONSORING MILITARY ACTIVITY
	Space Systems Division Air Force Systems Command Los Angeles, California

13. ABSTRACT

The amplitude and power of a large family of radio signals are observed to have log-normal probability density functions. Among these are signals propagated through random inhomogeneous media, a notable examplabe being low frequency atmospheric radio noise. Of greater importance are certain radar targets that have been observed to have essentially log-normal density functions. Both ships and space vehicles may fall into this category. Curves of probability of detection versus signal-to-noise ratio for the case of log-normal signals in Gaussian noise have been computed and are presented in this paper. The curves apply for square-law detection with varying degrees of post-detection linear integration. Both slowly and rapidly fluctuating signals are considered. It is shown that for log-normal signal distributions having large variances the probability of detection differs significantly from that obtained using curves based on an assumed Rayleigh signal distribution.

14.	KEY WORDS
Radar Detection Probability Curves Fluctuating Targets Log-Normal Cross Section Distributions Satellite Radar Cross Section Ship Radar Cross Section	

Abstract (Continued)